GABAergic Interneurons Control Spiking of Adult-born Hippocampal Granule Cells via Nonlinear α_5-GABA$_A$ Receptors

Inauguraldissertation

zur

Erlangung der Würde eines Doktors der Philosophie

vorgelegt der

Philosophisch-Naturwissenschaftlichen Fakultät

der Universität Basel

von

Meredith Lodge

von Neuseeland

2019

Genehmigt von der Philosophisch-Naturwissenschaftlichen Fakultät

auf Antrag von

Prof. Dr. Josef Bischofberger

Fakultätsverantwortlicher und Dissertationsleiter

Prof. Dr. Tania Rinaldi Barkat

Korreferentin

Basel, 19th November 2019

Prof. Dr. Martin Spiess
Dekan

Contents

1. Abstract

Excitatory GABAergic synapses have been shown to promote development and maturation of newborn granule cells in the adult hippocampus. In addition, strong GABAergic synaptic inputs are known to generate effective shunting inhibition in these young neurons. However, the functional properties of the GABA receptors mediating excitation and inhibition are largely unknown. Here we analyzed GABA receptors in young neurons activated by soma-targeting parvalbumin and dendrite-targeting somatostatin inhibitory interneurons. The synaptic $GABA_A$ receptors in young neurons show a pronounced non-linear voltage dependence and are assembled in part by α_5-subunits. As a consequence, synaptic conductance is 4-fold larger around the AP threshold (-35 mV) as compared to the resting potential (-80mV), independent of the interneuron subtype. By contrast, in mature granule cells, parvalbumin interneurons mediate linear GABAergic synaptic currents lacking α_5-subunits. Blocking α_5-$GABA_A$-receptor-mediated synaptic currents in young neurons not only reduced GABAergic depolarization, but also effectively reduced shunting inhibition of AP generation. Taken together, this data shows that nonlinear $GABA_A$ receptors support both GABAergic depolarization and effective GABAergic shunting inhibition in newborn young granule cells of the adult hippocampus.

2. Introduction

2.1 General introduction to the hippocampus memory system

The hippocampus- a deep-set area within the medial temporal lobe in humans- was named after the genus *Hippocampus* due to its seahorse-like structure. In rodents, a cross section of the cashew-like shape shows the classic 'trisynaptic loop' in which this area is known for. The entorhinal cortex feeds excitatory inputs into the dentate gyrus (DG), via the perforant path. The DG then feeds information through to the CA3 region via mossy-fiber terminals. Finally, CA3 projects onto CA1 via the Schaffer Collateral pathway and CA1 pyramidal neurons project back to the entorhinal cortex (Fig. 1A). As a whole, the hippocampus is widely recognised as the main center of memory formation, a view that has been strengthened by the discovery of place cells in the hippocampus, and head direction cells, and grid cells in the entorhinal cortex of the rodent (Knierim, 2015). Additionally, human lesion studies have further shown the importance of the hippocampus in episodic memory formation (memories of one's experience) and semantic memory (factual knowledge). Patients with hippocampal damage have difficulty remembering the details of their daily life, however, can often remember personal events that occurred prior to the time of damage, suggesting that memories are further consolidated in other regions (potentially the neocortex). This was famously illustrated by the case of H.M who, in 1957, underwent a bilateral medial temporal lobe resection to treat severe epilepsy. As a result, he lost the ability to form new declarative memories while maintaining old memories that were acquired years before surgery (Dossani et al., 2015).

The seminal studies of Marr suggested that the mammalian hippocampal formation constitutes an auto-associative memory storage based on CA3 connectivity (Marr, 1971). Auto-associative memory allows the retrieval of a complete piece of data with the presentation of only a partial sample (to recall the whole using only some of its parts). This allows an individual to 'fill in the blanks' or adapt a memory as it changes- for example the ability to recognise the same person as they age or alter their appearance over time. However, it was pointed out that selectively retrieving a specific firing pattern among several learned neuronal activity patterns stored in the

same set of recurrent synapses is highly complex (Treves and Rolls, 1992). While auto-associative memory storage systems show the potentially useful property of memory retrieval by partial cues, they also tend to generalize, strongly limiting storage capacity. Computational modeling suggested that this problem could be reduced in the hippocampus by sparse and orthogonal activity in the dentate-gyrus mossy-fiber system, acting as a 'director' for the CA3 network (Treves and Rolls, 1994).

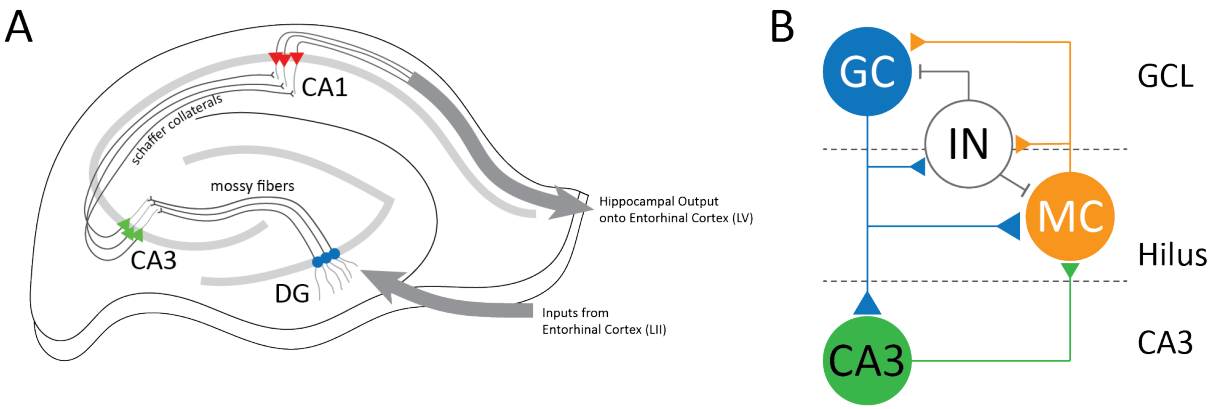

Figure 1. The hippocampus forms a 'trisynaptic loop'. A) Simplified schematic representation of the basic hippocampal circuit The DG receives inputs from the entorhinal cortex and granule cells feed information to CA3 through the mossy fibers. CA3 connects to CA1 via Schaffer collaterals, and CA1 projects back to the entorhinal cortex. Please note for simplicity many other details of connectivity have been excluded. B) A simplified diagram of the main connections of the DG between GCs (GCL), mossy cells (hilus) and CA3 neurons and their interaction with INs (hilus and GCL) within the dentate gyrus. Adapted from GoodSmith et al. (2017).

Indeed sparse activity patterns in dentate were later confirmed by many experimental studies, showing that only about 2% of dentate granule cells are active during a certain behavioral task (Jung and McNaughton, 1993; Chawla et al., 2005; Bakker et al., 2008; Hainmueller and Bartos, 2018). However, within the CA3 region the relative proportion of active cells is typically an order of magnitude larger (30-40%). This is partially due to the dense recurrent network formed by CA3 pyramidal cells, with each neuron receiving about 4000 EC inputs and more than 10000 recurrent collateral synapses. In contrast, a single CA3 pyramidal cell receives inputs from only a few mossy fibers (~50) with exceptionally strong synaptic weight. Therefore, although the mossy-fiber input is sparse, a brief burst in a single GCs is able to discharge a CA3 pyramidal neuron (Henze et al., 2002; Bischofberger et al., 2006). As dentate GCs are active in parallel to the direct perforant-path input onto CA3, a sparse and orthogonal mossy fiber input might therefore help to form distinct cell assemblies during learning for different memory items (Treves and Rolls, 1994). This

sparse population coding is thought to help increase storage capacity of the hippocampus, and GABAergic interneurons play a key role in this process.

2.2 The dentate gyrus

The dentate gyrus is comprised of three layers. The hilus, a polymorphic layer, includes a number of different cell types including GABAergic interneurons and most notably, the excitatory mossy cells. Surrounding the hilus on three sides is the granule cell layer, which contains the principle cells of the DG which are densely packed together with a thickness of four to eight neurons (approximately 60μm thick). The outer layer of the dentate gyrus is the molecular layer. This reasonably cell free layer is mainly occupied by the dendrites of granule cells, as well as the input fibers from the perforant pathway (Amaral et al., 2007). A simplified schematic of the connections between granule cells, mossy cells, and interneurons of the DG with CA3 neurons is shown in Fig. 1B (adapted from GoodSmith et al. 2017).

Functionally, the dentate gyrus has long been thought to play a crucial role in pattern separation, with the anatomy, activity and connectivity of granule cells lending themselves favorably to this notion. Pattern separation involves the transformation of similar memories into highly non-overlapping separate representations. Computational models have highlighted the importance of the dentate and its output connections onto CA3 (Treves and Rolls, 1992, 1994; Treves et al., 2008; Rolls, 2013). Behavioral studies, like that done by Leutgeb et al. (2007) have confirmed that both areas are important in pattern separation and completion. When exposing rodents to minimal changes in the shape of an environment, the correlated activity patterns of granule cells were significantly altered but remained stable in CA3. However, when environments were made increasingly different, new cells were recruited in CA3 and the DG. Thus, inputs from the entorhinal cortex can be ‘fine-tuned’ in response to small changes through altered firing patterns in the dentate, while gross changes result in the recruitment of non-overlapping cell assemblies in CA3.

2.3 GABAergic connectivity within the dentate gyrus

GABAergic interneurons within the dentate gyrus form a heterogenous population, with individual subtypes serving distinct network roles based on the inputs they receive and the outputs they generate. Two major classes populate the DG: basket cell (BC) interneurons (INs) and hilar perforant path associated (HIPP) cells which are defined by morphology and the target selectivity of their axon. BC INs are parvalbumin (PV) positive, have their soma and axon terminal in the granule cell layer and selectively form somatic-synapses onto granule cells. These fast-spiking neurons represent approximately 30% of the interneuron population (Freundl and Buzsáki, 1996). In contrast, HIPP INs are somatostatin (SOM) positive, have their soma present in the hilus- and as the name suggests- project their axons out into the molecular layer (where perforant path fibers reside) to form dendritic-synapses onto granule cells (Lee et al., 2016). These SOM-INs account for approximately 50% of the interneuron population. Although the interneuron population within the dentate includes multiple other subtypes (for example neurogliaform and cholecystokinin INs), the majority of research has focused on PV and SOM interneurons due to their selective synapse location.

The role of these two main subtypes in higher network functions is thought to be tightly linked to the inputs they receive as well as their intrinsic properties. Feedforward and feedback inhibition microcircuits recruit distinct interneuron populations to control network activity within the DG. Feedforward inhibition is thought to rely on fast-spiking PV-INs, due to the direct inputs they receive from perforant-path terminals, and their low-activation threshold and rapid firing (Ewell and Jones, 2010). Additionally, PV basket cells receive inputs from granule cells. However, they preferentially inhibit those granule cells from which they receive no input, producing strong lateral inhibition and a ‘winner-takes-all’ mechanism (Espinoza et al., 2018). Thus, granule cells that receive strong excitatory inputs will direct DG activity, while those with weak inputs will be rapidly inhibited. In contrast, the feedback inhibitory microcircuit recruits both PV and SOM INs, as granule cells synapse directly onto both populations.

Postsynaptically, GABAergic inputs are modulated by the receptor subtypes found in the synapses of granule cells. $GABA_A$ receptors are a pentamer, composed of subunits derived from the α, β, γ, δ, θ, ε, and π gene families. Most commonly, $GABA_A$ receptors ($GABA_ARs$) are comprised of two α-subunits, two β-subunits and a γ-subunit, which join together to form a central chloride ion channel pore. The subunit composition not only shapes the kinetic properties of the receptor but has been found to be tied to the location of the receptor- either synaptic or extrasynaptic (Hannan et al., 2019). Within the dentate, the α_1, α_4, α_5, γ_2, and δ subunits are expressed (Sun et al., 2004), with α_1-containing 'fast' receptors found within synapses, and α_4, α_5 and δ containing 'slow' receptors localised in the extrasynaptic membrane (Wei et al., 2003; Smith, 2013; Engin et al., 2015). However, recent studies suggest that slow dendritic inhibition within the hippocampus may be mediated by postsynaptic α_5-$GABA_ARs$, suggesting that typically 'extrasynaptic' GABA receptors may also be found synaptically (Collinson et al., 2002; Zarnowska et al., 2009; Vargas-Caballero et al., 2010; Schulz et al., 2018).

2.4 Adult neurogenesis in the dentate gyrus

The addition of new neurons in the brain throughout adulthood has long been a topic of controversy within the neuroscience field. Traditionally, the brain has been viewed as a constant, stable unit- in stark contrast to the developmental growth seen during embryogenesis. Leading neuroscientists like Ramón y Cajal, believed that the neurons that were present after birth would remain throughout adulthood, however, this theory has been challenged multiple times in the last few decades. In 1962 Altman injected radioactive thymidine-H^3 intracranially, and found labelled neurons, suggesting the presence of neuronal proliferation. By measuring the concentration of nuclear-bomb-test-derived C^{14} in genomic DNA it has been concluded that in humans 700 new neurons are added to the hippocampus every day through neurogenesis (Spalding et al., 2013). More recent work from the Llorens-Martín group examining human post-mortem tissue have found that immunohistochemical markers for neurogenesis are present up to the ninth decade of life (Moreno-Jiménez et al., 2019a). Therefore, this long-held dogma of the stability of the human brain has been called into question. The wider field now accepts that mammalian species do indeed produce newborn neurons

well into adulthood through two distinct regions which give rise to progenitor cells. The subventricular zone (SVZ), located in the walls of the lateral ventricles, produces a large number of neuroblasts that are able to migrate rostrally to the olfactory bulb, where they then differentiate into neurons (Doetsch and Alvarez-Buylla, 1996; Doetsch et al., 1999; Lim and Alvarez-Buylla, 2016). The subgranular zone (SGZ) however, is found between the granule cell layer of the dentate gyrus and the hilus, where radial glia-like neural stem cells exit the quiescent stage and give rise to amplifying neural progenitor cells that finally divide to adopt a neuronal cell fate (Kaplan and Hinds, 1977) (Fig. 2, adapted from Bischofberger, 2007). Whether neurogenesis occurs in areas of the brain other than the SVG or SGZ is still debated, with some evidence supporting cell proliferation in the neocortex, striatum, amygdala and substantia nigra (reviewed by Rakic, 2002; Gould, 2007).

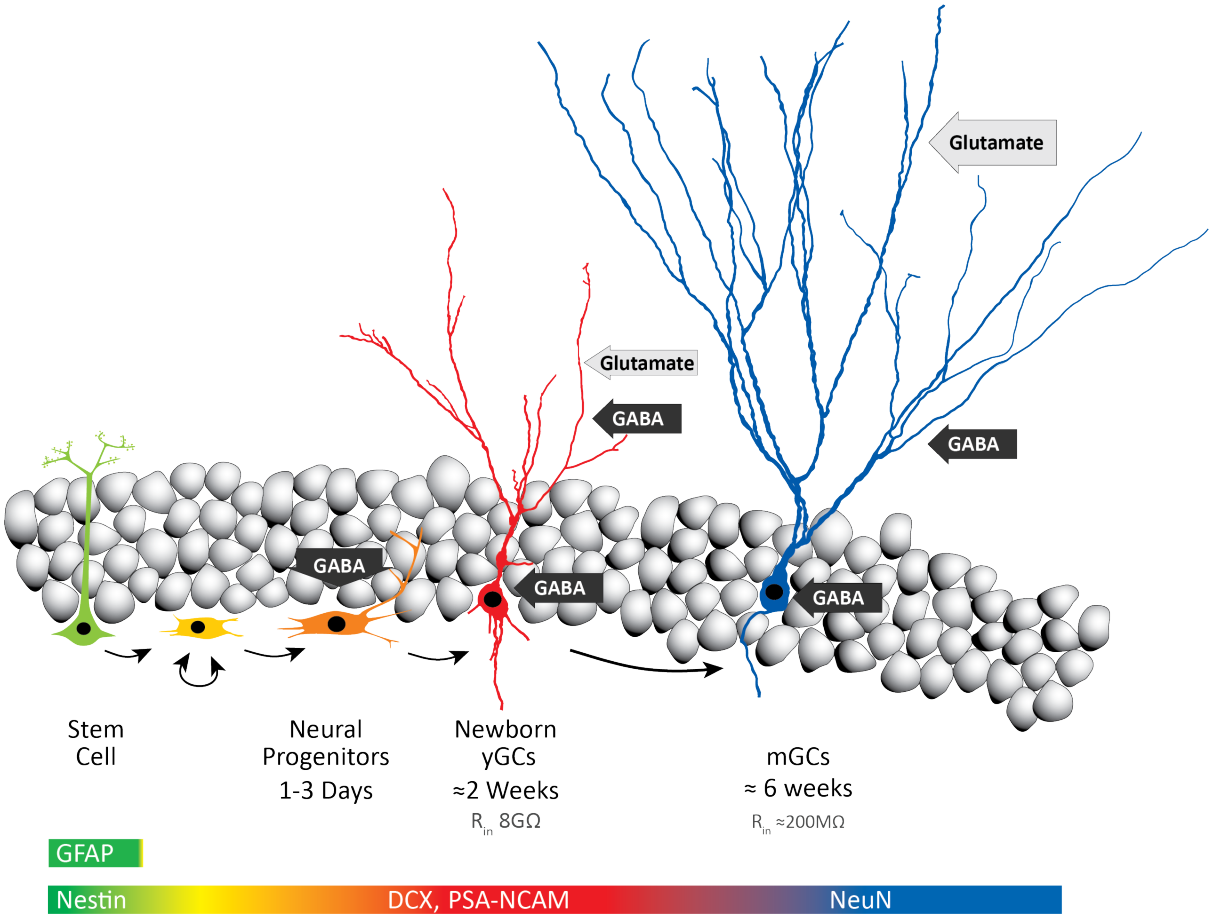

Figure 2. Maturation of newly generated granule cells in the adult hippocampus. Schematic representation of the development of a newly-generated granule cell including cell morphology, neuronal marker expression and inputs during different maturation time points. Adapted from Bischofberger, (2007).

Establishing functional analysis using patch-clamp recordings from adult-born hippocampal granule cells (van Praag et al., 2002), was a major step forward in establishing adult neurogenesis as a widely accepted phenomenon within the broader neuroscience community. Subsequently, several studies appeared showing distinct functional properties of newborn neurons in the adult brain, including enhanced excitability and enhanced synaptic plasticity, relative to the mature granule cell (GC) population (Schmidt-Hieber et al., 2004; Ge et al., 2007). Furthermore, GABAergic synapses were shown to be initially depolarizing until 3 weeks of age (Overstreet-Wadiche et al., 2005a; Ge et al., 2006; Heigele et al., 2016), followed by a phase with a hyperpolarized GABA reversal potential (E_{GABA}) and a slower time course of the GABAergic synaptic inhibition (Marín-Burgin et al., 2012). At 8 weeks post mitosis, adult born granule cells were found to finally show GABAergic inhibition identical to mature GCs (Laplagne et al., 2006).

2.5 Regulation of adult neurogenesis

While neurogenesis does seem to occur continuously throughout adulthood, different environmental and physiological stimuli have been found to regulate the rate of neurogenesis and cell survival. Overall increased neuronal network activity has been found to positively modulate neurogenesis (Deisseroth et al., 2004), with learning (Tronel et al., 2010), social interaction (Hsiao et al., 2014), physical exercise (van Praag et al., 1999; Zhao et al., 2006; Vivar et al., 2012; Deshpande et al., 2013) and enriched environments (Kempermann et al., 1997a; Bergami et al., 2015) all promoting increased cell proliferation and survival. Pathological increases of neuronal activity through epileptic seizures is also able to increase neurogenesis (Bengzon et al., 1997; Parent et al., 1997; Gray and Sundstrom, 1998; Jessberger et al., 2005), supporting the notion that network activity is important.

Several factors can also act to downregulate neurogenesis, with social stress (Gould et al., 1998; Mouri et al., 2018), substance abuse (Eisch et al., 2000; Vetreno and Crews, 2015) and even cessation of voluntary exercise (Nishijima et al., 2017) reducing cell proliferation within the dentate. Genetic background can produce variability in the rate of neurogenesis, with Kempermann et al. (1997b) finding differences between different mouse strains commonly used in research. Additionally,

a decline in neurogenesis is present during ageing, with a 75% loss of progenitor neurons in mid to old age compared with young mice (Jin et al., 2003; Lugert et al., 2010; Apple et al., 2017). This drop in proliferation has been linked with a decrease in growth factors including brain-derived neurotrophic growth factor (Marlatt et al., 2012; Apple et al., 2017). However, voluntary running in aged mice has partially been able to reverse these effects (Marlatt et al., 2012; Trinchero et al., 2017). Several pathological conditions have been linked to reduced neurogenesis including Alzheimer's, schizophrenia, anxiety and depression (Malberg et al., 2000; Heckers, 2001; Sigurdsson et al., 2010; Hill et al., 2015; Miller and Hen, 2015; Moreno-Jiménez et al., 2019b). Taken together, these studies show that despite adult-neurogenesis being a robust phenomenon in healthy adults, multiple factors can impact the rate of granule cell proliferation.

2.6 Identification of newly-generated young granule cells

In order to study neurogenesis in the dentate gyrus multiple methods to label and identify newborn and immature neurons have been established. One of the first approaches developed was intraperitoneal injections of Bromodeoxydine (BrdU), a thymidine analog that is incorporated into the DNA of dividing cells during the S-phase cycle for around 2 days post injection. Immunohistochemical analysis can be performed on tissue, allowing young cells to be identified and 'birth-dated' (Takahashi et al., 1992). However, BrdU can also be incorporated into DNA during other synthesis events such as cellular repair or gene duplication, so can produce an overestimate of the number of newly proliferated neurons (Taupin, 2007). Thus, BrdU is best combined with post-hoc analysis for markers specific to immature neurons, such as polysialylated-neural cell adhesion molecule (PSA-NCAM) or double-cortin (DCX) which are transiently expressed throughout maturation (Fig. 2).

An important milestone in the identification of young neurons was the development of fluorescent labelling that allowed for the visualization of newborn neurons in live tissue experiments. The development of a retrovirus that could be intracranially injected to label proliferating cells with a green fluorescent protein (GFP), allowed for both cell identification in live slices and morphological analysis including the neuronal processes (van Praag et al., 2002). The ability to birth-date neurons and

conduct electrophysiological recordings from the same animals allowed for the correlation of intrinsic properties and synaptic connections of young neurons with their precise age (Espósito et al., 2005; Ge et al., 2007; Alvarez et al., 2016; Sah et al., 2017).

One shortcoming of viral injections is that their expression is restricted to the injection site. In recent years, transgenic mouse lines expressing fluorescent proteins under the control of promoters specific to immature neurons have overcome this limitation. This allows fluorescent proteins to be expressed transiently and -in the case of neurogenic promoters- throughout the entire dentate gyrus. For example, Overstreet et al. (2004) utilized a mouse line with the enhanced green fluorescent protein expressed under the control of the proopiomelanocortin promoter (POMC-eGFP), labelling young granule cells up to 2 weeks of age. Additionally, Couillard-Despres et al. (2006) developed a mouse line where the red fluorescent protein (DsRed) was expressed under the control of the doublecortin promoter, labeling cells between one and four weeks of age. The ability to effectively visualize and identify young neurons *in vivo* has allowed for the investigation of both the intrinsic properties of young cells and their synaptic connectivity during maturation.

2.7 Enhanced excitability of young granule cells

The structure and function of young GCs differ from mature cells in the dentate gyrus in a substantial number of ways, including synaptic connectivity, firing patterns and membrane excitability (Fig. 3, adapted from Heigele et al., 2016). Post mitotic development of young GCs has been extensively studied in adult mice. After cell division the young neurons rapidly start to grow, showing a total dendritic length (TDL) of about 500 µm at 2 weeks post mitosis (wpm) and further increasing to 1000 µm at 3 wpm (Zhao et al., 2006; Sun et al., 2013; Gonçalves et al., 2016). In Fig. 3A-B a 2.5 week old biocytin filled neuron is shown with an immature dendritic tree, which fired action potentials (AP) with excitatory currents in the range of a few picoampere (pA) - two orders of magnitude lower than typical mature GCs (Fig. 3D-E). This early growth period is followed by synaptic refinement and dendritic pruning, until the neurons resemble fully mature granule cells with a TDL of about 2 mm at around 6-8 weeks post mitosis (Schmidt-Hieber et al., 2007; Gonçalves et al., 2016). The cell

capacitance is initially very small, around 20 pF when the first synapses are formed (about 1 wpm), and increases up to 60-70 pF during the next 4-6 weeks (Ambrogini et al., 2004; Mongiat et al., 2009; Heigele et al., 2016). In addition, young GCs have initially a high membrane resistivity, resulting in a remarkably high electrical input resistance (R_{in}) of about 32 GΩ compared to about 200 MΩ in mature GCs. This means that small currents generate relatively large membrane depolarizations in the young neurons. The high membrane resistance also leads to a slow membrane time constant of about 150ms at 1-2 wpm, promoting temporal integration of synaptic potentials (Fig. 3C) (Overstreet et al., 2004; Schmidt-Hieber et al., 2004; Heigele et al., 2016). Subsequently, the R_{in} decays exponentially with a 4-fold decrease per week resulting in about 8 GΩ, 2 GΩ and 0.5 GΩ at 2, 3 and 4 weeks, respectively (Fig. 3G) (Heigele et al., 2016; Li et al., 2017). The change in R_{in} with maturation is most likely generated by an activity-dependent upregulation in the density of inward-rectifier potassium channels (Kir2, Kir3.2) and ion channels from the two-pore-domain (K2P) family (Mongiat et al., 2009; Young et al., 2009; Gonzalez et al., 2018), which also directly generates a pronounced developmental speed up of the membrane time constant at about 3-4 wpm (Fig. 3H).

The high input resistance together with the slow membrane time constant renders young GCs very sensitive to small excitatory currents. As shown in Figure 3I, the rheobase varies from about 5 pA in young up to 200 pA in fully mature cells, spanning almost two orders of magnitude. In addition there are low-threshold calcium spikes generated by somato-dendritic T-type calcium channels, which further boost small EPSPs towards the action potential (AP) threshold (Ambrogini et al., 2004; Schmidt-Hieber et al., 2004; Stocca et al., 2008).

Before 3 weeks, young GCs show a higher AP threshold of about -35 mV in contrast to -45 mV in mature GCs (Heigele et al., 2016). Additionally the voltage-gated sodium and potassium currents were found to be smaller in young as compared to mature GCs, which reduces the AP amplitude, the maximal rate of rise (Fig. 3J) and most importantly the maximal firing frequency (Mongiat et al., 2009; Heigele et al., 2016). As a result, young GCs fire only one or a few spikes during persistent current injection before 3 wpm (Fig. 3B). Finally, the density of excitatory synapses and the amplitude of excitatory synaptic currents are much smaller in young GCs up to 4 weeks of age

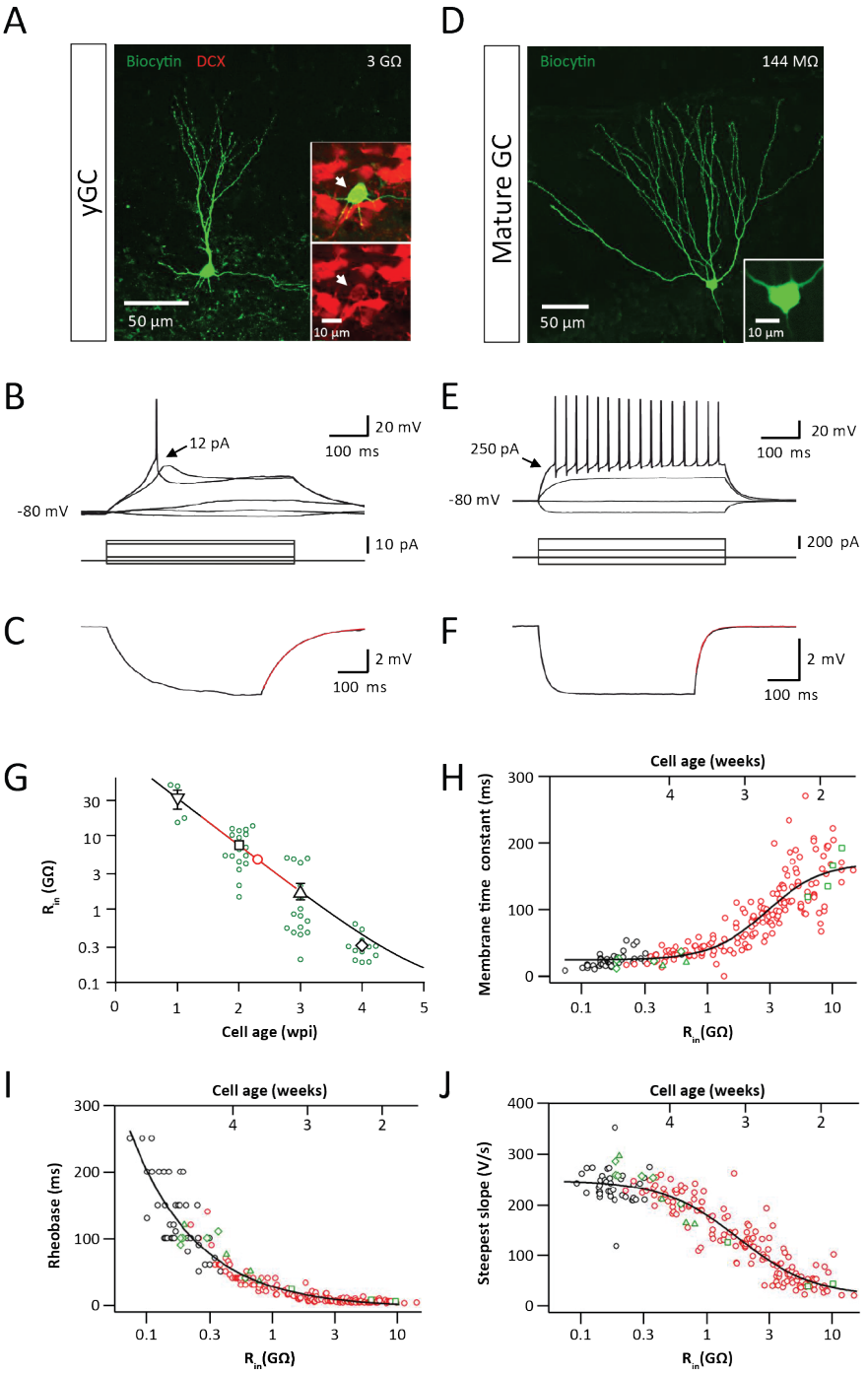

Figure 3. Intrinsic properties differ between young and mature granule cells. (A) Confocal image of a biocytin-filled (green) newborn granule cell with an input resistance of 3 GΩ corresponding to 2.5 weeks post mitosis. Inset images show immunohistochemical staining of DCX expression (red). (B) Low-threshold Ca^{2+}-spike and AP induced by somatic current injection (same cell as A). Minimal current for AP induction is indicated. (C) Decay after a small hyperpolarization revealed a slow membrane time constant (τ_m = 94ms, monoexponentially fit in red). (D) Morphology of a mature granule cell with an input resistance of 144 MΩ. (E) Mature firing pattern for the cell in (D). (F) Voltage decay after the current pulse revealed a fast τ_m of 23ms. (G) Semi-logarithmic plot showing that input resistance (R_{in}) decreases with maturation. Green circles represent individual GFP-positive birth-dated GCs. Black circles represent the mean ± s.e.m. of GFP-positive neurons. Red line indicates the range of the R_{in} of recorded DCX+ neurons (1.5–18 GΩ) corresponding to 1.5 to 3 weeks post mitosis. (H-J) Semi-logarithmic plots of membrane time constant (H), threshold current to evoke an AP (rheobase) (I) and steepest slope of APs (J) of mature GCs (black), $DsRed^+$ young (red) and GFP-positive birth-dated GCs (green). Lines represent sigmoidal (H, J) or double exponential (I) fits. Adapted from Heigele et al. (2016).

(see below). Thus, the high R_{in} compensates for the smaller glutamatergic synaptic currents, to obtain a synapse-evoked spiking probability in young 2-4 wpm GCs, which is relatively similar to mature cells – at least in the absence of GABAergic inhibition (Mongiat et al., 2009; Dieni et al., 2013; Li et al., 2017).

2.8 Formation and function of glutamatergic synapses in yGCs

Glutamatergic synapses have been found to form around 7 days post mitosis, potentially originating from hilar mossy cells (Deshpande et al., 2013; Chancey et al., 2014; Sah et al., 2017). During the second post mitotic week further glutamatergic synaptic contacts are made from lateral and medial entorhinal cortex (LEC, MEC)(Deshpande et al., 2013; Woods et al., 2018). Therefore, young neurons form synapses with the major afferent glutamatergic input pathways early on.

Until 3 wpm glutamatergic synapses show immature functional properties including preferential expression of NR2B-containing NMDA receptors (Ge et al., 2007; Chancey et al., 2013, 2014; Li et al., 2017). Similarly, the extrasynaptic membrane of newborn granule cells harbors a large number of NMDA receptors, even in the youngest cells without any synapses (Schmidt-Salzmann et al., 2014). The extrasynaptic NMDA/AMPA receptor conductance ratio is 3-times higher in young GCs before 3 wpm and declines towards a mature ratio of about 1:1 after the loss of DCX expression. These findings suggest that extrasynaptic NMDA receptors are key players in the process of new synapse formation in newly generated granule cells. They might be activated by extrasynaptic glutamate spillover from neighboring preexisting axon terminals and thereby initiate growth of new filopodia and spines in a competitive manner (Toni et al., 2007; Mu et al., 2015; Adlaf et al., 2017). Furthermore, NMDAR activation between 1-2 wpm was shown to be important for survival of the newborn cells, which are otherwise eliminated via apoptosis (Tashiro et al., 2006).

The synaptic NMDAR/AMPAR conductance ratio is initially 10:1 at 2 wpm, substantially higher than the extrasynaptic ratio of 3:1 (Schmidt-Salzmann et al., 2014; Li et al., 2017), indicating that NMDA receptors are selectively enriched and targeted into developing postsynaptic filopodia. This not only supports synapse formation but

also lays the foundation for the adjustment of synaptic strength during activity-dependent synaptic plasticity (see below, Schmidt-Hieber et al., 2004; Ge et al., 2007). The high expression of NMDARs in newly formed synapses of young GCs generates pronounced NMDA-dependent electrogenesis, resulting in highly non-linear summation of glutamatergic EPSPs (Li et al., 2017). As shown in Fig. 4 (adapted from Li et al., 2017), electrical stimulation of glutamatergic synapses in the molecular layer with a low intensity readily evokes subthreshold EPSPs in mature as well as in 2 week old GCs. In contrast to mature neurons, the EPSPs in young neurons are highly sensitive to the NMDAR antagonist AP5 (Fig. 4AB). Furthermore, brief burst stimulation (5@50Hz) generates non-linear NMDAR-dependent summation of EPSPs in young GCs with a 10-times larger peak amplitude relative to single EPSPs. In contrast, EPSP summation is sublinear in mature GCs (Fig. 4CD). As a consequence, the peak amplitude of burst EPSPs in mature and 2 week old neurons is not significantly different using the same stimulation intensity (Li et al., 2017). Increasing stimulation intensity generates spiking in young cells as well as in mature cells (Fig. 4E+F). Unlike mature cells however, spiking in young neurons is critically dependent on NMDA receptors. This is supported by the small membrane capacitance (20 pF) and high electrical input resistance before 3 wpm (2-30 GΩ), which renders young GCs electrotonically compact and creates a single electrotonic compartment (Heigele et al., 2016)

The addition of AMPA receptors into glutamatergic synapses of young cells is thought to be activity-dependent. AMPAR integration (“synapse unsilencing”) is dependent on sufficient depolarization at the synapse to remove the Mg^{2+} block and activate NMDARs. This activation leads to the rapid addition of AMPA receptors into the synapse. Interestingly, increasing network activity by placing mice in an enriched environment for two weeks significantly increased the percentage of newborn GCs with AMPAR EPSCs which was not associated with enhanced maturation (Chancey et al., 2013). The AMPAR contribution dramatically increases between 2-4 weeks post mitosis, with AMPA-dependent spiking occurring at 4wpm (Mongiat et al., 2009; Gu et al., 2012; Dieni et al., 2013, 2016).

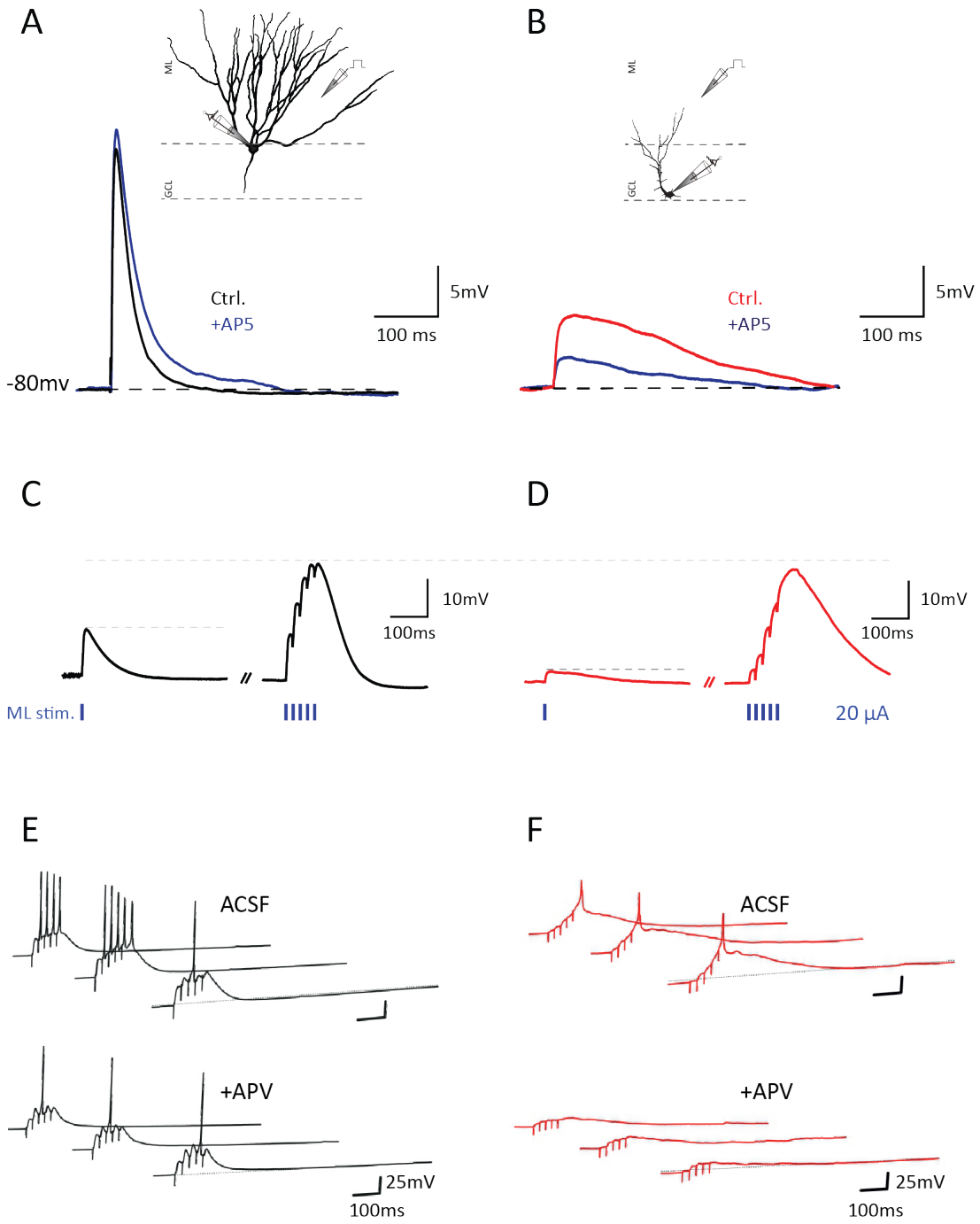

Figure 4. NMDA-dependent electrogenesis in young GCs. (A, B) Application of AP5 (50µM) does not significantly affect EPSP amplitude in mature granule cells (A) but decreases EPSP amplitude in a young neuron (B) at 2.5 weeks post mitosis (wpm). There is a significantly larger contribution of AP5-sensitive NMDA receptors to the EPSP in 2–3 week old DsRed+ neurons than in mature GCs. (C, D) Subthreshold summation of five EPSPs evoked by brief burst stimuli (5@50 Hz, 20µA) in a mature (C) and a young 2.5 week old GC (D). The ratio of burst EPSP amplitude to single EPSPs is significantly higher in young GCs relative to mature GCs.(E, F) Increasing burst stimulation intensity (5 @ 50Hz, 30 µA) evoked AP firing in both mature (E) and young (F) cells. With the application of AP5 (50µM) firing was still possible in mature neurons, however, it was largely blocked in young GCs showing strong NMDA-receptor dependent spiking. Adapted from Li et al. (2017).

There are a number of important factors counterbalancing excitability in young granule cells. Most importantly, the number of synaptic connections is dramatically smaller at young developmental stages. It was estimated that the density of immature glutamatergic synapses at 2 and 3 wpm corresponds to only about 2% and 20% of mature values, respectively (Zhao et al., 2006; Li et al., 2017). At 4 wpm the synapse density is still only 35% of mature and further increases during the following weeks (Dieni et al., 2016). Remarkably, synapse-evoked spiking probability at 2-4 wpm was reported to be very similar in young and mature neurons, using local afferent fiber stimulation in the molecular layer (Mongiat et al., 2009; Dieni et al., 2016; Li et al., 2017). This suggests that the high sensitivity for small excitatory currents and NMDA-dependent electrogenesis in young cells does not generate hyperexcitability, but rather balances low connectivity and compensates for the low number of input synapses.

2.9 GABAergic synaptic inputs onto adult-born granule cells drive both excitation and shunting inhibition

Newborn granule cells begin to develop GABAergic synaptic contacts as early as 4 days post mitosis (Song et al., 2013) and these synapses gradually increase in strength during the next 6 weeks (Espósito et al., 2005; Ge et al., 2006; Sah et al., 2017). The first interneurons which were found to contact young GCs at about 1 wpm were NO-synthase (NOS) positive neurogliaform/ivy cells and parvalbumin-positive (PV) basket cells (Markwardt et al., 2011; Alvarez et al., 2016). In a study by Linda Overstreet-Wadiche and colleagues it was shown that these early GABAergic synaptic currents have slow time course and small amplitudes, but are nevertheless generated by bona fide synapses and do not represent spillover from neighboring synapses (Markwardt et al., 2009).

Similar to embryonic brain development the GABA reversal potential (E_{GABA}) in young neurons is relatively depolarized to about -35 mV until 3 weeks post mitosis in contrast to about -80 mV measured in mature GCs (Fig. 5, adapted from (Heigele et al., 2016) (Overstreet-Wadiche et al., 2005b; Ge et al., 2006; Karten et al., 2006; Heigele et al., 2016). This is due to a relatively high internal chloride concentration (~25 mM) generated by high expression of NKCC1 and the low expression of KCC2

chloride transporters and has important consequences for the development and survival of young neurons (Ben-Ari, 2002; Ge et al., 2006; Jagasia et al., 2009). More specifically, it has been shown that feedback inhibition via PV interneurons is critically important for mediating the survival-promoting effect of environmental enrichment during the first 2 weeks after mitosis (Alvarez et al., 2016). It has also been shown that depolarizing GABAergic synapses can powerfully unblock NMDA receptors and may thereby induce enough calcium influx to stimulate phosphorylation of CREB and other growth promoting proteins, as well as the unsilencing of glutamatergic synapses (Jagasia et al., 2009; Chancey et al., 2013).

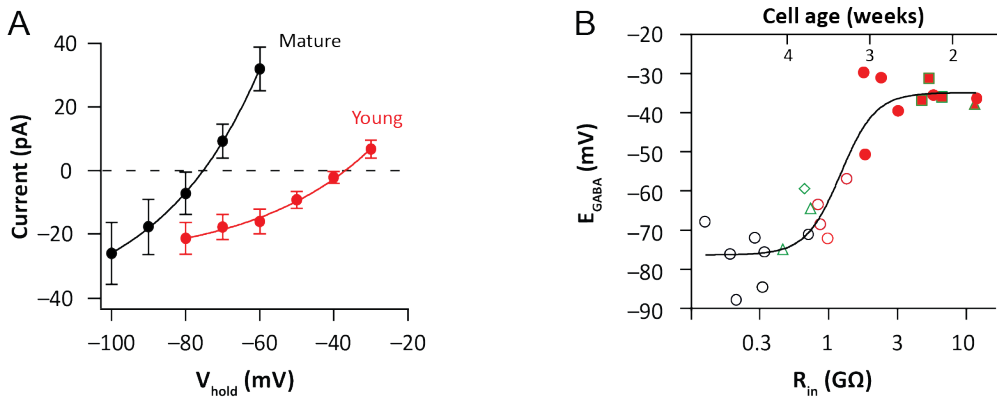

Figure 5. GABA-reversal of young granule cells is more depolarized than in mature cells. Gramicidin perforated-patch recordings of GABAergic synaptic currents in young and mature granule cells. (A) The average amplitudes of GABAergic synaptic currents from young (red) and mature (black) GCs show a reversal potential of -35 mV and -80 mV, respectively (data presented as mean ± s.e.m). (B) E_{GABA} in individual granule cells was plotted against input resistance (R_{in}) for DCX-DsRed+ young (red), GFP virus–labeled (green symbols) and mature GCs (black circles). Adapted from Heigele et al., (2016).

Does a depolarized reversal potential of -35 mV mean that GABA is always excitatory? An important factor in this context is the AP threshold. If E_{GABA} is above the AP threshold, excitation is expected to be the predominant outcome. In the case that E_{GABA} is below the threshold, but more depolarized than the resting potential, GABA is expected to generate depolarizing shunting inhibition. In contrast to hyperpolarizing inhibition, shunting inhibition is silent without glutamatergic excitatory synaptic inputs. But when combined with glutamatergic EPSPs, AP initiation is blocked by short circuiting depolarization beyond E_{GABA}.

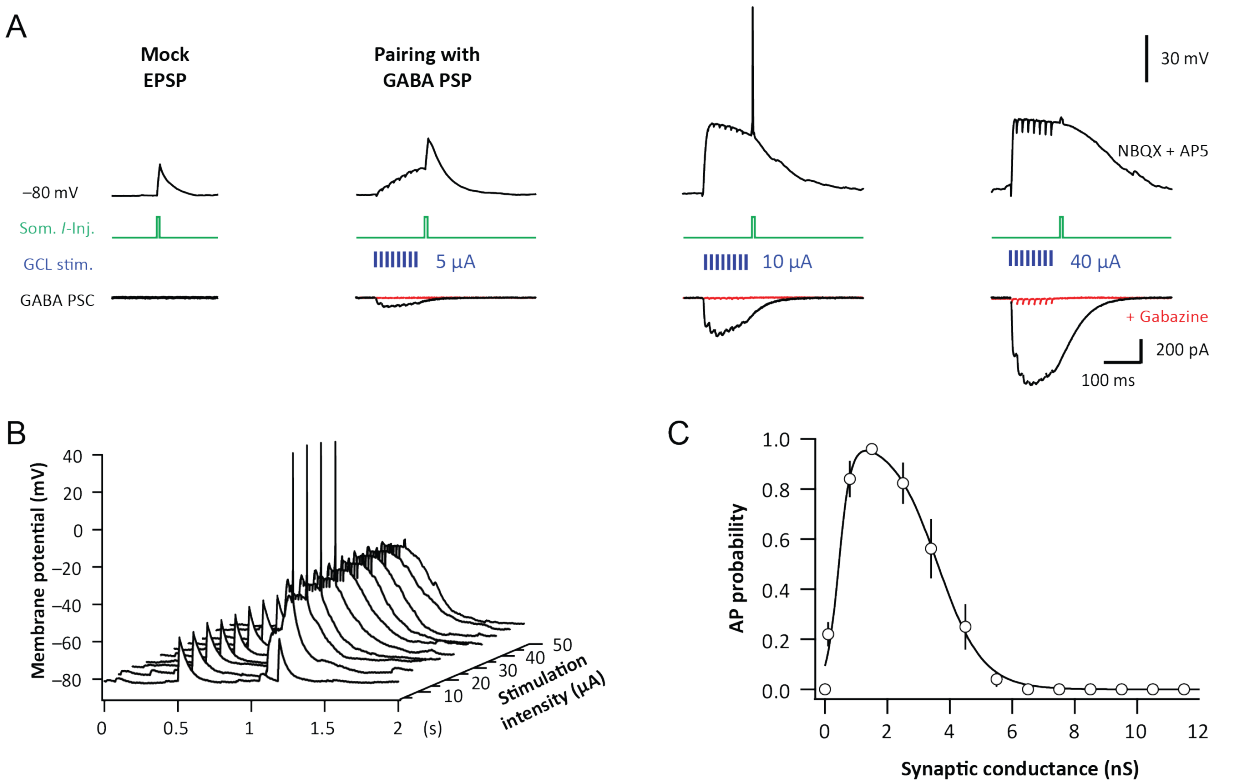

Figure 6. GABA-induced excitation and inhibition of AP firing in young granule cells. (A) Mock EPSPs were generated by a somatic current injection (10ms, green) and paired with GABAergic postsynaptic potentials (PSPs) evoked by stimulation pulses of increasing intensity (200 µs, eight times at 50 Hz) in the presence of NBQX and AP5 (upper traces). Lower traces show GABA PSCs using the same stimulation intensity before (black) and after application of gabazine (red). (B) A sequence of traces showing pairing with increasing synaptic stimulation intensity, as indicated on the right axis. Spiking is restricted to low stimulation intensities. (C) Firing probability is plotted against the GABA PSC conductance, showing that firing could only be evoked in a certain conductance range (0.4-4 nS). Continuous line represents a fitted curve consisting of the product of a sigmoidal rise and decay. Data are presented as mean ± s.e.m. From Heigele et al., (2016).

In young GCs before 3 wpm it turned out that E_{GABA} is sitting pretty much exactly at the AP threshold (-35 mV) (Heigele et al., 2016). This has important consequences. When only about 10% of connected presynaptic GABAergic interneurons (3-4 cells) fire a brief burst of APs, an average synaptic conductance of about 1.5 nS is generated in a typical 2-3 week old cell. This conductance was indeed shown to facilitate the generation of APs in young GCs (Fig. 6A, adapted from Heigele et al., 2016). However, a larger number of active GABAergic synapses (>30% of available connections) was shown to inhibit firing via shunting inhibition of AP initiation (Fig. 6B-C) (Heigele et al., 2016). This large GABAergic conductance promotes rapid depolarization towards E_{GABA}, but at the same time prevents further depolarization beyond this point. Thereby, AP initiation in young GCs can be powerfully controlled by the number of active GABA interneurons.

At 4 weeks post mitosis, E_{GABA} becomes very similar to mature GCs sitting close to the resting potential of about -80 mV (Fig. 5B) (Marín-Burgin et al., 2012; Heigele et al., 2016). Nevertheless, GABAergic synapses are still not fully mature at this stage. As pointed out by Alejandro Schinder and colleagues, a prominent feature at this developmental stage still is the slower time course of perisomatic inhibition mediated by PV interneurons relative to mature GCs (Marín-Burgin et al., 2012). Although local stimulation of perforant path (PP) fibers in the molecular layer can generate a ratio of GABAergic and glutamatergic peak conductance in young GCs similar to mature cells, the slower rise time of inhibitory currents provides a window of spiking opportunity. While inputs from soma-targeting PV INs onto yGCs have been studied, the presence of dendritic inhibition from the other main subtype- SOM-INs- has remained largely uninvestigated. Additionally, the slow time course of the kinetics may point to different post synaptic GABAR composition in young cells than in mature, however, the $GABA_A$ receptor subtypes present in the synapses of young GCs is unknown.

2.10 The aims of this study

What remains unclear in the neurogenesis field is the precise mechanisms that underlie the bidirectionality of the GABA transmission present in these developing neurons, which is key to maintaining low levels of firing. Given that GABA plays such a crucial role in the growth and maturation of adult-born neurons, we wanted to investigate the specific properties of GABAergic transmission that mediates the fine balance between excitatory promotion of activity and inhibitory control onto these cells by addressing the following questions:

Firstly, which interneuron subpopulations form somatic and dendritic inhibitory GABAergic synapses onto young granule cells?

Secondly, which postsynaptic GABA receptors are present in the inhibitory synapses of young cell?

And thirdly, what are the functional properties of the postsynaptic $GABA_A$Rs present on young granule cells? Do they have any voltage-dependence and how are they involved in shunting inhibition?

In the present study, whole-cell patch-clamp recordings were used to address these questions in newborn hippocampal granule cells of the adult mouse brain.

3. Methods

3.1 Mouse lines

Electrical stimulation experiments were performed on transgenic mice of both genders, expressing the red fluorescent protein DsRed under the control of the doublecortin (DCX) promoter maintained in a C57Bl/6 background (Couillard-Despres et al., 2006). Labelling of doublecortin positive cells with a fluorescent protein allows for the visual identification of adult-born granule cells in acute brain slices. Optogenetic experiments were performed with virally injected animals (PVCre x DCX-DsRed or SOMCre x DCX-DsRed). To generate lines for viral injection homozygous PV-Cre (B6;129P2-*Pvalb*$^{tm1(Cre)Arbr}$/J) or SOM-Cre (*SST* $^{tm2.1(cre)Zjh}$/J) mice were crossed with homozygous DCX-DsRed mice (*Dcx-DsRed,* Couillard-Despres et al., 2006). All mice were obtained from The Jackson Laboratory, except for the DCX-DsRed animals which were gifted from Ludwig Aigner (PMU, Salzburg). In order to increase adult neurogenesis, mice were housed in an enriched environment for a minimum of 10 days prior to experiments. Groups of 3-6 animals were placed in large cages (595x380x200 mm, Figure 7) on a 12:12hr light/dark cycle, with running wheels, tunnels and houses. Animals had ad libitum access to food and water. All experiments were approved by the Basel Cantonal Committee on Animal Experimentation according to federal and cantonal regulations.

Figure 7. Environmentally enriched cages for increased neurogenesis. Mice were house in large cages with mouse houses, tubes and running wheels for 1-4 weeks pre-experiment.

3.2 Stereotaxic viral injections

To selectively activate synaptic inputs from GABAergic interneurons onto young granule cells, an optogenetic approach was used. Parvalbumin-positive interneurons were targeted with the PV-Cre x DCX-DsRed mouse line while Somatostatin positive interneurons were targeted with SOM-Cre x DCX-DsRed mouse line. To allow for selective excitation of these interneurons, an excitatory floxed-channelrhodopsin was expressed in the ventral dentate gyrus (AAV-EF1a-DIO-hChR2(H134R)-EYFP, UNC Vector Core). 4-5 week old mice were anaesthetized using a 4% concentration of isoflurane and maintained with continuous inhalation of isoflurane at a 2% concentration. The animal was then placed in a stereotaxic frame, and the skull levelled using bregma and lambda. A small incision was made in the skin over the skull and 0.8mm holes were drilled above the injection site. Injections were made using pulled glass micropipettes (BLAUBRAND Intramark micropipettes) and a picospritzer (version III Parker Hannifin, 2-15ms air pulses at 1Hz, between 10-20 psi). Injection co-ordinates were selected from a mouse brain atlas (Franklin and Paxinos, 2007) and optimized through a series of control injections. The following co-ordinates for the ventral dentate gyrus were used, with four injection sites along the dorsal-ventral plane: anterior-posterior= -3.2mm, medial-lateral= $\pm$3.0mm, dorsal/ventral=-4.5mm, -4.0mm, -3.5mm and -3.00mm. Silk-based sutures were used to close the wound, and animals were given rimadyl for analgesia post-surgery. Animals were placed in recovery cages with a heating pad until fully alert, then they were returned to their home cage.

3.3 Slice preparation

Experiments were performed on both male and female mice between 4-10 weeks of age (mostly 6-10 weeks). Animals were anaesthetised with isoflurane (4% in O2, Vapor, Draeger) and once sufficiently unresponsive, were killed by decapitation in accordance with national and institutional guidelines. To increase cell survival, animals were placed in an oxygen-enriched environment for a minimum of ten minutes prior to anaesthetisation. The brain was then removed in ice-cold sucrose-based solution (approximately 4°C), which was aerated with carbogen (a mixture of 95% O_2 and 5% CO_2). The brain was transferred to fresh sucrose-based solution (see 3.9), where the two hemispheres were separated with a single scalpel cut. Each hemisphere had an angled portion of dorsal cortex removed, similar to that described in Heigele et al. (2016), to produce dentate slices with healthy and intact dendrites

of the granule cells. The two hemispheres were then glued, with the cut side down, onto a small metal plate and transferred into the cutting chamber which was filled with ice-cold sucrose-based solution. Transverse 350μm thick hippocampal slices were cut with an approximate 20° angle to the dorsal surface, using a Leica VT1200 vibratome (velocity of 0.04 mm/s and a lateral vibrating amplitude of 1.8 mm). Slices were incubated at 35°C in the same sucrose-based solution for 30 minutes and then stored at room temperature until experiments were conducted.

3.4 Electrophysiology

Electrophysiological recordings of acute brain slices were conducted within 8 hours of slice preparation. Slices were placed into a bath chamber, with continuous perfusion of oxygenated artificial cerebrospinal fluid (ACSF, pH 7.4, Osmolarity 315-25 mOsm, equilibrated with 95% O_2 and 5% CO_2). Granule cells were visualised with an infrared differential interference contrast (IR-DIC) microscope (Examiner.D1, Zeiss, Oberkochen, Germany) using a 63x objective (numerical aperture 1.0, Zeiss, Oberkochen, Germany).

Voltage-clamp recordings of young and mature granule cells were conducted with patch pipettes (3-6 MΩ) pulled from borosilicate glass tubes with 2.0 mm outer diameter and 0.5 mm wall thickness (Hilgenberg, Malsfeld, Germany; Flaming-Brown P-97 puller, Sutter Instruments, Novato, USA). Intracellular solutions are described in 3.9.

Current-clamp recordings of newborn granule cells were conducted with thicker walled glass (2.00mm outer diameter, 0.7mm wall thickness) with higher resistances (6-12MΩ) and low capacitance (≈5pF). These pipettes allowed for the accurate measurement of steady-state potentials and fast voltage fluctuations. Additionally, the thicker walls of the glass allow for a tight seal (R_{seal}) with the cell membrane, reducing current loss, and shunting of the cell. This is particularly important in current clamp recordings, as low seal resistances result in a depolarized resting membrane potential, and even prevent AP firing due to the loss of inward currents generated by voltage-gated-Na^+-channels. To further increase the likelihood of large R_{seal} values, pipettes were fire-polished on a micro-forge prior to use. The average seal resistance obtained in these recordings was 25.45GΩ corresponding to 6.36 times more than the R_{in} (R_{seal} 25.45±1.28GΩ, R_{in} 4.00± 0.27 GΩ, n= 31).

Voltage and current clamp recordings were both obtained using a Multiclamp 700B amplifier (Molecular devices Devices, Palo Alto, CA, USA), filtered at 10 kHz, and digitized at 20kHz with a CED Power 1401 interface (Cambridge Electronic Design, Cambridge, UK). Bridge balance was used to compensate the series resistance (R_s) in current clamp recordings ($R_s \approx$ 10-50MΩ). In most voltage clamp recordings, series resistance was compensated with an 80% correction. All voltage-clamp experiments were performed at room temperature (22-24°C), while current clamp recordings were obtained at high temperature(30-33°C).

Data acquisition and analysis were achieved using a custom software (FPulse, U. Fröbe, Physiological Institute Freiburg) running under IGOR Pro 6.31 (WaveMetrics, Lake Oswego, Oregon) and the open source analysis software Stimfit (http://code.google.com/p/stimfit, C. Schmidt-Hieber, Institut Pasteur, Paris).

3.5 Identification of new born granule cells

Adult-born granule cells between 1 and 3-weeks of age were identified by detection of DsRed fluorescence using a cooled CCD camera system (SensiCam, TILL Photonics, now FEI Munich GmbH, Gräfelfing, Germany). Ds-Red positive cells were detected using a light source with an excitation wavelength of 555nm (Polychrome V, TILL Photonics), which was connected to the microscope using a quartz fiber optic light guide. The illumination intensity was kept low to avoid possible photo-bleaching of the neurons and subsequent phototoxicity. As DS-Red expression can continue beyond the expression of doublecortin, young cells were also identified using cell morphology, location and input resistance. Newly generated young cells are found within the inner border of the granule cell layer, with small soma, and input resistances larger than 2.0GΩ. Therefore, DCX^+ granule cells with a $R_{in} \geq$ 2.0 GΩ were classified as young. In accordance with previous publications, mature granule cells were identified as having larger soma restricted to the outer border of the GCL and a $R_{in} \leq$ 400 MΩ (Schmidt-Hieber et al., 2004; Heigele et al., 2016; Li et al., 2017). Due to the larger cell membrane size (Li et al., 2017) and expression of potassium channels (Gonzalez et al., 2018) mature granule cells have small input resistances that allow them to be reliably distinguished from yGCs. Input resistance was converted to age in days as per Heigele et al. (2016).

3.6 Synaptic stimulation

Electrical stimulation

To electrically stimulate synaptic inputs, 12-15 MΩ pipettes were filled with a HEPES-buffered sodium rich solution to apply short negative current pulses (5-40 μA, 200 μs). To stimulate axons of soma-targeting GABAergic interneurons, the stimulation pipette was placed in the outer third of the granule cell layer (GCL), with a minimal lateral distance of 100 μm from the recorded cell. To stimulate axons of dendrite-targeting GABAergic interneurons, the stimulation pipette was placed in the outer third of the molecular layer to target the outer molecular layer (OML). To isolate GABAergic inputs, all electrical stimulation recordings were done in the presence of glutamatergic AMPAR and NMDAR blockers (10μM NBQX (2,3-dioxo-6-nitro-1,2,3,4- tetrahydrobenzo[*f*]quinoxaline-7-sulfonamide and 25μM AP5 (D-(-)-2-amino-5-phosphonopentanoic acid).

For voltage-clamp recordings single stimulations were used to produce inhibitory post-synaptic currents (IPSCs) in the recorded cell. For current clamp recordings a burst stimulation paradigm was used to evoke synaptic GABA release with 3 or 8-stimuli at 50Hz.

Optogenetic stimulation

Channelrhodopsin was genetically expressed in PV-cre or SOM-cre animals to enable the selective activation of either parvalbumin-positive or somatostatin-positive GABAergic interneurons. Interneurons were activated using a diode laser with a 473nm excitation wavelength (Rapp OptoElectronic, Hamburg, Germany). The field of illumination was targeted to the granule cell layer when stimulating parvalbumin interneurons, and the hilus or outer molecular layer when targeting somatostatin positive interneurons. For paired-pulse experiments, two light pulses were used 200ms apart. For rectification experiments a single light-pulse of varying intensities was delivered to produce a post-synaptic current around 200pA in amplitude (5-20mW, 5ms) at -80mV.

3.7 Data Analysis

Analysis of patch-clamp data was performed offline using the open-source analysis software Stimfit (https://neurodroid.github.io/stimfit) and customized scripts written in Python.

Intrinsic cell properties

The intrinsic properties of recorded neurons were determined in the first initial minutes of a whole cell configuration. Once the membrane was ruptured, the input resistance was measured in voltage clamp using the current response to a negative voltage step (-5mV, 500ms pulse). All cells were clamped at -80mV. Series resistance was also determined using this negative voltage step. For IPSCs, the decay τ was the weighted average of a biexponential fit only to the decay phase of the PSC starting at 95% of its amplitude. Resting membrane potentials were measured in the I=0 mode. Action potential properties were determined in the current-clamp configuration. A step protocol (500ms, 4, 10 or 50pA) was used to elicit a single spike in both young (DCX^+) or mature neurons.

Rectification index

Normalized conductance was calculated for each experiment individually by dividing PSC amplitudes by the difference of the voltage command from the estimated reversal potential. For the visualization of the outward rectification of GABAR-mediated currents, current amplitudes were normalized by the value at –80 mV (I_{norm}). The normalized currents were fitted in GraphPad Prism6 using a sigmoidal voltage- dependent conductance:

$$I_{norm}(v) = (v - E_{rev}) \times \left(g_{min} + \frac{g_{max} - g_{min}}{1 + e^{(v_{50} - v)/Slope}}\right)$$

With v representing the membrane potential, E_{rev} the $GABA_A$ reversal potential, g_{min} and g_{max} the minimal and maximal conductance, v_{50} the membrane potential at half-maximal, voltage-dependent conductance increase, and Slope determining the steepness of the sigmoidal, which was constrained to be at least the voltage difference between two adjacent data points.

To compare the strength of the observed rectification across different experimental conditions, we calculated a rectification index (RI) that was quantified as the ratio of the conductance obtained from the linear fit to the outward currents divided by the value measured at –80 mV (1 = no deviation).

PSP analysis

Mean burst PSPs were analysed to obtain peak amplitude and integral. The analysis of burst PSPs in current-clamp recordings testing shunting inhibition was performed on single-trial data to avoid distortion by AP discharge. In cases of AP firing, APs were digitally removed by cutting off spikes at the AP threshold, defined by the voltage slope (10 Vs−1) before calculating the integral.

Statistical analysis

Statistical analysis was performed with GraphPad Prism 8. We did not rely on the assumption that our data followed a normal distribution, and thus used non parametric tests. In most instances, statistical significance of paired data, in particular normalized data relative to 100% control, was derived from the Wilcoxon matched-pairs signed-rank test. The Mann-Whitney test was used for all unpaired comparisons. A two-tailed test was used, except for current clamp pharmacology experiments where a one-tailed test was used. The significance level was set to P=0.05. All data are shown as mean ± s.e.m if not stated otherwise. The sample size was determined by the reproducibility of the experiments and based on our experience with similar experiments (Heigele et al., 2016; Li et al., 2017; Schulz et al., 2018). The number *n* of observations indicated reflects the number of cells recorded from.

3.8 Immunohistochemistry

Immunohistochemical analysis was done with 350μm horizontal slices taken during electrophysiological preparation (method detailed in 3.2 slice preparation).Slices were fixed in 4% paraformaldehyde for 90mins to maintain the integrity of the postsynaptic density. Washing was done with a step-wise protocol using a tris-buffered saline solution, and 1% triton solution. Slices were transferred to the same tris-buffered saline containing Bovine

serum albumin (BSA, 1%) for two hours to provide sufficient blocking. Incubation with a primary antibody (VGAT; 1:500, $GABA_A$ receptor α_5; 1:500 both from Synaptic Systems) in 1% BSA was done for 24-48 hours at 4°C. Subsequently, slices were rinsed with tris-buffered saline solution and incubated with the secondary antibody at room temperature for 2 hours (Alexa Fluor 488-conjugated donkey anti-rabbit Ig; 1:1000 and Alexa Fluor 568 conjugated Streptavidin from MoBiTec, Alexa Fluor 647-conjugated donkey anti-guinea pig Ig; 1:1000, from Millipore Bioscience Research Reagents, DAPI; 1:10,000 from Sigma Aldrich). After the final rinsing, slices were mounted with ProLong Gold Antifade (Invitrogen, Thermofisher, California, United States), and imaged using a Zeiss LSM700 confocal microscope (Oberkochen, Germany). Image analysis and processing was done using the Zeiss ZEN software and ImageJ freeware (https://imagej.net/).

3.9 Solutions

ACSF

For electrophysiological recordings, slices were continuously perfused with artificial cerebrospinal fluid (ACSF) containing (in mM): 125 NaCl, 25 $NaHCO_3$, 25 glucose, 2.5 KCl, 1 NaH_2PO_4, 2 $CaCl_2$, 1 $MgCl_2$ (pH 7.4, equilibrated with 95% O_2/ 5% CO_2, Osmolarity 314-325 mOsm).

Sucrose

For cutting and storage, a sucrose-based solution was used, containing (in mM): 87 NaCl, 25 $NaHCO_3$, 2.5 KCl, 1.25 NaH_2PO_4, 75 sucrose, 0.5 $CaCl_2$, 7 $MgCl_2$ and 10 glucose (equilibrated with 95% O_2/ 5% CO_2, Osmolarity 325-328 mOsm).

Internal solutions

Voltage clamp recordings for connectivity and rectification experiments of both young and mature granule cells were conducted with high chloride internal solutions to increase the amplitudes of inward currents recorded from young granule cells. A potassium-chloride based intracellular solution containing symmetrical chloride was used to give a reversal potential around 0mV (KCl140, see Table 1). To determine the physiological level of rectification in young cells, we used an internal solution with physiological levels of chloride

in order to obtain a GABA reversal potential comparable to perforated-patch measurements (Heigele et al., 2016). Additionally, we used this internal solution for all current clamp recordings to have close to physiological AP firing responses (KCl25, see Table 1). For voltage clamp recordings targeting dendritic inputs, cesium-based internal solutions were used to block dendritic potassium channels and increase resolution of dendritic currents (CsCl100 and CsCl8, see Table 1) except in Fig.4F where KCl140 was used to boost small dendritic currents onto yGCs. In some internal solutions we added 5mM QX314-Cl to block voltage-gated sodium channels and prevent action currents in voltage clamp. Low-chloride solutions were adjusted to maintain the original chloride concentration.

Internal Solution	Composition (in mM)	Osmolarity (mOsm)	pH
KCl140	140 KCl, 10 EGTA, 10 HEPEs, 2 $MgCl_2$, 2 Na_2ATP, 1 Phosphocreatine, 0.3 GTP	305-310	adjusted to 7.3 with KOH
KCl25	122 K-Gluconate, 21 KCl, 10 HEPEs, 10 EGTA, 2 $MgCl_2$, 2 Na_2ATP, 1 Phosphocreatine, 0.3 GTP	305-310	adjusted to 7.3 with KOH
CsCl100	100 CsCl, 40 Cs-gluconate, 10 HEPEs, 10 EGTA, 2 $MgCl_2$, 2 Na_2ATP, 1 Phosphocreatine, 0.3 GTP	305-310	adjusted to 7.3 with CsOH
CsCl8	135 Cs-gluconate, 2 CsCl, 10 HEPEs, 10 EGTA, 2 $MgCl_2$, 2 Na_2ATP, 2 TEACl	305-310	adjusted to 7.3 with CsOH

Table 1. Internal solution compositions.

Pharmacology

A stock solution was prepared for the drugs indicated below, which were subsequently stored at -20°C (Table 2). Working solutions were prepared as needed by dissolving the stock in ACSF to make up the correct concentration. The following drugs were abbreviated in text for simplicity: NBQX (2,3-Dioxo-6-nitro-1,2,3,4-tetrahydrobenzo[*f*]quinoxaline-7-sulfonamide), AP5 (D-(-)-2-Amino-5-phosphonopentanoic acid), CGP55462 ([*S*-(*R**,*R**)]-[3-[[1-(3,4-Dichlorophenyl)ethyl]amino]-2-hydroxypropyl](cyclohexylmethyl) phosphinic acid), NO711 (1,2,5,6-Tetrahydro-1-[2-[[(diphenylmethylene)amino]oxy]ethyl]-3-pyridinecarboxylic acid hydrochloride), QX314 (*N*-(2,6-Dimethylphenylcarbamoylmethyl)triethylammonium chloride), gabazine (6-Imino-3-(4-methoxyphenyl)-1(6*H*)-pyridazinebutanoic acid hydrobromide). All

drugs were obtained from Tocris (Essex, England), except for dextran which was obtained from Sigma-Aldrich (Steinheim, Germany) and α5-NAM RO4938581 which was obtained from F. Hoffmann-La Roche (Basel, Switzerland).

Drug	Dissolved in	Stock Solution (mM)	Working Concentration
NBQX	DMSO	20mM	10μM
AP5	Water	50mM	25μM
α5-NAM RO4938581	DMSO	10mM	1μM
CGP54626	DMSO	10mM	1μM
NO711		10mM	10μM
Dextran	ACSF	N/A	5%
QX314 (in pipette)	Internal	N/A	5mM
Gabazine (SR95531)	Water	10mM	0.2μM/10μM

Table 2. Stock and working concentrations of pharmacological agents used in electrophysiology.

4. Results

4.1 GABAergic inputs onto young granule cells are non-linear and outwardly rectifying.

Dendritic inhibition of pyramidal cells of CA1 has been shown to exhibit outwardly-rectifying properties, while basket-cell mediated somatic inhibition is more linear and voltage-independent. (Pavlov et al., 2009; Schulz et al., 2018). To examine the voltage dependence of somatic inhibition onto granule cells of the dentate, we performed whole cell voltage-clamp recordings in acute hippocampal brain slices from 5-10 week old animals. We locally stimulated the granule cell layer (GCL) to target peri-somatic inputs, with the aim of comparing newly-generated and mature granule cells. To identify newly generated young granule cells (yGCs) we used transgenic animals expressing DsRed under the control of the doublecortin promoter (Brown et al., 2003; Couillard-Despres et al., 2006), while input resistance was used to predict cell age based on Heigele et al. (2016). 2-3 week old yGCs were DsRed positive with an input resistance between 2-8GΩ, while 3-4 week old cells were also DsRed positive, but their recorded input resistance was between 500MΩ and 2GΩ. Mature cells lacked DsRed fluorescence and had an input resistance below 400MΩ. GPSCs were recorded at different holding potentials from -80mV to +60mV in the presence of glutamatergic blockers (10μM NBQX + 25μM AP5)(Fig. 8). In symmetrical chloride conditions (144mM chloride in the potassium-based pipette solution) the outward GPSCs increased linearly with holding potentials above 0mV. Similar to somatic inhibition in CA1, mature and 3-4 week old granule cells had inward GPSCs that also followed this linear behaviour at negative potentials (Fig. 8B+D). Surprisingly, 2-3 week old GCs had inward GPSCs that increasingly deviated from the linear behaviour at more negative potentials (Fig. 8F), producing large rectification at -80mV. The rectification index (RI) was quantified as the ratio of the conductance obtained from the linear fit to the outward currents above 0mV divided by the value measured at -80mV close to the resting potential. A rectification index equal to 1 indicates no deviation from the linear fit. Outward rectification was significantly larger in GABAergic synapses onto 2-3 week old granule cells (RI = 1.90±0.08, n=8), than in 3-4 week old granule cells (RI = 1.29±0.12, n=8 $P \leq 0.001$), or mature granule cells (RI = 1.14±0.08, n=8 $P \leq 0.001$) (Fig. 8G). We also recorded from yGCs with a pipette solution that mimics the

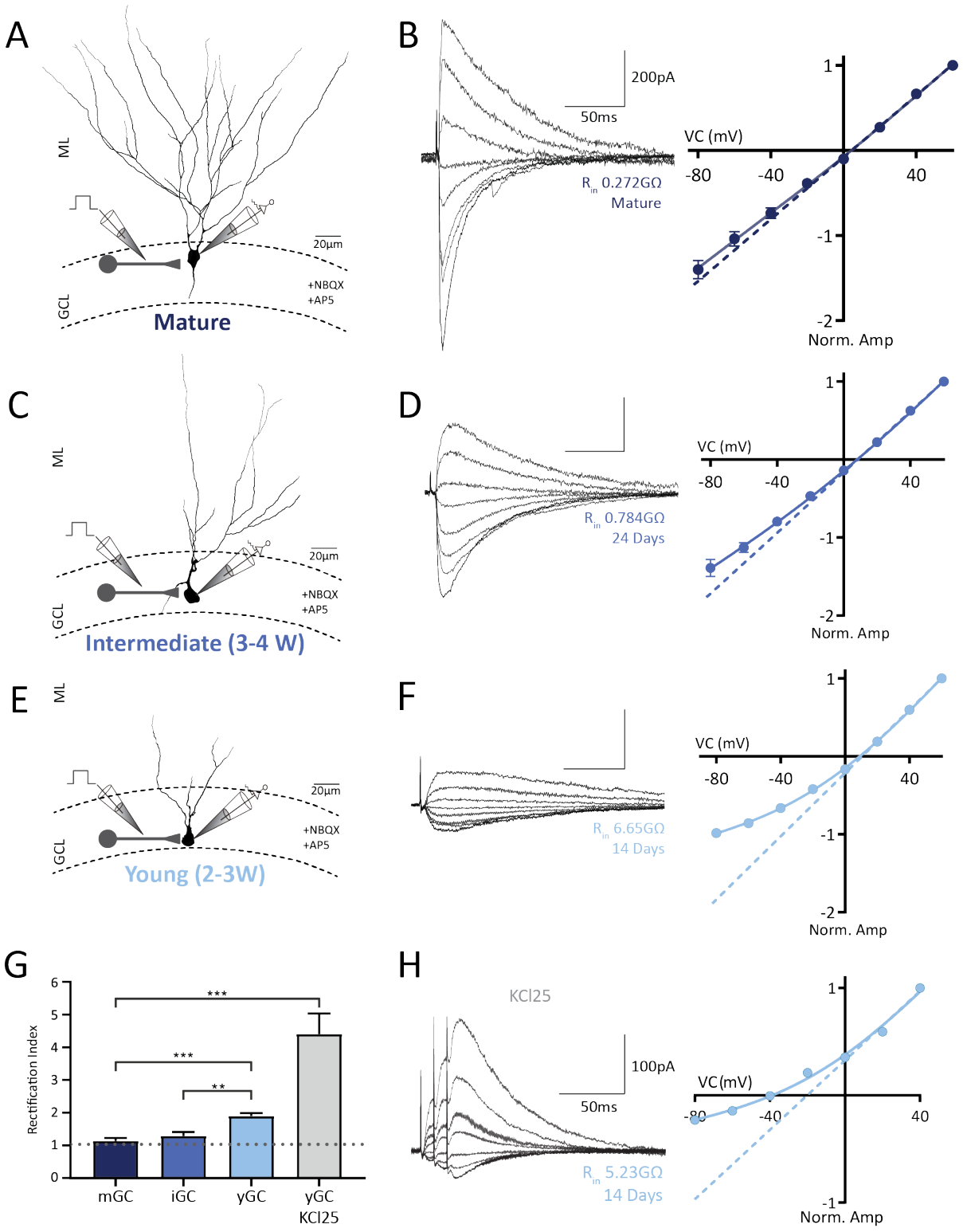

Fig. 8 Young GCs receive non-linear and outwardly rectifying GABAergic inputs. A, C+ E) Experimental design. Electrical stimulation of the GCL was used to target somatic inputs onto mature, intermediate and young granule cells (GCs) (5-20µA). Cells were classified based on the measured input resistance. Mature cells were defined as having an input resistance less than 400MΩ, intermediate cells had an input resistance between 500MΩ and 2GΩ corresponding to 3-4 weeks of age, and young GCs with input resistances between 2 and 8 GΩ, corresponding to 2-3 weeks of age. All young cells recorded were also DCX-DsRed positive. B) IPSCs from mature GCs were recorded at increasing membrane potentials (-80mV to +60mV) in symmetrical chloride conditions. The dashed line represents a linear fit to the outward current (+20 to +60mV), while the solid line

represents a non-linear fit obtained with the equation outlined in methods. Recordings were done in the presence 10 µM NBQX and 25 µM AP5. The corresponding current vs. voltage plot of the normalized amplitude is shown, with a linear line fitted to the outward IPSCs. D+F) as in B, but for intermediate and young GCs respectively. The current vs. voltage plot of young GCs clearly shows the non-linearity of the recorded IPSCs. G) Mean rectification indices (RI) were quantified as the expected conductance extrapolated from the linear fit to the outward currents (above 0mV) divided by the measured value at -80mV (where 1= no deviation, indicated by grey dashed line). The mean RI was significantly larger in young GCS than in mature in both symmetrical and physiological chloride (KCl25). H) IPSCs and current vs. voltage plot of yGCs recorded using an internal solution with physiological chloride (KCl25). A brief burst of 3 pulses (50Hz) was used to produce a larger inward current at -80mV. (Significance indicated in figure as *: P>0.05, **: P> 0.01, *** P>0.001).

physiological chloride concentration in young cells of 25mM (Heigele et al., 2016) and recorded GPSCs at different membrane potentials from -80 to +40mV. Under these conditions young cells showed even higher rectification, with a four-fold larger outward synaptic conductance than at resting-potential (RI=4.40±0.6, *n*=6)(Fig. 8G+H). These data show that electrical stimulation of GABA synapses at mature GC somata is very similar to somatic inhibition in CA1 pyramidal cells. In contrast, the voltage-dependence of GABAergic inhibition of young GCs is more similar to dendritic inhibition in CA1.

4.2 SOM- and PV-interneurons activate rectifying GABARs in young GCs.

Electrical stimulation potentially recruits a mixed population of presynaptic GABAergic fibers. To more selectively target identified populations of interneurons we used optogenetics. To characterize the connectivity between yGCs and the two major classes of soma-targeting and dendrite-targeting INs, we used a virus to express channelrhodopsin-2 (ChR2) in PV or SOM interneurons (see Fig 10A-B). To do so, PV-cre and SOM-cre mouse lines were crossed with the DCX-DsRed line and injected with a floxed-ChR2 virus. This allowed for both the selective expression of ChR2 in each interneuron subtype, and the visualization of newborn granule cells between one and four weeks of age. For soma-targeting PV inputs we utilized a potassium-based pipette solution, while analysis of dendritic inputs was performed using a cesium-based solution to block dendritic potassium channels and to increase the resolution of the recorded GPSCs. Both pipette solutions contained a high concentration of chloride to obtain symmetrical chloride conditions. To examine the voltage-dependence of soma- and dendrite-targeting interneurons similar to those seen in Schulz et al. (2018), we again recorded GPSCs at different holding potentials (from -80 to +60mV) in response to ChR2 light activation. Similar to what was found in CA1, somatic GABAergic inputs onto mGCs from PV-INs are linear (Fig. 9B), showing no rectifying properties. However, PV inputs onto young

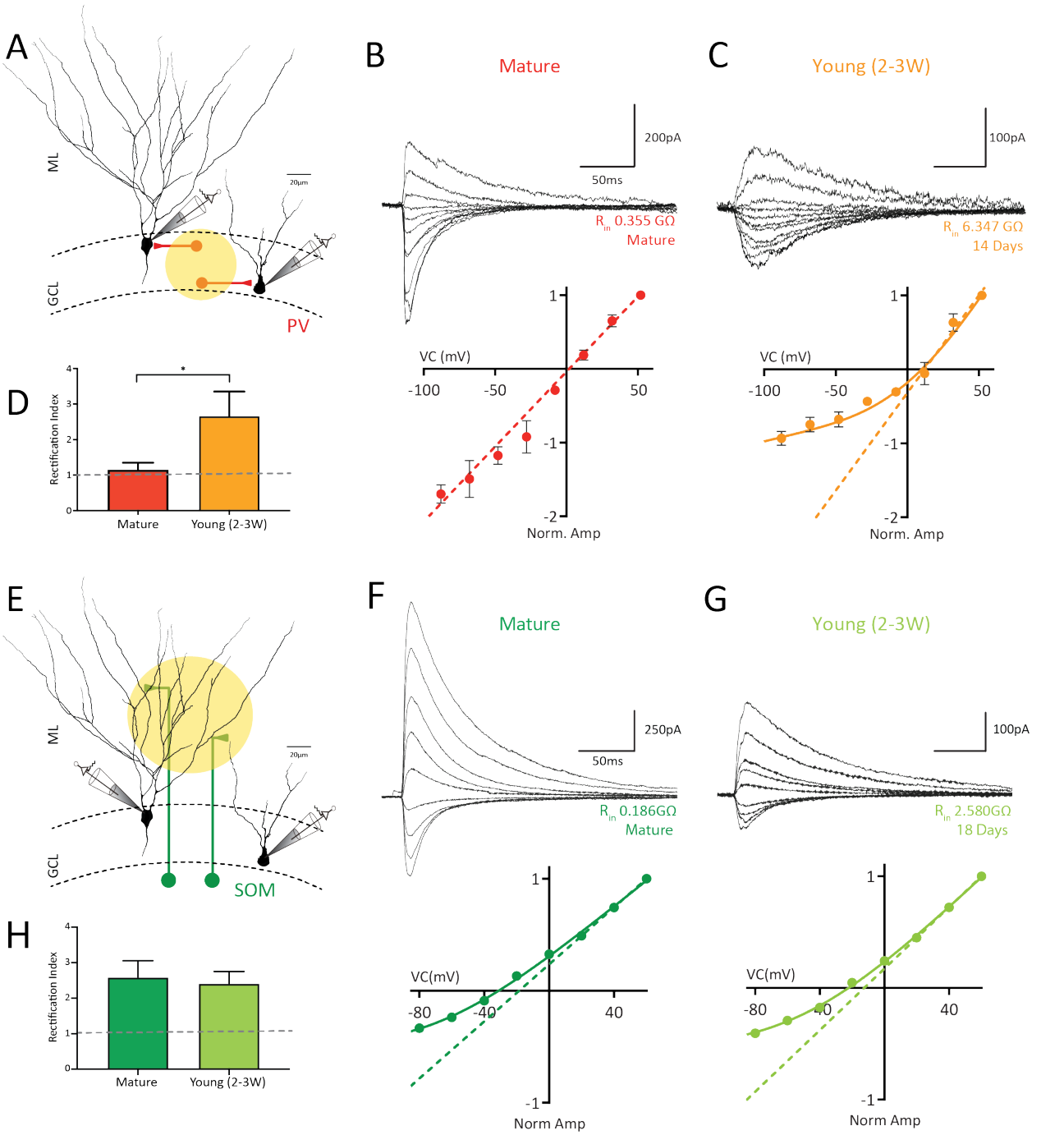

Fig. 9 Presynaptic interneuron subtype does not alter post-synaptic rectification in yGCs. A) Experimental design. PVcre x DCX-DsRed mice were injected with a floxed-ChR2 in the vDG. Optogenetic stimulation of the GCL was used to excite somatic inputs onto mature and young granule cells. Young granule cells were identified by the presence red fluorescence as well as their measured input resistance. B-C) GPSCs were recorded from mature (B) and young (C) GCs at increasing membrane potentials (-80mV to +60mV) in symmetrical chloride conditions. The corresponding normalised current vs. voltage plots show that mature GCs follow a linear transmission, while PV inputs onto young GCs are highly rectifying. D) The mean rectification index of PV inputs was significantly higher in yGCs than mature. E) Experimental design for SOMcre x DCX-DsRed mice injected with floxed ChR2 in the vDG. Optogenetic stimulation of the molecular layer (ML) was used to target dendritic inputs onto mature and young GCs. F-G) GPSCs were recorded from mature (F) and young (G) GCs. Normalised voltage vs. current plots show that inputs from SOM INs onto both mGCs and yGCs are non-linear. H) The mean rectification index of SOM inputs was not significantly different between mature and young GCs.

GCs are highly non-linear (Fig. 9C), comparable to electrical stimulation in the GCL (Fig. 8F). The rectification index was significantly different between mature and young granule cells (mGCs RI = 1.15±0.2, *n*=7, yGC RI=2.66±0.68, *n*=4 *P* =0.012)(Fig. 9D). These results show that PV-basket cells of the DG activate different postsynaptic GABA receptors in young vs mature granule cells.

Dendrite-targeting synapses from SOM-INs were found to be highly non-linear in mature GCs, consistent with what was described in CA1 pyramidal cells (Schulz et al., 2018)(Fig. 9F). Dendritic inputs onto young GCs were also non-linear (Fig. 9G) showing no significant difference to the rectification index found in mature GCs (mGCs RI = 2.585±0.47, *n*=8, yGC RI=2.409±0.343, *n*=9 *P*=0.89)(Fig. 9H). Interestingly, the rectification index from PV- and SOM-IN inputs onto young cells is very similar, suggesting that postsynaptic GABAR composition in young granule cells maybe homogenous across the cell body and dendritic tree. In mature cells however, the differences in rectification suggests that postsynaptic receptor composition is different in dendritic vs somatic synapses.

4.3 Inputs onto yGCs from SOM- and PV-interneurons have slow kinetics

To investigate kinetic properties of SOM or PV inputs onto young GCs and mature GCs, we again used viral ChR2 expression in PVcre x DCX-DsRed or SOM-cre x DCX-DsRed. Viral expression was restricted to each interneuron subtype, with GFP-positive PV basket-cell bodies and axons in the granule cell layer (Fig. 10A), while GFP-positive SOM INs had their cell bodies in the hilus, and axons terminating in the outer molecular layer (Fig. 10B). As reported by Alvarez et al. (2016), PV inputs onto young GCs show significantly slower rise times and decays than mature GCs. However, it remains unclear if this also applies to SOM inputs. Therefore, we looked at the rise and decay time course of optogenetically evoked GPSCs at -80mV from both PV and SOM INs. Similar to what was already described, inputs from PV-INs had significantly faster rise times in mature GCs than young GCs (mature 1.55± 0.4ms, *n*=7; young 4.36± 0.89ms, *n*=8 *P* =0.029)(Fig. 10C+E). Decay τ was calculated by fitting a monoexponential curve for mGCs, and a biexponential curve for yGCs. Perisomatic GPSCs onto young granule cells showed a prolonged decay (mature 20.7± 0.6ms; young 52.0± 3.7ms, *P* =0.001)(Fig. 10F). However, dendritic inputs from SOM-INs did not show

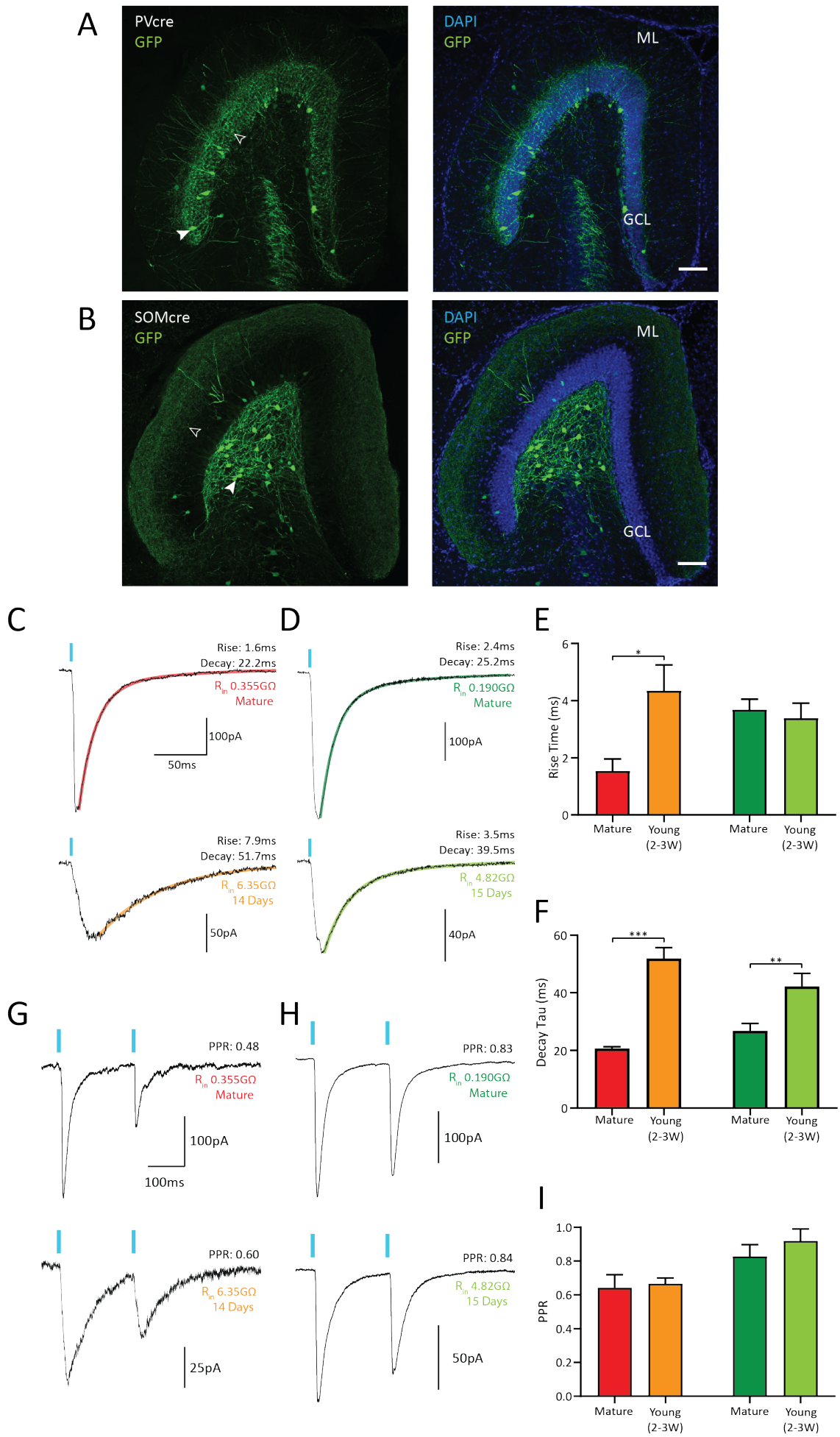

Fig. 10 Kinetics properties of GPSCs onto young GCs are different to those onto mature GCs.

any difference in rise time course between young and mature GCs (mature 3.70± 0.36ms, *n*=8; young 3.40± 0.51ms, *n*=9 *P* =0.61)(Fig. 10D+E), while the decay τ was significantly different (mature 26.79± 4.6ms, *n*=7; young 42.2± 4.6ms, *P* =0.006)(Fig. 10F). This large decrease in rise time with maturation in perisomatic connections suggests that 2-3 week old GCs have relatively immature synapses. Additionally, the difference in decay kinetics in young and mature GCs suggests that postsynaptic receptor composition may be different, with yGCs having a higher contribution from GABARs with slow kinetic profiles.

We additionally sought to examine whether dendritic or perisomatic presynaptic terminals were different between young and mature GCs. For this we utilized paired ChR2 pulses delivered with a 200ms interval. When comparing the second pulse with the first, we found that all granule cells displayed depression of the second pulse, irrespective of the presynaptic interneuron (Fig. 10G+H). However, the level of depression was different between PV and SOM INs. Inputs from PV-basket cells showed large depression, with the second pulse reduced to 64% of the first. Interestingly, this effect was consistent between young and mature GCs (mature 0.64± 0.07; young 0.67± 0.03, *P* =0.66). SOM inputs however, showed much less reduction of the second pulse, and again this was very similar between young and mature GCs (mature 0.83± 0.07; young 0.92± 0.07, *P* =0.28)(Fig. 10I). This is turn indicates that the presynaptic release-probability of dendritic and peri-somatic inputs onto yGCs is not dependent on postsynaptic cell age but determined by the fully mature presynaptic interneurons.

Fig. 10 Kinetics properties of GPSCs onto young GCs are different to those onto mature GCs. A) Confocal image of the viral expression of floxed-GFP in the vDG of PVcre animals. GFP^{+ve} PV cell bodies are present in the GCL (one cell body indicated with filled arrowhead). Consistent with basket cell morphologies GFP^{+ve} axons terminate in the GCL (indicated with the arrow outline). Right image includes merge with DAPI, note the densely packed GCL. Scale bar 100μm . B) Viral injection of floxed-GFP into the vDG of SOMcre animals shows selective expression of GFP in cell bodies located in the hilus. Axon terminals are present in the outer molecular layer, allowing synapse formation onto the dendrites of granule cells. Scale bar 100μm. C) Optogenetically evoked GPSCs from PV-INs recorded at -80mV in mature (top) and young (bottom) granule cells. 20-80% rise time was measured for each cell, and the decay τ was calculated using a mono- or bi-exponential fit (young and mature cells respectively). D) Example traces of optogenetically evoked GPSCs from SOM-INs. E) Rise time was significantly slower in GPSCs onto yGCs from PV-INs, while there was no difference in GPSCs from SOM. F) Decay τ was prolonged in yGCs. G) Example paired-pulse GPSCs in mature (top) and young (bottom) using optogenetic stimulation of PV-INs. Two 5ms light pulses were delivered 200ms apart to test for short-term plasticity. H) same as in F) but with optogenetic activation of SOM-INs. I) Mean PPR for perisomatic and dendritic inputs were not significantly different in mature vs. young granule cells.

4.4 α_5-containing $GABA_A$Rs mediate synaptic inhibition onto adult-born granule cells.

So far, we have found that the time course and voltage dependence of postsynaptic $GABA_A$-Rs in yGCs is very different from receptors in mGCs. This strongly suggests that the postsynaptic receptor composition may be different. α5-containing $GABA_A$Rs have been shown to be present in both CA1 and the dentate gyrus (Collinson et al., 2002; Zarnowska et al., 2009; Vargas-Caballero et al., 2010; Engin et al., 2015) , however the precise location of these receptors (within the synapse or the extra-synaptic membrane) has remained controversial (Farrant and Nusser, 2005; Serwanski et al., 2006; Capogna and Pearce, 2011; Hausrat et al., 2015). The recent study by Schulz et al. (2018) showed that α_5-containing $GABA_A$Rs mediate synaptic inhibition onto apical dendrites of pyramidal cells of CA1, which also displayed strong outward rectification.

To test the contribution of α_5-$GABA_A$Rs we used RO4938581, a highly selective negative allosteric modulator (α_5-NAM, 1μM)(Ballard et al., 2009). Electrical stimulation in the granule cell layer or outer molecular layer (ML) were used to target perisomatic or dendritic inputs respectively in the presence of NBQX and APV. Fast PSCs from GCL stimulation in mature GCs showed no significant change in amplitude with the application of α_5-NAM (to 100.6 ± 4.6%, *n*=4 *P* =0.88)(Fig. 11A+C), while in contrast stimulation of dendritic inputs produced a significant decrease (to 80.4 ± 2.7%, *n*=9 *P* =0.004)(Fig. 11B+C). Similarly, the decay τ for soma-targeting GABAergic inputs were not changed with α_5-NAM application (58.86 ± 5.42ms to 52.01 ± 6.855ms, *P* =0.063), while the decay of dendritic inputs was significantly decreased (69.42 ± 4.35ms to 57.63 ± 3.30ms, *P* =0.004)(Fig. 11D). This suggests that α_5-$GABA_A$Rs are selectively targeted to dendritic synapses in mature cells.

In 2-3 week old GCs both somatic and dendritic inputs were reduced with α_5-NAM application. PSC amplitudes from GCL stimulation decreased to 76.3% ± 2.7%, of control (*n*=6 *P* =0.031)(Fig. 11E+G), while the decay τ was also significantly reduced (157.2 ± 16.03ms to 137.4 ± 13.95ms, *P* =0.016)(Fig. 11H). Similarly, PSC amplitudes from OML stimulation decreased to 70.2% ± 2.7% of control (*n*=6 *P* =0.031), with a reduction in decay τ from 173.4 ± 14.15ms to 129.4 ± 11.96ms (*P* =0.031)(Fig. 11H). The comparable effect of α_5-NAM on both perisomatic and dendritic inputs in yGCs indicates that GABAR distribution

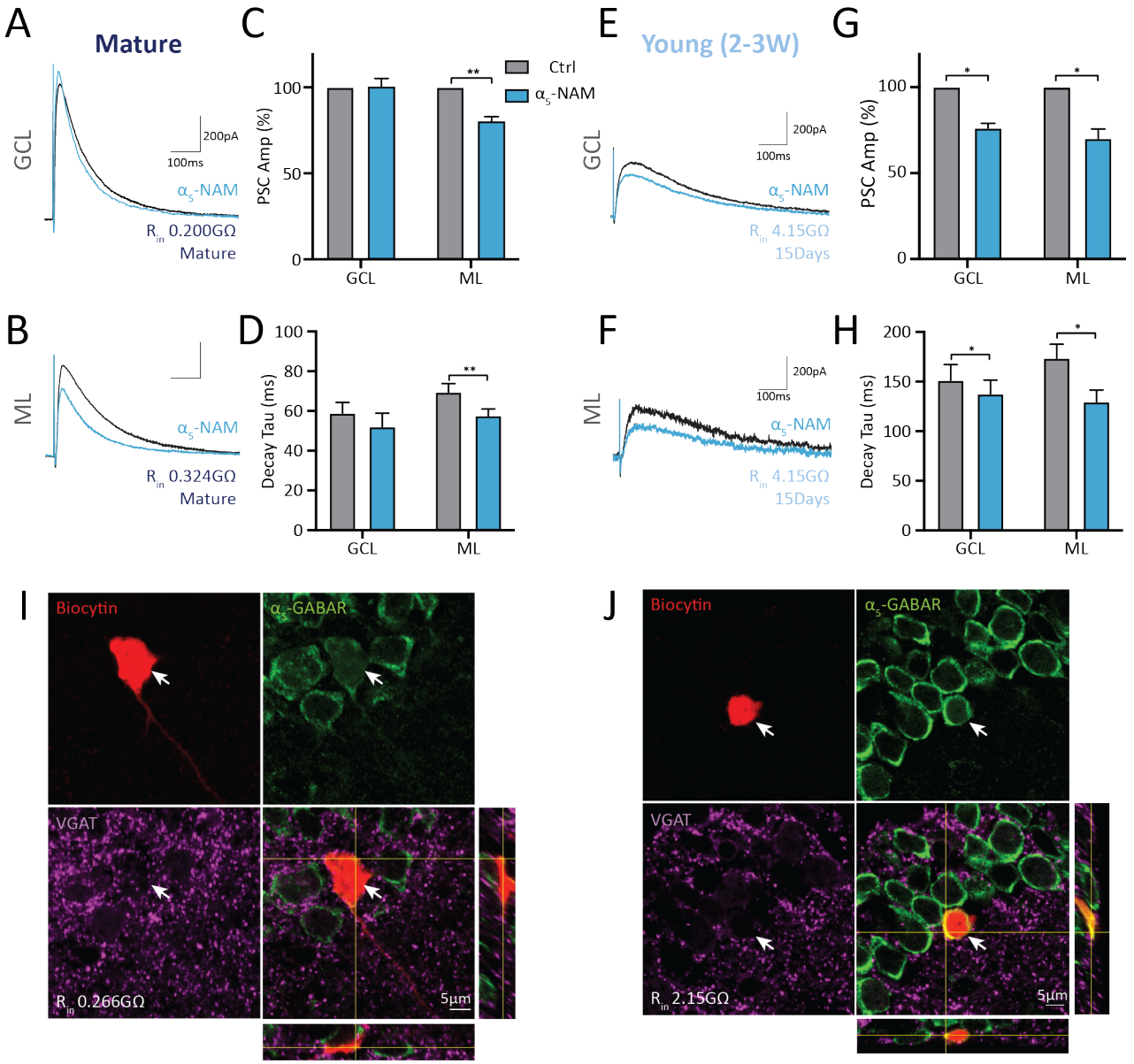

Fig. 11 α5-GABA$_A$Rs mediate dendritic and somatic Inhibition onto adult-born granule cells. A-B) Electrical stimulation of the GCL or ML was used to target somatic or dendritic inputs onto mature GCs respectively. IPSCs were recorded at +60 mV in the presence of 10 µM NBQX and 25 µM APV using a CsCl-based pipette solution. Representative mean IPSCs before and after addition of the α5-NAM RO4938581 (1 µM, blue) show that dendritically evoked IPSCs were reduced, but not somatic (C). D) α5-NAM reduced the decay in dendritic IPSCs. E-F) Representative mean IPSCs recorded from young GCs in a potassium-chloride-based pipette solution. Application of the α5-NAM (blue) show that both dendritic and somatic inputs onto young GCs are modulated by α5-containing GABA$_A$Rs. G-H) Both normalised PSP amplitudes and decay were significantly decreased in young GCs. I) Example of immunohistochemically labelled α5-GABA$_A$Rs (green) and VGAT puncta (magenta) on a biocytin-filled (red) mature granule cell (0.266GΩ). J) The same labelling as in I) on a 2-week-old young granule cell (2.15GΩ).

may be homogeneous across the cell membrane, whereas in mature cells there is a clear distinction between dendritic (containing α_5-$GABA_A$Rs) and somatic (lacking α_5-$GABA_A$Rs) synapses. Additionally, although RO4938581 is very selective for α_5-containing $GABA_A$Rs, the maximal efficiency is only about 50% (Ballard et al., 2009). Thus, the contribution of these receptors is approximately two times as large, suggesting that around 50% or the GPSCs in 2-3 week old GCs is generated by GABA receptors that contain α_5-subunits. Similarly, in dendritic synapses of mature GCs, approximately 40% of the inhibitory PSC is mediated by α_5-$GABA_A$Rs.

Biocytin filling and immunohistochemical staining of mature and young granule cells was used to test for the presence of the α_5-GABAR combined with a marker for GABAergic presynaptic terminals, VGAT. Mature GCs did not have strong α_5-labelling in the soma, consistent with the pharmacological data in A, however VGAT puncta were present around the cell body and proximal dendrite (*n*=4)(Fig. 11I). In contrast, young GCs had robust α_5-GABAR labelling throughout the soma, as well as surrounding VGAT (*n*=5)(Fig. 11J). Taken together, these results suggest that granule cells within the dentate utilize high-affinity α_5-containing $GABA_A$Rs, with mature cells selectively expressing them in dendritic synapses, while yGCs show a homogenous distribution across both dendritic and somatic synapses.

4.5 Increasing spillover of GABA to the extrasynaptic membrane increases rectification in mGCs.

α_5-$GABA_A$Rs are traditionally considered to be extrasynaptic receptors. However Schulz et al., (2018) not only showed that they are present in dendritic synapses but also that they have a non-linear voltage-dependence. As rectification was not present in somatic synapses onto mGCs, we sought to test whether enhancing extrasynaptic receptor activation could increase the non-linearity of GABA transmission at these synapses. In order to increase GABA spillover, we compared the effect of the GAT1 transporter inhibitor NO711 (1μM) on peri-somatic inputs of both mature and 2-3 week old granule cells. By blocking GABA re-uptake through the GAT1 transporter we increased GABA overflow into the extrasynaptic space. Additionally, we blocked presynaptic $GABA_B$ receptors using CGP54626 (1μM) to prevent changes in GABA release. Local stimulation of the GCL was used in order to target peri-

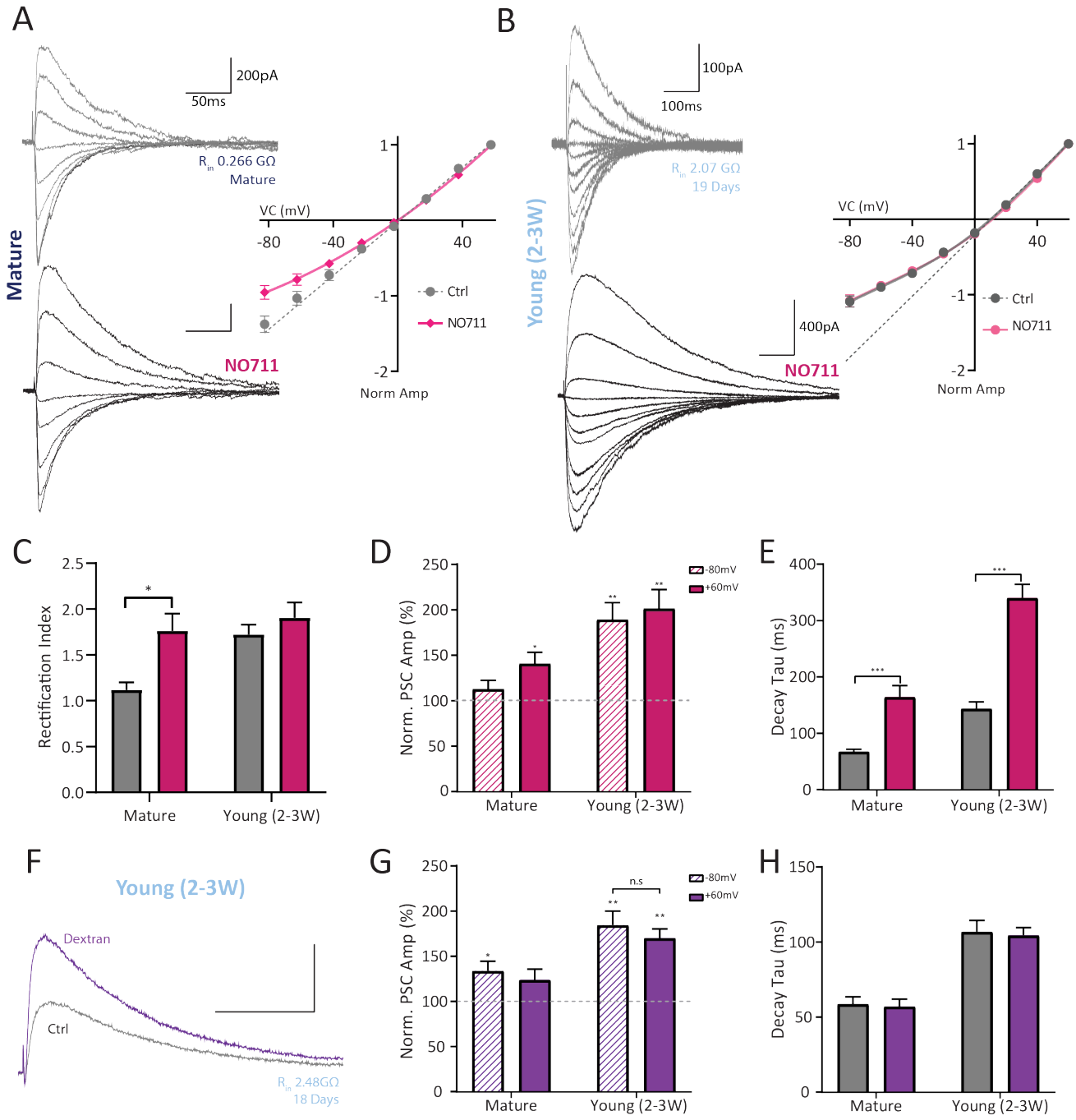

Fig. 12 Increasing peri-synaptic receptor activation increases rectification in mature GCs. A) Electrical stimulation of the GCL was used to target somatic GABAergic inputs onto mature GCS (with 1μM CGP545626, 10μM NBQX, 25μM APV). The GABA reuptake transport blocker NO711 (1μM) was used to increase peri- and extra-synaptic receptor activation (top, control in grey, bottom NO711 in black). IPSCs were recorded at increasing membrane potentials (-80mV to +60mV) in symmetrical chloride conditions. Outward IPSCs in mature cells showed greater increases in amplitude. The corresponding current vs. voltage plot shows the normalised amplitudes in control (grey) and post NO711 (maroon) application, with a linear line fitted to the outwards IPSCs, and a non-linear fit to the post-NO711 data. B) IPSCs from young GCs showed a large increase in amplitude of both inward and outward currents, producing similar rectification post-NO711 application. C) The rectification index of mature GCs significantly increases with more spill over and extrasynaptic receptor activation, while in young GCs this remains the same. D) The outward PSCs of mature GCs increased significantly with NO711 application, while the inward current remained unchanged. In yGCs, both outward and inward currents were significantly increased. E) The decay τ of both mature and young GCs

were significantly increased. F) 5% dextran was used to confirm synaptic transmission in yGCs. Example traces of IPSCs recorded at +60mV show a large increase in amplitude and similar decay τ with dextran wash-in. G) Young GCs showed a significant increase in the normalised amplitude with dextran application but showed no significant increase in decay (H), suggesting that young cells do receive synaptic inputs but that post-synaptic GABA receptors are not saturated.

somatic inputs, and GPSCs were recorded at different holding potentials (from -80 to +60mV)(Fig. 12A+B). Interestingly, mature granule cells showed a smaller increase in amplitudes of inward currents compared to outward currents (inward current to 111.2± 11.25%, *n*= 13 *P* =0.41, outward current to 139.3± 13.94%, *P* =0.033)(Fig. 12A+D). When plotted against each holding potential the GPSC peak amplitudes at negative potentials also deviated from the linear fit, producing strong rectification after NO711 application.

Conversely, 2-3 week old GCs showed a uniform increase in amplitude across the different holding potentials (inward current to 188.0± 19.85%, *n*= 11 *P* =0.002, outward current to 199.9± 22.29%, *P* =0.002)(Fig. 12B+D). Decay τ was significantly prolonged in both mature and young GCs, consistent with the block of GABA reuptake (Fig. 12E). The rectification index was increased in mature granule cells (from 1.12± 0.08 to 1.76± 0.18, *n*= 8 *P* =0.016) (Fig. 12C) pointing to the role of extra- or peri-synaptic $GABA_A$ receptors in producing rectification- similar to that seen by Pavlov et al. (2009). The rectification index in young GCs remained unchanged with the application of NO711 (from 1.725± 0.10 to 1.90± 0.16, *P* =0.25). Interestingly, the rectification index of mature GCs post NO711 application was not significantly different to that seen in young GCs (1.76± 0.18 vs 1.90± 0.16, *n*= 8 *P*= 0.57). Thus, with NO711 application and increased extrasynaptic $GABA_A$Rs activation we were able to make mature perisomatic synapses behave similarly to newborn GCs, with increased outward rectification and slower decay. Additionally, the stability of the rectification index in young cells with increased spillover further confirms that yGCs may have homogeneous receptor distribution between the synapse and peri- or extrasynaptic space.

As rectification in yGCs was not changed with NO711, we sought to confirm the presence of true synaptic transmission and to ensure that GABAergic signalling onto young GCs is not mediated by spillover. To slow-down diffusion of GABA out of the synaptic cleft we used dextran- a branched molecule with high molecular weight- in order to increase the viscosity of the extracellular space (Nielsen et al., 2004; Markwardt et al., 2009). This

effectively blocks spillover transmission from the synapse while enhancing the synaptic concentration of neurotransmitter. The decreased mobility of GABA and thus higher concentration within the synaptic cleft increases the occupation and activation of both pre- and postsynaptic receptors. In order to prevent changes in GABA release we blocked presynaptic $GABA_B$ receptors using CGP54626 (1μM). If newborn granule cells would only receive GABAergic inputs from spill-over of neighbouring mature synapses we would expect to see a decrease in GPSC amplitude with dextran application. In contrast, if yGCs do receive synaptic inputs, we would expect the amplitudes to remain the same or increase with dextran.

In mature granule cells, the wash-in of dextran significantly increased the amplitude of the inward current (-80mV)(133.8± 10.69%, *n*= 9 *P* =0.014). Similarly, the outward current was increased, although this was not significant (to 124.0 ± 11.73%, *P* =0.6) (Fig. 12G). This is consistent with a higher concentration of GABA within the synaptic cleft due to reduced diffusion. There was no effect on decay τ in mGCs (Fig. 12H). Likewise, young granule cells showed a significant increase in IPSC amplitude from baseline (inward current to 184.6 ± 15.32%, *n*= 9 *P* =0.004, outward current to 170.2 ± 10.07%, *P* =0.004)(Fig. 12F+G), again with no increase in decay τ (Fig. 12H). This increase in amplitude confirms that yGCs do indeed receive synaptic inputs, and not spillover from neighbouring synapses. Furthermore, the large increase in amplitude in 2-3 week old GCs suggests that GABA receptors are far from saturation. With the application of dextran and resulting increase of GABA concentration within the synaptic cleft, postsynaptic receptors have a higher occupancy. Additionally, the stability of the rise time after dextran application (+60mv, mGCs 2.07±0.54ms to 2.01±0.51ms, *n*=9 *P* =0.84; yGCs 5.97±0.53 to 5.46±0.32, *P* =0.20) further suggests that inputs onto yGCs are synaptic. In case all GPSCs would be mediated by extrasynaptic $GABA_A$Rs, we would see a pronounced increase in rise time with dextran application. Finally, as dextran application increased both inward and outward currents equally (inward to 184.6 ± 15.32%, outward to 170.2 ± 10.07%, *n*= 9 *P* =0.30)(Fig. 12G), there was no change in rectification. Thus, voltage-dependent non-linear $GABA_A$Rs are present synaptically in soma-targeting synapses of young granule cells.

4.6 α_5-GABA$_A$Rs promote NMDAR-mediated excitation.

What is the functional role of synaptic α_5-GABA$_A$Rs in adult-born granule cells? As synaptic α_5-GABA$_A$Rs have slow kinetics similar to that of NMDA receptors, we wanted to know if the slow GABAergic depolarisation mediated by these receptors helps to facilitate NMDAR activation in yGCs. To test whether α_5-GABA$_A$Rs modulate NMDA receptor activation, we performed whole-cell current clamp recordings in the absence of any blockers. To maintain the physiological chloride reversal potential in yGCs and therefore depolarizing GABAergic inputs, we used a potassium gluconate-based pipette solution with 25mM chloride (Heigele et al., 2016; Li et al., 2017). The membrane potential was kept constant and close to the resting potential of -80mV. By stimulating in the molecular layer (brief burst of 3 pulses at 50Hz) we were able to effectively recruit both glutamatergic and GABAergic inputs onto young GCs and record subthreshold PSPs with an average depolarization of 35.31±1.04 mV (*n*= 12; Fig. 13A+D). Bath application of α_5-NAM (1μM) resulted in a large and significant 32.9% reduction of the burst amplitude (to 67.09± 7.87% of control, *n*=7 *P* =0.008) and 43.9% reduction of the integral (to 56.15± 8.764% of control, *P* =0.008). Subsequent wash-in of AP5 (50μM) resulted in a smaller decrease of amplitude by 14.7% (to 52.44 ± 6.01% of baseline, *P* =0.016) and integral by 15.3% (to 40.83 ± 5.92% of baseline, *P* =0.008)(Fig. 13A-C). In contrast, application of AP5 in ACSF caused only a 21.9% reduction in amplitude (to 78.1± 7.2% of control, *n*= 5 *P* =0.016) and a 28.5% reduction in integral (to 71.5± 7.3% of control, *P*=0.031). Additional wash in of α_5-NAM further removed GABAergic depolarization reducing the PSP and integral further (54.98± 11.28% of baseline, *P* =0.016, and 49.23± 10.59% of baseline, *P* =0.016, respectively)(Fig. 13D-F). Furthermore, we compared the NMDAR-sensitive reduction of PSP amplitude and integral in both control and in the presence of α_5-NAM (Fig. 13G+H). As expected, the wash-in of AP5 from control had a larger effect than when applied sequentially after α_5-NAM. This can be explained by the voltage-dependence of the NMDARs. The reduced depolarization after the block of α_5-GABARs, leads to reduced activation of NMDARs. Both PSP amplitude (Ctrl 21.9± 5.9%, *n*=6; in presence of α_5-NAM 14.7±3.9%, *n*=7, *P* =0.15) and integral (Ctrl 34.0± 2.6%; in presence of α_5-NAM 15.3±5.0%, *P* =0.015) showed a smaller NMDA-sensitive component in the presence of α_5-NAM. However, only the effect on the integral was large and robust enough to reach significance.

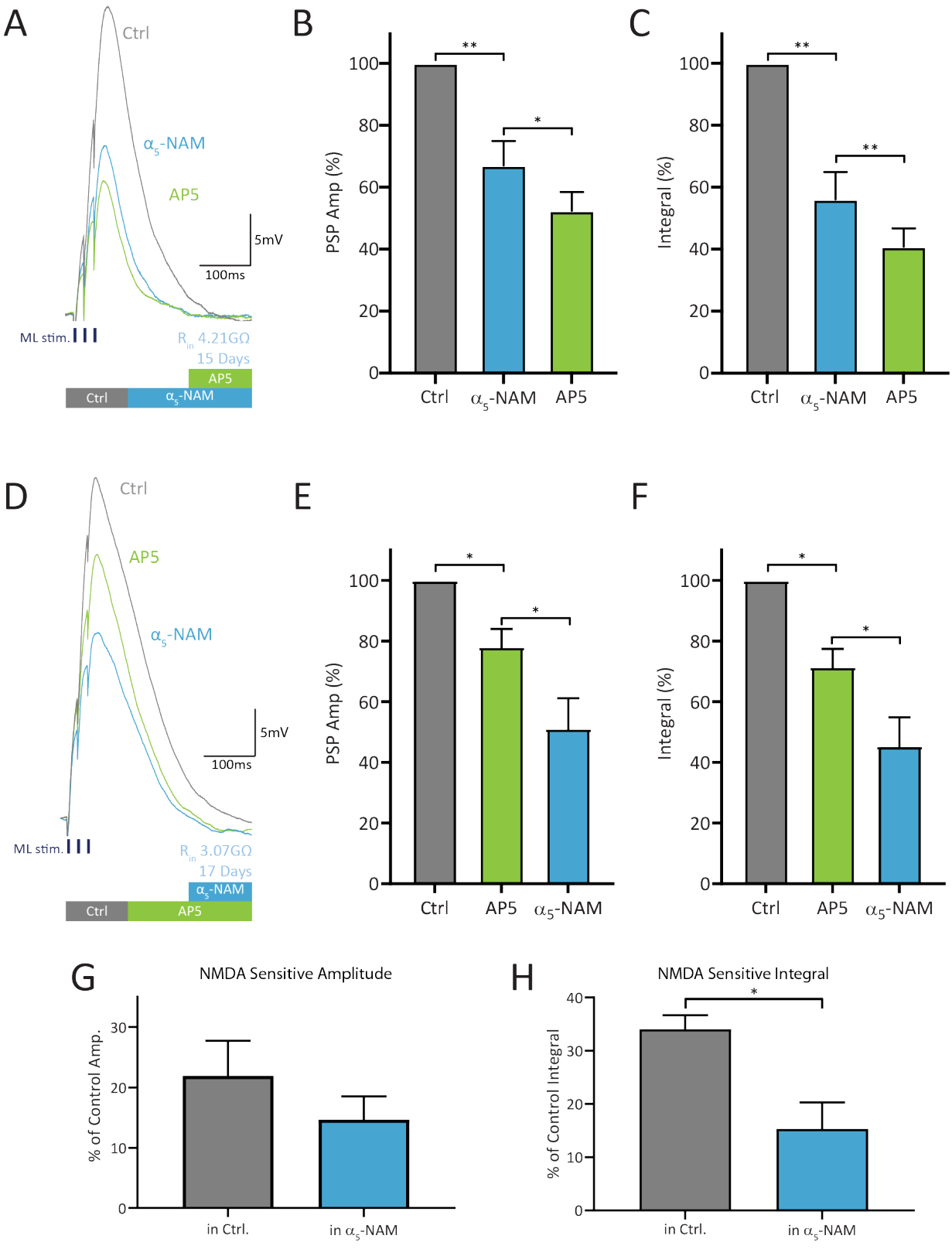

Fig. 13 Activation of depolarizing α5-GABA$_A$Rs controls NMDAR recruitment. A) NMDAR contribution to PSPs in yGCs after blocking 50% α5-containg GABARs with the application of α5-NAM. A short burst (3 pulses, at 50Hz) of electrical stimulation of the GCL was used to evoke a PSP≈35mV. B-C) PSP amplitude and integral area dramatically dropped with α5-NAM application, while APV (50 μM) application produced a significant but modest reduction. D-F) APV application in control ACSF produced a small but significant change in PSP amplitude and integral, while subsequent application of α5-NAM resulted in a significant decrease in both amplitude and integral. G-H) The NMDA-sensitive amplitude and integral was smaller in the presence of α5-NAM than in control.

Thus, we show that α_5-GABARs promote GABAergic depolarization of young GCs, which increases the activation of voltage-sensitive NMDA receptors.

4.7 α_5-GABA$_A$Rs bidirectionally mediate excitation and shunting inhibition of adult-born granule cells.

Although GABAergic inputs are initially depolarizing in adult-born GCs, GABA can still be inhibitory through shunting inhibition (Heigele et al., 2016). GPSCs mediated by α_5-GABA$_A$Rs promote NMDAR activation, however, we also wanted to investigate whether they played a similar role in shunting inhibition. To do this, we performed whole-cell current clamp recordings in the presence of NBQX and AP5 to block glutamatergic inputs (10μM and 25μM respectively). Local electrical stimulation of the GCL was used in order to target peri-somatic GABAergic inputs at the lowest intensity required to produce effective shunting inhibition (30-60μA). To simulate a controlled glutamatergic input, we evoked a coincident mock EPSP via current injection to produce a 20mV depolarisation (Fig. 14A). We were able to effectively evoke action potential firing with a short burst protocol (3 pulses at 50Hz) and produce strong shunting inhibition with a long burst protocol (8 pulses at 50Hz). The application of α_5-NAM (1μM) had a differential effect in that AP firing in response to the short burst was largely unaffected (from 85.1± 12.3% to 74.2± 11.4% , *n*= 8 *P* =0.15), however shunting inhibition was strongly reduced, with a significant increase in AP firing probability with the long burst (from 15.3± 10.0% to 53.0± 13.9% *n* =8 *P*=0.016) (Fig. 14B). However, both 3- and 8-stimulation paradigms showed a decrease in PSP integral (3stim 74.6± 3.1%, *P* =0.004; 8 stim 78.1± 4.7%, *P* =0.004) as expected with a reduction in GABAergic depolarisation. This suggests that α_5-containing GABARs powerfully control shunting inhibition, while having a relatively mild effect on GABAergic excitation. This is consistent with the biophysical properties of the α_5-containing GABARs in yGCs showing about a four-fold larger conductance close to the AP threshold (-35mV) compared to -80mV (see Fig. 8H). Thus, blocking α_5GABARs widens the action potential window in young cells, increasing overall excitation.

Heigele et al. (2016) found that shunting inhibition was strongly reduced when 50% of GABA receptors were blocked using a low concentration of gabazine (SR95531, 0.2μM), while excitation was shifted towards stronger stimulation intensities. As approximately 50% of the

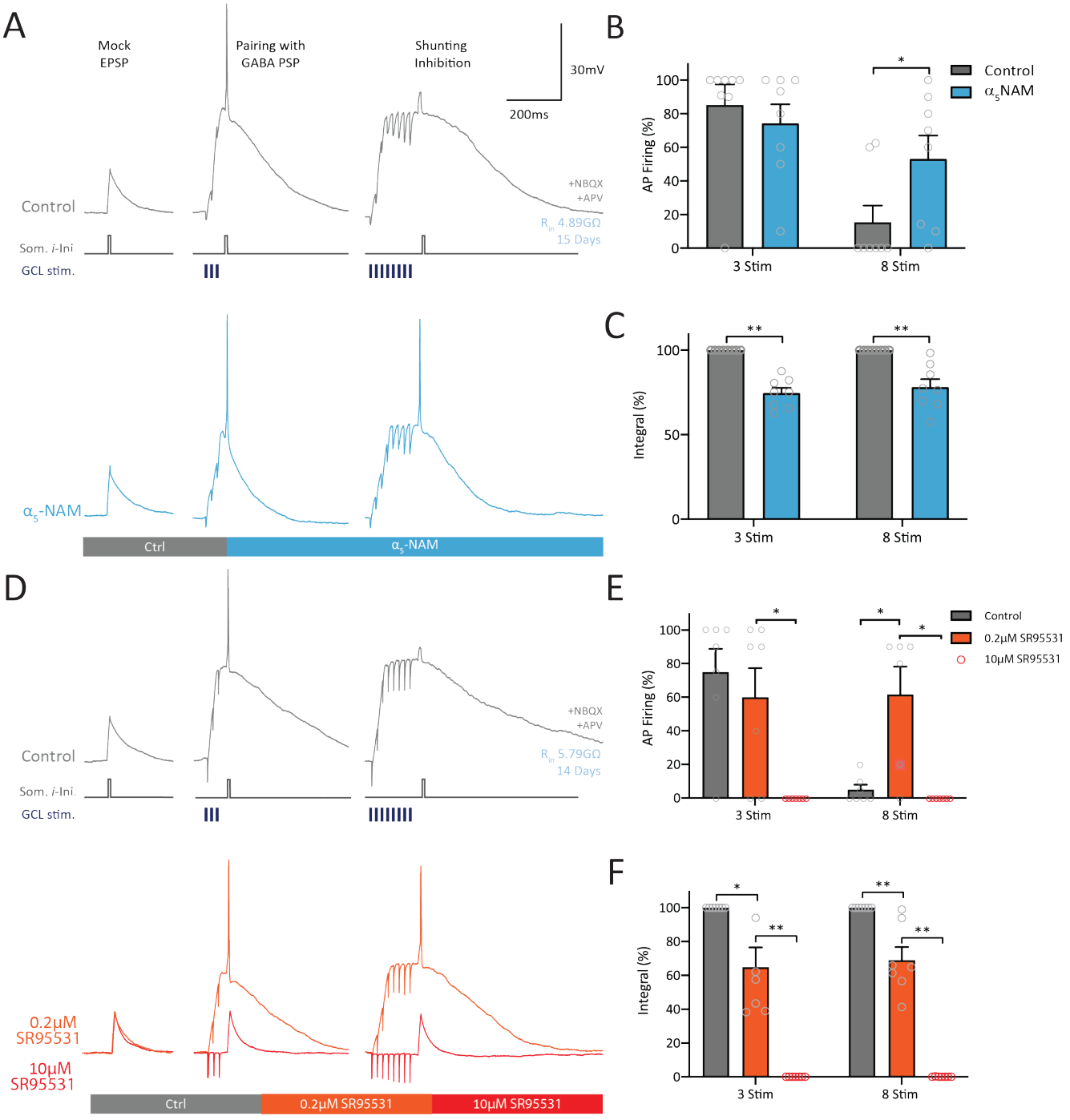

Fig. 14 α_5-GABA$_A$Rs maintain sparse-firing in yGCs with shunting inhibition. A) Experimental design. A somatic current injection (10ms, about 20mV) was delivered alone, or paired with 3 or 8 pulse bursts of stimulation in the GCL (50Hz) in the presence of NBQX (10μM) and APV (25μM). The lowest stimulation intensity that produced shunting inhibition with the 8-stim burst was chosen (30-60μA). Example traces are shown in control (grey) and with the application of α_5-NAM (1μM, blue), B) Mean AP firing probability of the 3- and 8-stim burst PSPs. AP firing was not significantly affected with α_5-NAM application, however shunting inhibition of the 8-stim burst was significantly reduced with α_5-NAM application, resulting in a large increase in AP firing. The integral of the 8-stim PSP was significantly decreased with the application of both α_5-NAM and gabazine. Grey open circles represent individual cells. C) Mean PSP integrals show similar reductions with α_5-NAM application. D) Example traces of control (grey) with sequential application of 0.2μM (orange) and 10μm red) gabazine (SR95531). E) Similarly, to α_5-NAM 0.2μM did not affect AP firing with the 3-stim burst, but significantly reduced shunting inhibition, resulting in a large increase of AP firing with the 8-stim burst. Subsequent application of 10μM gabazine (red open circles) abolished all AP firing. F) Mean integrals were reduced with 0.2μM gabazine, while 10μM gabazine fully blocked the remaining GPSPs.

GPSCs in young GCS are mediated by α_5-containing GABARs we wanted to see whether a low concentration of gabazine had a similar effect to that of α_5-NAM. Similarly, we found that low gabazine had little effect on GABAergic excitation, with the short burst protocol showing similar AP probabilities (from 75.0± 13.7% to 60.0± 17.3%, *n*= 7 *P* =0.34)(Fig. 14D+E). However, shunting inhibition was strongly reduced, allowing effective AP firing (from 5.8± 3.3% to 61.7± 16.6% , *n*= 6 *P* =0.031). Integrals for both the 3-stim and 8-stim bursts were significantly decreased (3stim 64.8± 11.69%, *P* =0.023; 8 stim 68.9± 7.8%, *P* =0.008)(Fig. 14F). Subsequent application of 10μM gabazine was sufficient to fully block any remaining PSP, thus showing that all synaptic responses are indeed GABA receptor mediated (Fig. 14D-F). Taken together, the comparable effect of the 0. 2μM gabazine (which binds non-specifically to $GABA_ARs$) and the α_5-NAM in reducing shunting inhibition, further indicates that $GABA_ARs$ are homogenous in yGCs.

5. Discussion

This study describes a novel dendritic GABAergic input onto young GCs originating from somatostatin positive interneurons from as early as 2 weeks post mitosis. Additionally, the presence of perisomatic inhibition from parvalbumin interneurons was confirmed. Further investigation into the postsynaptic $GABA_AR$ composition of young cells revealed that the α_5-subunit was present in approximately 50% of the receptors in both perisomatic and dendritic inhibitory synapses. The α_5-$GABA_AR$ showed non-linear outward rectification with around 4-fold larger conductance at depolarized membrane potentials above -40mV relative to the resting membrane potential. Consistent with this voltage dependence, α_5-containing GABARs were found to act bidirectionally- facilitating subthreshold depolarisation and NMDAR activation, while also powerfully controlling shunting inhibition.

5.1 Adult born granule cells receive synaptic GABA inputs from PV and SOM interneurons

The development of GABAergic synaptic contacts onto young granule cells has been shown to begin as early as 4 days post mitosis (Song et al., 2013), continuing to increase in strength during the next 6 weeks of maturation (Espósito et al., 2005; Ge et al., 2006; Sah et al., 2017). NOS-positive neurogliaform interneurons and parvalbumin-positive basket cells have been found to form GABAergic synapses from 1-week post mitosis (Markwardt et al., 2011; Alvarez et al., 2016), forming synapses on the proximal dendrites and soma respectively. However, what remained unclear was whether yGCs receive distal dendritic inputs from an early age. Consistent with the work of Alvarez et al. (2016) we were able to confirm the presence of perisomatic inputs from soma-targeting PV-INs using optogenetic stimulation. We also identified the novel presence of distal dendritic inputs from SOM-INs from as early as 2 weeks post mitosis. Both interneuron subtypes support feedback inhibition, while PV-INs also support feedforward inhibition (Ewell and Jones, 2010). The involvement of adult-born granule cells in both inhibitory microcircuits suggests that yGCs likely contribute to the network in a functional manner from as early as 2 weeks after mitosis.

Dendritic and perisomatic synaptic inputs onto 2-3 week old granule cells showed slow kinetic properties and small conductance, similar to that previously described (Espósito et al.,

2005; Ge et al., 2006; Markwardt and Overstreet-Wadiche, 2008; Markwardt et al., 2011; Song et al., 2013; Alvarez et al., 2016; Sah et al., 2017). Slow GPSCs have been attributed to synapses with characteristics in between tonic and phasic inhibition (Szabadics et al., 2007), or to non-specific GABA spillover from neighboring synapses (Rossi and Hamann, 1998). Thus, the slow kinetic profile of PSCs of young cells has been suggested to be spillover from neighboring mature synapses, allowing the activation of extrasynaptic receptors present homogenously over yGCs (Wei et al., 2003). However, similar to the work done by Markwardt et al. (2009) we confirmed that GABAergic transmission onto young cells is indeed synaptic, and not spillover from neighboring mature synapses. Application of dextran and the resulting reduction of GABA diffusion out of the synapse did not result in a decrease in GPSC amplitude in young cells, but rather an increase.

While we were able to show that GABAergic inputs onto yGCs were synaptic and not spillover, the kinetics of these inputs were still slow. In contrast to the fast-kinetic responses of perisomatic inputs on mature GCs, young GCs showed slow inputs from PV-INs. Likewise, dendritic inputs onto yGCs displayed prolonged rise and decay time courses. To ensure that the pre-synaptic terminals of GABAergic INs were not different between young and mature GCs we compared paired-pulse ratio, finding that the release probability was the same irrespective of age of the postsynaptic cell. However, PV-INs showed a larger paired-pulse depression than SOM-INs. The unchanged paired-pulse depression between 2-3 weeks post mitosis and full maturity indicates that release probability in the presynapse remains constant and that presynaptic contacts from PV and SOM INs are fully established.

5.2 GABAergic inputs onto young granule cells are highly non-linear

Similar to the study done by Schulz et al. (2018), we found that dendrite targeting inputs from SOM INs onto both young and mature GCs are non-linear and voltage dependent, comparable to that seen in CA1 pyramidal cells. This non-linearity of GABAergic dendritic inhibitory inputs of mature GCs probably acts to balance NMDA-receptor-mediated synaptic depolarization. In contrast, perisomatic inhibitory inputs from PV interneurons onto mature GCs not only showed faster kinetics, but also linear transmission with no rectification. However, perisomatic inputs onto young cells did show strong voltage dependence, behaving in a similar way to dendritic inputs. This suggests that synapses across the somatodendritic

cell membrane of young GCs are largely homogenous. Whereas, in mature cells the properties of somatic and dendritic synapses are different, with slow rectifying receptors restricted to the dendritic domain. Additionally, as 3-4-week-old cells already lose this non-linearity in somatic synapses, maturation of granule cells is accompanied by the conversion of slow rectifying synaptic $GABA_A$Rs at the soma to linear fast receptors.

In addition to the finding in CA1 by Schulz et al. (2018), we showed that the voltage-dependence of GPSCs onto young GCs and dendritic inputs onto mature GCs is present in symmetrical chloride conditions. It is expected from Goldman-Hodgkin-Katz (GHK) rectification that unsymmetrical distribution of ions generates different currents in inward vs outward directions. Indeed, we have found that rectification is smaller in symmetrical chloride than in 25mM chloride. Nevertheless, the presence of rectification in symmetrical chloride shows that rectification is a property of the post-synaptic GABA receptors. This suggests that the outwardly-rectifying transmission found in granule cells is actually due to voltage sensitive GABA receptors that have different opening probabilities at different membrane potentials.

5.3 α_5-containing $GABA_A$ receptors are present in somatic and dendritic synapses of yGCs

α_5-containing-GABARs have traditionally been viewed as extrasynaptic, mediating tonic inhibition with slow kinetic properties. However, as Schulz et al. (2018) demonstrated the presence of α_5-$GABA_A$Rs in dendritic synapses of CA1 pyramidal cells, we sought to investigate whether α_5-$GABA_A$Rs may be present in granule cells of the dentate. Similar to CA1 pyramidal cells, mature granule cells have α_5-$GABA_A$Rs in dendritic synapses targeted by SOM interneurons. Additionally, α_5-$GABA_A$Rs have been shown to be rectifying, accounting for the non-linearity seen in mGCs. Using computational modeling, Schulz et al. (2018) found that the slow kinetics and voltage-dependence of α_5-$GABA_A$Rs are ideally suited to temporally and spatially control the non-linear NMDAR activation in fine dendritic tufts, while also preventing NMDAR-dependent burst firing. We propose that in mature granule cells- where GABA is inhibitory- the role of α_5-GABARs is likely similar, in order to maintain sparse activity.

Additionally, we found that both perisomatic and dendritic synapses of young GCs contain the α_5-subunit, which mediates approximately 50% of GABA inputs onto yGCs. This suggests that postsynaptic receptor composition in young cells is homogenous at 2-3 weeks post mitosis, however as the cell matures these α_5-$GABA_A$Rs are removed from perisomatic synapses but largely persist in dendritic synapses. The speed up of kinetics in somatic synapses with development is also consistent with the removal of α_5-GABARs, due to their slow kinetics. Interestingly, when we increased spillover of perisomatic synapses in mature GCs with application of NO711, we were able to enhance rectification, by recruiting perisynaptic α_5-$GABA_A$Rs. This suggests that α_5-$GABA_A$Rs are not completely lost from the somatic cell membrane, but instead are specifically targeted to the extrasynaptic membrane, where they might contribute to tonic inhibition.

5.4 α_5-$GABA_A$Rs promote shunting inhibition, maintaining sparse firing of yGCs

Similar to embryonic development, the E_{GABA} of adult born granule cells is at -35mV, substantially more positive than the resting membrane potential of -80mV. Therefore, GABA signaling onto young cells is initially depolarizing (Ge et al., 2006; Karten et al., 2006; Chancey et al., 2013). However, multiple behavioural studies have shown that the number of activated newly generated young GCs is comparable with the activity of mature GCs. Using immediate early gene expression, the proportion of active 4-week-old GCs was found to be slightly larger (~4%) than the proportion of active mature GCs within the general NeuN-positive GC population under identical conditions (~1-2%) (Ramirez-Amaya et al., 2006; Kee et al., 2007; Tashiro et al., 2007; Krzisch et al., 2016) . Similarly, *in vivo* calcium imaging has shown that cells younger than 6 wpm are on average 1.5-fold more active than mature GCs (Danielson et al., 2016). These *in vivo* results are fully consistent with the view that young cells are slightly more active than mature GCs, but still maintain a sparse activity one order of magnitude lower than reported activities in CA3. How they maintain low activation levels despite their intrinsic properties has been unclear until the recent study by Heigele et al. (2016) discovered that GABAergic inputs are able to act bidirectionally, promoting depolarization as well as an inhibitory control of AP firing through shunting inhibition.

GABAergic synapses contact yGCs as soon as 1wpm from a number of interneuron subpopulations; including PV-positive basket cells, neurogliaform/ivy cells and now from this

study SOM-positive HIPP cells (Markwardt et al., 2011; Deshpande et al., 2013; Song et al., 2013). All of these inputs might provide GABAergic excitation as well as shunting inhibition. Heigele et al. (2016) carefully investigated the GABAergic conductance onto newborn granule cells, mimicking sequential feedforward (PV-mediated) and feedback (SOM-mediated) inhibition with a brief burst stimulation in the GCL (2-8pulses at 50Hz) followed by stimulation of the ML (2 pulses at 100Hz). At low intensities, action potentials were reliably generated while at higher intensities this was shunted. The minimal synaptic conductance needed to generate AP firing was found to be 0.28nS, close to the unitary conductance reported for neurogliaform INs–evoked GPSCs (0.23 nS)(Markwardt et al., 2011). Additionally, the peak firing probability was found to be around 1.5nS, consistent with a brief burst activity of only 3-4 interneurons. However, they described a maximal conductance onto yGCs of 12nS, which reliably produced shunting inhibition from 4nS upwards. Thus, strong network activity recruiting more than 33% of dentate interneurons produces robust GABAergic inhibition onto yGCs, effectively blocking AP firing.

What is the functional role of α_5-GABARs in young granule cells? Firstly, we found that in young GCs α_5-GABARs promote depolarization up to the $E_{GABA;}$ facilitating NMDAR activation. Thus, α_5-GABARs play a role in the GABAergic depolarization of yGCs. Secondly, we tested the contribution of α_5-GABARs to shunting inhibition. Using the same stimulation paradigm as Heigele et al. (2016)- combining burst stimulation of the GCL with a mock EPSP- we were able to elicit both excitation (short burst, 3 pulses at 50Hz), and shunting inhibition (long burst, 8 pulses at 50Hz). Blocking 50% of the α_5-GABARs reliably reduced shunting inhibition, resulting in a significant increase of AP firing. However, there was little effect on the short burst protocol which remained excitatory, suggesting that reducing the GABAergic conductance onto yGCs was able to widen the AP window. The biophysical properties of α_5-GABARs perfectly supports shunting inhibition as the voltage-dependence produces a conductance four-fold larger around the action potential threshold (-35mV) than at rest (-80mV).

5.5 The functional significance of GABAergic inhibition within the dentate gyrus

As we have recently reviewed (Lodge and Bischofberger, 2019), the dentate gyrus represents a highly competitive ‘winner-takes all’ network. (Geiger et al., 1997; Temprana et

al., 2015; Espinoza et al., 2018). Strong lateral feedback inhibition from PV-positive basket cells can be easily recruited by a small number of active mature GCs, exerting strong control over neighboring GCs locally restricted within about 200 µm (Ewell and Jones, 2010; Sambandan et al., 2010; Espinoza et al., 2018). *In vivo* recordings in awake animals showed that mature GCs are under strong inhibitory control by local PV-basket cells during theta-nested gamma oscillations (Pernía-Andrade and Jonas, 2014). Only a small proportion of winner GCs escape from this inhibition from time to time, generating the well-known sparse population activity of the dentate gyrus GCs (Jung and McNaughton, 1993; Chawla et al., 2005; Bakker et al., 2008; Hainmueller and Bartos, 2018). Due to the high level of inhibition needed to maintain such a sparse network activity, it is expected that during behavior young GCs receive substantial GABAergic inputs. However, unlike mature GCs, the depolarised E_{GABA} of yGCs generates both GABAergic excitation (when only ~10% of GABAergic synapses are active) as well as shunting inhibition (when >30% of GABAergic synapses are active), to maintain sparse activity in the network.

While adult neurogenesis has been found to increase pattern separation, this seems to be in contrast to the intrinsic properties of yGCs, including the high input resistance. Several studies have demonstrated the importance of newborn GC age, with 4-week-old neurons facilitating pattern separation during learning, while older cells are less effective (Gu et al., 2012; Nakashiba et al., 2012). Furthermore, modeling studies have suggested that hippocampal pattern separation is dependent on sparse activity and orthogonal coding of neuronal information in the dentate gyrus-mossy fiber system (Treves and Rolls, 1992, 1994). This contradiction to the intrinsic ‘hyperexcitable’ properties of young cells reinforces the importance of a true inhibitory input onto these neurons. This was clearly shown in a study by Krzisch et al. (2016) where an increase in spine density in yGCs as a result of Neuroligin-2 overexpression increased yGC activation during learning from 4 to 9% (Arc^+ neurons). After this increase in young cell activity, learning was impaired. Thus, sparse AP firing in young cells is necessary to improve hippocampal functioning via adult neurogenesis. Perisomatic and dendritic GABAergic inputs onto yGCs that target synaptic α_5-containing GABARs allow bidirectional modulation of AP firing. Whereas small inputs increase firing, large inputs shunt firing, ensuring specificity and sparsity of the neuronal code for new information. Thus, α_5-$GABA_AR$s allow young granule cells to tightly control the AP firing window, generating improved pattern separation.

5.5 Conclusions

Through this study we were able to identify the neuronal subtypes that provide somatic and dendritic inhibition onto young granule cells. From as early as 2 weeks post mitosis we found that young granule cells receive inhibitory inputs from both parvalbumin and somatostatin interneurons. Additionally, we found that the synaptic $GABA_A$ receptors in young cells showed a pronounced non-linear voltage-dependence. This was explained by the presence of α_5-containing $GABA_A$Rs which were also found in dendritic synapses of mature granule cells. As a consequence of this voltage-dependence, the synaptic conductance in young cells was four-fold greater at depolarized potentials than at rest. We found that this receptor property facilitates sub-threshold depolarization. However, its main role in young cells is probably the shunting of action potential generation as conductance is 4-times larger at depolarized potentials around the AP threshold. Taken together, our new findings reinforce the concept that α_5-$GABA_A$Rs play an important role in maintaining the inhibitory function of GABA onto young cells, preventing over-excitation and producing sparse firing. This data suggests that the synaptic GABA receptor profile in yGCs strongly supports pattern separation by allowing both GABAergic depolarization and effective shunting inhibition in newborn granule cells of the hippocampus.

6. References

Adlaf EW, Vaden RJ, Niver AJ, Manuel AF, Onyilo VC, Araujo MT, Dieni C V, Vo HT, King GD, Wadiche JI, Overstreet-Wadiche L (2017) Adult-born neurons modify excitatory synaptic transmission to existing neurons. Elife 6, e19886.

Altman J (1962) Are new neurons formed in the brains of adult mammals? Science 135:1127–1128.

Alvarez DD, Giacomini D, Yang SM, Trinchero MF, Temprana SG, Büttner KA, Beltramone N, Schinder AF (2016) A disynaptic feedback network activated by experience promotes the integration of new granule cells. Science (80-) 354:459–465.

Amaral DG, Scharfman HE, Lavenex P (2007) The dentate gyrus: fundamental neuroanatomical organization (dentate gyrus for dummies). Prog Brain Res 163.

Ambrogini P, Lattanzi D, Ciuffoli S, Agostini D, Bertini L, Stocchi V, Santi S, Cuppini R (2004) Morpho-functional characterization of neuronal cells at different stages of maturation in granule cell layer of adult rat dentate gyrus. Brain Res 1017:21–31.

Apple DM, Solano-Fonseca R, Kokovay E (2017) Neurogenesis in the aging brain. Biochem Pharmacol 141:77–85.

Arnold Bakker, C. Brock Kirwan, Michael Miller CELS (2007) Pattern Separation in the Dentate Gyrus and CA3 of the Hippocampus. Science (80-) 315:961–966.

Bakker A, Kirwan CB, Miller M, Stark CEL (2008) Pattern Separation in the Human Hippocampal CA3 and Dentate Gyrus. Science (80-) 319:1640–1642.

Ballard TM, Knoflach F, Prinssen E, Borroni E, Vivian JA, Basile J, Gasser R, Moreau JL, Wettstein JG, Buettelmann B, Knust H, Thomas AW, Trube G, Hernandez MC (2009) RO4938581, a novel cognitive enhancer acting at GABAA α5 subunit-containing receptors. Psychopharmacology (Berl) 202:207–223.

Ben-Ari Y (2002) Excitatory actions of gaba during development: the nature of the nurture. Nat Rev Neurosci 3:728–739.

Bengzon J, Kokaia Z, Elmér E, Nanobashvili A, Kokaia M, Lindvall O (1997) Apoptosis and proliferation of dentate gyrus neurons after single and intermittent limbic seizures. Proc Natl Acad Sci U S A 94:10432–10437.

Bergami M, Masserdotti G, Temprana SG, Motori E, Eriksson TM, Göbel J, Yang SM, Conzelmann K-K, Schinder AF, Götz M, Berninger B (2015) A Critical Period for Experience-Dependent Remodeling of Adult-Born Neuron Connectivity. Neuron 85:710–

717.

Bischofberger J (2007) Young and excitable: new neurons in memory networks. Nat Neurosci 10:273–275.

Bischofberger J, Engel D, Frotscher M, Jonas P (2006) Timing and efficacy of transmitter release at mossy fiber synapses in the hippocampal network. Pflügers Arch - Eur J Physiol 453:361–372.

Bolz L, Heigele S, Bischofberger J (2015) Running Improves Pattern Separation during Novel Object Recognition. Brain Plast 1:129–141.

Brown JP, Couillard-Després S, Cooper-Kuhn CM, Winkler J, Aigner L, Kuhn HG (2003) Transient Expression of Doublecortin during Adult Neurogenesis. J Comp Neurol 467:1–10.

Capogna M, Pearce RA (2011) GABAA,slow: Causes and consequences. Trends Neurosci 34:101–112.

Chancey JH, Adlaf EW, Sapp MC, Pugh PC, Wadiche JI, Overstreet-Wadiche LS (2013) GABA Depolarization Is Required for Experience-Dependent Synapse Unsilencing in Adult-Born Neurons. J Neurosci 33:6614–6622.

Chancey JH, Poulsen DJ, Wadiche JI, Overstreet-Wadiche L (2014) Hilar mossy cells provide the first glutamatergic synapses to adult-born dentate granule cells. J Neurosci 34:2349–2354.

Chawla MK, Guzowski JF, Ramirez-Amaya V, Lipa P, Hoffman KL, Marriott LK, Worley PF, McNaughton BL, Barnes CA (2005) Sparse, environmentally selective expression ofArc RNA in the upper blade of the rodent fascia dentata by brief spatial experience. Hippocampus 15:579–586.

Collinson N, Kuenzi FM, Jarolimek W, Maubach KA, Cothliff R, Sur C, Smith A, Otu FM, Howell O, Atack JR, McKernan RM, Seabrook GR, Dawson GR, Whiting PJ, Rosahl TW (2002) Enhanced Learning and Memory and Altered GABAergic Synaptic Transmission in Mice Lacking the α5 Subunit of the GABA $_A$ Receptor. J Neurosci 22:5572–5580.

Couillard-Despres S, Winner B, Karl C, Lindemann G, Schmid P, Aigner R, Laemke J, Bogdahn U, Winkler J, Bischofberger J, Aigner L (2006) Targeted transgene expression in neuronal precursors: watching young neurons in the old brain. Eur J Neurosci 24:1535–1545.

Danielson NB, Kaifosh P, Zaremba JD, Lovett-Barron M, Tsai J, Denny CA, Balough EM, Goldberg AR, Drew LJ, Hen R, Losonczy A, Kheirbek MA (2016) Distinct Contribution of

Adult-Born Hippocampal Granule Cells to Context Encoding. Neuron 90:101–112.

Deisseroth K, Singla S, Toda H, Monje M, Palmer TD, Malenka RC (2004) Excitation-Neurogenesis Coupling in Adult Neural Stem/Progenitor Cells. Neuron 42:535–552.

Deshpande A, Bergami M, Ghanem A, Conzelmann K-K, Lepier A, Götz M, Berninger B (2013) Retrograde monosynaptic tracing reveals the temporal evolution of inputs onto new neurons in the adult dentate gyrus and olfactory bulb. Proc Natl Acad Sci U S A 110:E1152-61.

Dieni C V., Panichi R, Aimone JB, Kuo CT, Wadiche JI, Overstreet-Wadiche L (2016) Low excitatory innervation balances high intrinsic excitability of immature dentate neurons. Nat Commun 7:11313.

Dieni C V, Nietz AK, Panichi R, Wadiche JI, Overstreet-Wadiche L (2013) Distinct determinants of sparse activation during granule cell maturation. J Neurosci 33:19131–19142.

Doetsch F, Alvarez-Buylla A (1996) Network of tangential pathways for neuronal migration in adult mammalian brain. Proc Natl Acad Sci U S A 93:14895–14900.

Doetsch F, Caillé I, Lim DA, García-Verdugo JM, Alvarez-Buylla A (1999) Subventricular Zone Astrocytes Are Neural Stem Cells in the Adult Mammalian Brain. Cell 97:703–716.

Dossani RH, Missios S, Nanda A (2015) The Legacy of Henry Molaison (1926-2008) and the Impact of His Bilateral Mesial Temporal Lobe Surgery on the Study of Human Memory. World Neurosurg 84:1127–1135.

Eisch AJ, Barrot M, Schad CA, Self DW, Nestler EJ (2000) Opiates inhibit neurogenesis in the adult rat hippocampus. Proc Natl Acad Sci U S A 97:7579–7584.

Engin E, Zarnowska ED, Benke D, Tsvetkov E, Sigal M, Keist R, Bolshakov VY, Pearce RA, Rudolph U (2015) Tonic Inhibitory Control of Dentate Gyrus Granule Cells by α5-Containing GABAA Receptors Reduces Memory Interference. J Neurosci 35:13698–13712.

Espinoza C, Guzman SJ, Zhang X, Jonas P (2018) Parvalbumin+ interneurons obey unique connectivity rules and establish a powerful lateral-inhibition microcircuit in dentate gyrus. Nat Commun 9:4605.

Espósito MS, Piatti VC, Laplagne DA, Morgenstern NA, Ferrari CC, Pitossi FJ, Schinder AF (2005) Neuronal differentiation in the adult hippocampus recapitulates embryonic development. J Neurosci 25:10074–10086.

Ewell LA, Jones M V. (2010) Frequency-Tuned Distribution of Inhibition in the Dentate Gyrus.

J Neurosci 30:12597–12607.

Farrant M, Nusser Z (2005) Variations on an inhibitory theme: Phasic and tonic activation of GABA A receptors. Nat Rev Neurosci 6:215–229.

Franklin KB, Paxinos G (2007) The mouse brain in stereotaxic coordinates, 3rd ed. New York.

Freundl TF, Buzsáki G (1996) Interneurons of the Hippocampus. Hippogimpus 6:347–470.

Ge S, Goh ELK, Sailor KA, Kitabatake Y, Ming G, Song H (2006) GABA regulates synaptic integration of newly generated neurons in the adult brain. Nature 439:589–593.

Ge S, Yang C, Hsu K, Ming G, Song H (2007) A Critical Period for Enhanced Synaptic Plasticity in Newly Generated Neurons of the Adult Brain. Neuron 54:559–566.

Geiger JR., Lübke J, Roth A, Frotscher M, Jonas P (1997) Submillisecond AMPA Receptor-Mediated Signaling at a Principal Neuron–Interneuron Synapse. Neuron 18:1009–1023.

Gonçalves JT, Bloyd CW, Shtrahman M, Johnston ST, Schafer ST, Parylak SL, Tran T, Chang T, Gage FH (2016) In vivo imaging of dendritic pruning in dentate granule cells. Nat Neurosci 19:788–791.

Gonzalez JC, Epps SA, Markwardt SJ, Wadiche JI, Overstreet-Wadiche L (2018) Constitutive and Synaptic Activation of GIRK Channels Differentiates Mature and Newborn Dentate Granule Cells. J Neurosci 38:6513–6526.

GoodSmith D, Chen X, Wang C, Kim SH, Song H, Burgalossi A, Christian KM, Knierim JJ (2017a) Spatial Representations of Granule Cells and Mossy Cells of the Dentate Gyrus. Neuron 93:677-690.e5.

GoodSmith D, Chen X, Wang C, Kim SH, Song H, Burgalossi A, Christian KM, Knierim JJ (2017b) Spatial Representations of Granule Cells and Mossy Cells of the Dentate Gyrus. Neuron 93:677-690.e5.

Gould E (2007) How widespread is adult neurogenesis in mammals? Nat Rev Neurosci 8:481–488.

Gould E, Tanapat P, McEwen BS, Flugge G, Fuchs E (1998) Proliferation of granule cell precursors in the dentate gyrus of adult monkeys is diminished by stress. Proc Natl Acad Sci 95:3168–3171.

Gray WP, Sundstrom LE (1998) Kainic acid increases the proliferation of granule cell progenitors in the dentate gyrus of the adult rat. Brain Res 790:52–59.

Gu Y, Arruda-Carvalho M, Wang J, Janoschka SR, Josselyn SA, Frankland PW, Ge S (2012) Optical controlling reveals time-dependent roles for adult-born dentate granule cells. Nat Neurosci 15:1700–1706.

Hainmueller T, Bartos M (2018) Parallel emergence of stable and dynamic memory engrams in the hippocampus. Nature 558:292–296.

Hannan S, Minere M, Harris J, Izquierdo P, Thomas P, Tench B, Smart TG (2019) GABAAR isoform and subunit structural motifs determine synaptic and extrasynaptic receptor localisation. Neuropharmacology.

Hausrat TJ, Muhia M, Gerrow K, Thomas P, Hirdes W, Tsukita S, Heisler FF, Herich L, Dubroqua S, Breiden P, Feldon J, Schwarz JR, Yee BK, Smart TG, Triller A, Kneussel M (2015) Radixin regulates synaptic GABAA receptor density and is essential for reversal learning and short-term memory. Nat Commun 6:6872.

Heckers S (2001) Neuroimaging studies of the hippocampus in schizophrenia. Hippocampus 11:520–528.

Heigele S, Sultan S, Toni N, Bischofberger J (2016) Bidirectional GABAergic control of action potential firing in newborn hippocampal granule cells. Nat Neurosci 19:263–270.

Henze DA, Wittner L, Buzsáki G (2002) Single granule cells reliably discharge targets in the hippocampal CA3 network in vivo. Nat Neurosci 5:790–795.

Hill AS, Sahay A, Hen R (2015) Increasing Adult Hippocampal Neurogenesis is Sufficient to Reduce Anxiety and Depression-Like Behaviors. Neuropsychopharmacology 40:2368–2378.

Hsiao Y-H, Hung H-C, Chen S-H, Gean P-W (2014) Social Interaction Rescues Memory Deficit in an Animal Model of Alzheimer's Disease by Increasing BDNF-Dependent Hippocampal Neurogenesis. J Neurosci 34:16207–16219.

Jagasia R, Steib K, Englberger E, Herold S, Faus-Kessler T, Saxe M, Gage FH, Song H, Lie DC (2009) GABA-cAMP response element-binding protein signaling regulates maturation and survival of newly generated neurons in the adult hippocampus. J Neurosci 29:7966–7977.

Jessberger S, Römer B, Babu H, Kempermann G (2005) Seizures induce proliferation and dispersion of doublecortin-positive hippocampal progenitor cells. Exp Neurol 196:342–351.

Jin K, Sun Y, Xie L, Batteur S, Mao XO, Smelick C, Logvinova A, Greenberg DA (2003) Neurogenesis and aging: FGF-2 and HB-EGF restore neurogenesis in hippocampus and subventricular zone of aged mice.

Jung MW, McNaughton BL (1993) Spatial selectivity of unit activity in the hippocampal granular layer. Hippocampus 3:165–182.

Kaplan M, Hinds J (1977) Neurogenesis in the adult rat: electron microscopic analysis of light radioautographs. Science (80-) 197:1092–1094.

Karten YJG, Jones MA, Jeurling SI, Cameron HA (2006) GABAergic signaling in young granule cells in the adult rat and mouse dentate gyrus. Hippocampus 16:312–320.

Kee N, Teixeira CM, Wang AH, Frankland PW (2007) Preferential incorporation of adult-generated granule cells into spatial memory networks in the dentate gyrus. Nat Neurosci 10:355–362.

Kempermann G, Kuhn HG, Gage FH (1997a) More hippocampal neurons in adult mice living in an enriched environment. Nature 386:493–495.

Kempermann G, Kuhn HG, Gage FH (1997b) Genetic influence on neurogenesis in the dentate gyrus of adult mice. Proc Natl Acad Sci U S A 94:10409–10414.

Knierim JJ (2015) The hippocampus. Curr Biol 25:R1116–R1121.

Krzisch M, Fülling C, Jabinet L, Armida J, Gebara E, Cassé F, Habbas S, Volterra A, Hornung J-P, Toni N (2016) Synaptic Adhesion Molecules Regulate the Integration of New Granule Neurons in the Postnatal Mouse Hippocampus and their Impact on Spatial Memory. Cereb Cortex 27:4048–4059.

Laplagne DA, Espósito MS, Piatti VC, Morgenstern NA, Zhao C, van Praag H, Gage FH, Schinder AF (2006) Functional Convergence of Neurons Generated in the Developing and Adult Hippocampus Macklis J, ed. PLoS Biol 4:e409.

Lee CT, Kao MH, Hou WH, Wei YT, Chen CL, Lien CC (2016) Causal Evidence for the Role of Specific GABAergic Interneuron Types in Entorhinal Recruitment of Dentate Granule Cells. Sci Rep 6.

Li L, Sultan S, Heigele S, Schmidt-Salzmann C, Toni N, Bischofberger J (2017) Silent synapses generate sparse and orthogonal action potential firing in adult-born hippocampal granule cells. Elife 6, e23612.

Lim DA, Alvarez-Buylla A (2016) The Adult Ventricular-Subventricular Zone (V-SVZ) and Olfactory Bulb (OB) Neurogenesis. Cold Spring Harb Perspect Biol 8:a018820.

Lodge M, Bischofberger J (2019) Synaptic properties of newly generated granule cells support sparse coding in the adult hippocampus. Behav Brain Res:112036.

Lugert S, Basak O, Knuckles P, Haussler U, Fabel K, Götz M, Haas CA, Kempermann G, Taylor V, Giachino C (2010) Quiescent and Active Hippocampal Neural Stem Cells with Distinct Morphologies Respond Selectively to Physiological and Pathological Stimuli and Aging. Cell Stem Cell 6:445–456.

Malberg JE, Eisch AJ, Nestler EJ, Duman RS (2000) Chronic antidepressant treatment increases neurogenesis in adult rat hippocampus. J Neurosci 20:9104–9110.

Marín-Burgin A, Mongiat LA, Pardi MB, Schinder AF (2012) Unique processing during a period of high excitation/inhibition balance in adult-born neurons. Science 335:1238–1242.

Markwardt S, Overstreet-Wadiche L (2008) GABAergic signalling to adult-generated neurons. J Physiol 586:3745–3749.

Markwardt SJ, Dieni C V, Wadiche JI, Overstreet-Wadiche L (2011) Ivy/neurogliaform interneurons coordinate activity in the neurogenic niche. Nat Neurosci 14:1407–1409.

Markwardt SJ, Wadiche JI, Overstreet-Wadiche LS (2009) Input-specific GABAergic signaling to newborn neurons in adult dentate gyrus. J Neurosci 29:15063–15072.

Marlatt MW, Potter MC, Lucassen PJ, van Praag H (2012) Running throughout middle-age improves memory function, hippocampal neurogenesis, and BDNF levels in female C57BL/6J mice. Dev Neurobiol 72:943–952.

Marr D (1971) Simple Memory: A Theory for Archicortex. Philos Trans R Soc B Biol Sci 262:23–81.

Miller BR, Hen R (2015) The current state of the neurogenic theory of depression and anxiety. Curr Opin Neurobiol 30:51–58.

Mongiat LA, Espósito MS, Lombardi G, Schinder AF (2009) Reliable Activation of Immature Neurons in the Adult Hippocampus Reh TA, ed. PLoS One 4:e5320.

Moreno-Jiménez EP, Flor-García M, Terreros-Roncal J, Rábano A, Cafini F, Pallas-Bazarra N, Ávila J, Llorens-Martín M (2019a) Adult hippocampal neurogenesis is abundant in neurologically healthy subjects and drops sharply in patients with Alzheimer's disease. Nat Med 25:554–560.

Moreno-Jiménez EP, Flor-García M, Terreros-Roncal J, Rábano A, Cafini F, Pallas-Bazarra N, Ávila J, Llorens-Martín M (2019b) Adult hippocampal neurogenesis is abundant in neurologically healthy subjects and drops sharply in patients with Alzheimer's disease. Nat Med 25:554–560.

Mouri A, Ukai M, Uchida M, Hasegawa S, Taniguchi M, Ito T, Hida H, Yoshimi A, Yamada K, Kunimoto S, Ozaki N, Nabeshima T, Noda Y (2018) Juvenile social defeat stress exposure persistently impairs social behaviors and neurogenesis. Neuropharmacology 133:23–37.

Mu Y, Zhao C, Toni N, Yao J, Gage FH (2015) Distinct roles of NMDA receptors at different

stages of granule cell development in the adult brain. Elife 4, e07871.

Nakashiba T, Cushman JD, Pelkey KA, Renaudineau S, Buhl DL, McHugh TJ, Barrera VR, Chittajallu R, Iwamoto KS, McBain CJ, Fanselow MS, Tonegawa S (2012) Young Dentate Granule Cells Mediate Pattern Separation, whereas Old Granule Cells Facilitate Pattern Completion. Cell 149:188–201.

Nielsen TA, DiGregorio DA, Silver RA (2004) Modulation of Glutamate Mobility Reveals the Mechanism Underlying Slow-Rising AMPAR EPSCs and the Diffusion Coefficient in the Synaptic Cleft. Neuron 42:757–771.

Nishijima T, Kamidozono Y, Ishiizumi A, Amemiya S, Kita I (2017) Negative rebound in hippocampal neurogenesis following exercise cessation. Am J Physiol Integr Comp Physiol 312:R347–R357.

Overstreet-Wadiche L, Bromberg D, Bensen A, Westbrook G (2005a) GABAergic Signaling to Newborn Neurons in entate Gyrus. J Neurophysiol 94:4528–4532.

Overstreet-Wadiche L, Bromberg D, Bensen A, Westbrook G (2005b) GABAergic Signaling to Newborn Neurons in entate Gyrus. J Neurophysiol 94:4528–4532.

Overstreet LS, Hentges ST, Bumaschny VF, de Souza FSJ, Smart JL, Santangelo AM, Low MJ, Westbrook GL, Rubinstein M (2004) A transgenic marker for newly born granule cells in dentate gyrus. J Neurosci 24:3251–3259.

Parent JM, Yu TW, Leibowitz RT, Geschwind DH, Sloviter RS, Lowenstein DH (1997) Dentate granule cell neurogenesis is increased by seizures and contributes to aberrant network reorganization in the adult rat hippocampus. J Neurosci 17:3727–3738.

Pavlov I, Savtchenko LP, Kullmann DM, Semyanov A, Walker MC (2009) Outwardly rectifying tonically active GABAA receptors in pyramidal cells modulate neuronal offset, not gain. J Neurosci 29:15341–15350.

Pernía-Andrade AJ, Jonas P (2014) Theta-Gamma-Modulated Synaptic Currents in Hippocampal Granule Cells In Vivo Define a Mechanism for Network Oscillations. Neuron 81:140–152.

Rakic P (2002) Neurogenesis in adult primate neocortex: an evaluation of the evidence. Nat Rev Neurosci 3:65–71.

Ramirez-Amaya V, Marrone DF, Gage FH, Worley PF, Barnes CA (2006) Integration of New Neurons into Functional Neural Networks. J Neurosci 26:12237–12241.

Rolls ET (2013) The mechanisms for pattern completion and pattern separation in the hippocampus. Front Syst Neurosci 7:74.

Rossi DJ, Hamann M (1998) Spillover-mediated transmission at inhibitory synapses promoted by high affinity α6 subunit GABA(A) receptors and glomerular geometry. Neuron 20:783–795.

Sah N, Peterson BD, Lubejko ST, Vivar C, van Praag H (2017) Running reorganizes the circuitry of one-week-old adult-born hippocampal neurons. Sci Rep 7:10903.

Sambandan S, Sauer J-F, Vida I, Bartos M (2010) Associative plasticity at excitatory synapses facilitates recruitment of fast-spiking interneurons in the dentate gyrus. J Neurosci 30:11826–11837.

Schmidt-Hieber C, Jonas P, Bischofberger J (2004) Enhanced synaptic plasticity in newly generated granule cells of the adult hippocampus. Nature 429:184–187.

Schmidt-Hieber C, Jonas P, Bischofberger J (2007) Subthreshold dendritic signal processing and coincidence detection in dentate gyrus granule cells. J Neurosci 27:8430–8441.

Schmidt-Salzmann C, Li L, Bischofberger J (2014) Functional properties of extrasynaptic AMPA and NMDA receptors during postnatal hippocampal neurogenesis. J Physiol 592:125–140.

Schulz JM, Knoflach F, Hernandez M-C, Bischofberger J (2018) Dendrite-targeting interneurons control synaptic NMDA-receptor activation via nonlinear α5-GABAA receptors. Nat Commun 9:3576.

Serwanski DR, Miralles CP, Christie SB, Mehta AK, Li X, De Blas AL (2006) Synaptic and nonsynaptic localization of GABAA receptors containing the α5 subunit in the rat brain. J Comp Neurol 499:458–470.

Sigurdsson T, Stark KL, Karayiorgou M, Gogos JA, Gordon JA (2010) Impaired hippocampal–prefrontal synchrony in a genetic mouse model of schizophrenia. Nature 464:763–767.

Smith SS (2013) α4βδ GABAA receptors and tonic inhibitory current during adolescence: effects on mood and synaptic plasticity. Front Neural Circuits 7:135.

Song J, Sun J, Moss J, Wen Z, Sun GJ, Hsu D, Zhong C, Davoudi H, Christian KM, Toni N, Ming G, Song H (2013) Parvalbumin interneurons mediate neuronal circuitry–neurogenesis coupling in the adult hippocampus. Nat Neurosci 16:1728–1730.

Spalding KL, Bergmann O, Alkass K, Bernard S, Salehpour M, Huttner HB, Boström E, Westerlund I, Line Vial C, Buchholz BA, Ran Possnert G, Mash DC, Druid H, Frisé J (2013) Dynamics of Hippocampal Neurogenesis in Adult Humans. Cell 153:1219–1227.

Stocca G, Schmidt-Hieber C, Bischofberger J (2008) Differential dendritic Ca^{2+} signalling in

young and mature hippocampal granule cells. J Physiol 586:3795–3811.

Sun C, Sieghart W, Kapur J (2004) Distribution of α1, α4, γ2, and δ subunits of GABAA receptors in hippocampal granule cells. Brain Res 1029:207–216.

Sun GJ, Sailor KA, Mahmood QA, Chavali N, Christian KM, Song H, Ming G (2013) Seamless reconstruction of intact adult-born neurons by serial end-block imaging reveals complex axonal guidance and development in the adult hippocampus. J Neurosci 33:11400–11411.

Szabadics J, Tamás G, Soltesz I (2007) Different transmitter transients underlie presynaptic cell type specificity of GABAA,slow and GABAA,fast. Proc Natl Acad Sci U S A 104:14831–14836.

Takahashi T, Nowakowski RS, Caviness VS (1992) BUdR as an S-phase marker for quantitative studies of cytokinetic behaviour in the murine cerebral ventricular zone. J Neurocytol 21:185–197.

Tashiro A, Makino H, Gage FH (2007) Experience-Specific Functional Modification of the Dentate Gyrus through Adult Neurogenesis: A Critical Period during an Immature Stage. J Neurosci 27:3252–3259.

Tashiro A, Sandler VM, Toni N, Zhao C, Gage FH (2006) NMDA-receptor-mediated, cell-specific integration of new neurons in adult dentate gyrus. Nature 442:929–933.

Taupin P (2007) BrdU immunohistochemistry for studying adult neurogenesis: Paradigms, pitfalls, limitations, and validation. Brain Res Rev 53:198–214.

Temprana SG, Mongiat LA, Yang SM, Trinchero MF, Alvarez DD, Kropff E, Giacomini D, Beltramone N, Lanuza GM, Schinder AF (2015) Delayed Coupling to Feedback Inhibition during a Critical Period for the Integration of Adult-Born Granule Cells. Neuron 85:116–130.

Toni N, Teng EM, Bushong EA, Aimone JB, Zhao C, Consiglio A, van Praag H, Martone ME, Ellisman MH, Gage FH (2007) Synapse formation on neurons born in the adult hippocampus. Nat Neurosci 10:727–734.

Treves A, Rolls ET (1992) Computational constraints suggest the need for two distinct input systems to the hippocampal CA3 network. Hippocampus 2:189–199.

Treves A, Rolls ET (1994) Computational analysis of the role of the hippocampus in memory. Hippocampus 4:374–391.

Treves A, Tashiro A, Witter MP, Moser EI (2008) What is the mammalian dentate gyrus good for? Neuroscience 154:1155–1172.

Trinchero MF, Buttner KA, Sulkes Cuevas JN, Temprana SG, Fontanet PA, Monzón-Salinas MC, Ledda F, Paratcha G, Schinder AF (2017) High Plasticity of New Granule Cells in the Aging Hippocampus. Cell Rep 21:1129–1139.

Tronel S, Fabre A, Charrier V, Oliet SHR, Gage FH, Abrous DN (2010) Spatial learning sculpts the dendritic arbor of adult-born hippocampal neurons. Proc Natl Acad Sci U S A 107:7963–7968.

van Praag H, Kempermann G, Gage FH (1999) Running increases cell proliferation and neurogenesis in the adult mouse dentate gyrus. Nat Neurosci 2:266–270.

van Praag H, Schinder AF, Christie BR, Toni N, Palmer TD, Gage FH (2002) Functional neurogenesis in the adult hippocampus. Nature 415:1030–1034.

Vargas-Caballero M, Martin LJ, Salter MW, Orser BA, Paulsen O (2010) α5 Subunit-containing GABAA receptors mediate a slowly decaying inhibitory synaptic current in CA1 pyramidal neurons following Schaffer collateral activation. Neuropharmacology 58:668–675.

Vetreno RP, Crews FT (2015) Binge ethanol exposure during adolescence leads to a persistent loss of neurogenesis in the dorsal and ventral hippocampus that is associated with impaired adult cognitive functioning. Front Neurosci 9:35.

Vivar C, Potter MC, van Praag H (2012) All About Running: Synaptic Plasticity, Growth Factors and Adult Hippocampal Neurogenesis. In, pp 189–210. Springer, Berlin, Heidelberg.

Wei W, Zhang N, Peng Z, Houser CR, Mody I (2003) Perisynaptic localization of delta subunit-containing GABA(A) receptors and their activation by GABA spillover in the mouse dentate gyrus. J Neurosci 23:10650–10661.

Woods NI, Vaaga CE, Chatzi C, Adelson JD, Collie MF, Perederiy J V., Tovar KR, Westbrook GL (2018) Preferential Targeting of Lateral Entorhinal Inputs onto Newly Integrated Granule Cells. J Neurosci 38:5843–5853.

Young CC, Stegen M, Bernard R, Müller M, Bischofberger J, Veh RW, Haas CA, Wolfart J (2009) Upregulation of inward rectifier K $^{+}$ (Kir2) channels in dentate gyrus granule cells in temporal lobe epilepsy. J Physiol 587:4213–4233.

Zarnowska ED, Keist R, Rudolph U, Pearce RA (2009) GABAA receptor α5 subunits contribute to GABA A,slow synaptic inhibition in mouse hippocampus. J Neurophysiol 101:1179–1191.

Zhao C, Teng EM, Summers RG, Ming G-L, Gage FH (2006) Distinct morphological stages

of dentate granule neuron maturation in the adult mouse hippocampus. J Neurosci 26:3–11.

7. Scientific Publications

7.1 Review: Lodge & Bischofberger (2019). Synaptic properties of newly generated granule cells support sparse coding in the hippocampus. Behavioural Brain Research, 372:112036.

Behavioural Brain Research 372 (2019) 112036

Contents lists available at ScienceDirect

Behavioural Brain Research

journal homepage: www.elsevier.com/locate/bbr

Synaptic properties of newly generated granule cells support sparse coding in the adult hippocampus

Meredith Lodge, Josef Bischofberger*

Department of Biomedicine, University of Basel, Pestalozzistr. 20, CH-4056 Basel, Switzerland

ARTICLE INFO

Keywords:
Adult neurogenesis
Sparse coding
Hippocampus
Granule cells
Glutamatergic synapses
GABA receptors
NMDA receptors

ABSTRACT

In the adult hippocampus new neurons are continuously generated throughout life and integrate into the existing network *via* the formation of thousands of new synapses. Adult-born granule cells are known to improve learning and memory at about 3–6 weeks post mitosis by enhancing the brains ability to discriminate similar memory items. However, the underlying mechanisms are still controversial. Here we review the distinct functional properties of the newborn young neurons, including enhanced excitability, reduced GABAergic inhibition, NMDA-receptor dependent electrogenesis and enhanced synaptic plasticity. Although these cellular properties provide a competitive advantage for synapse formation, they do not generate 'hyperactivity' of young neurons. By contrast, *in vivo* evidence from immediate early gene expression and calcium imaging indicates that young neurons show sparse activity during learning. Similarly, *in vitro* data show a low number of high-impact synapses, leading to activation young cells by distinct subsets of afferent fibers with minimal overlap. Overall, the enhanced excitability of young cells does not generate hyperactivity but rather counterbalance the low number of excitatory input synapses. Finally, sparse coding in young neurons has been shown to be crucial for neurogenesis-dependent improvement of learning behavior. Taken together, converging evidence from cell physiology and behavioral studies suggests a mechanism that can explain the beneficial effects of adult neurogenesis on brain function.

1. Introduction

Establishing functional analysis using patch-clamp recordings from adult-born hippocampal granule cells [1], was a major step forward in establishing adult neurogenesis as a widely accepted phenomenon within the broader neuroscience community. Subsequently, several studies appeared showing distinct functional properties of newborn neurons in the adult brain, including enhanced excitability and enhanced synaptic plasticity, relative to the mature granule cell (GC) population [2,3]. Furthermore, GABAergic synapses were shown to be initially depolarizing until 3 weeks of age [4,5], followed by a phase with hyperpolarized E_{GABA} and a slower time course of the GABAergic synaptic inhibition [6]. At 8 weeks post mitosis, adult born granule cells were found to finally show identical GABAergic inhibition to mature GCs [7]. Based on these cell biological studies it was concluded that young neurons are 'hyperactive' and 'hyperexcitable' during learning behavior and memory processing [8,9]. Remarkably, on the behavioral level it was shown that adult neurogenesis improves learning by increasing the brains capability to distinguish between similar memory items, a process called pattern separation. Specifically, several studies showed that newborn 4-week-old neurons facilitate pattern separation during learning, while older neurons seem to be less effective [10,11] Modeling studies have suggested that hippocampal pattern separation is dependent on sparse activity and orthogonal coding of neuronal information in the dentate gyrus-mossy fiber system [12,13]. Therefore, cellular 'hyperactivity' of young neurons would be in conflict with improved behavioral pattern separation. This apparent paradox of hyperactive cells *versus* improved pattern separation, has been controversially discussed in the past years [14–17]. However, recent studies have provided a better understanding of the young neuron's excitability and their sparse connectivity, shedding new light onto this apparent discrepancy. These new results suggest that evidence from cell biology and behavioral studies are converging to a more coherent view.

2. Enhanced excitability of young granule cells

The structure and function of young GCs differ from mature cells in the dentate gyrus in a substantial number of ways, including synaptic connectivity, firing patterns and membrane excitability (Fig. 1). Post-mitotic development of young GCs has been extensively studied in adult

* Corresponding author.
E-mail address: Josef.Bischofberger@unibas.ch (J. Bischofberger).

https://doi.org/10.1016/j.bbr.2019.112036
Received 15 April 2019; Received in revised form 6 June 2019; Accepted 11 June 2019
Available online 13 June 2019

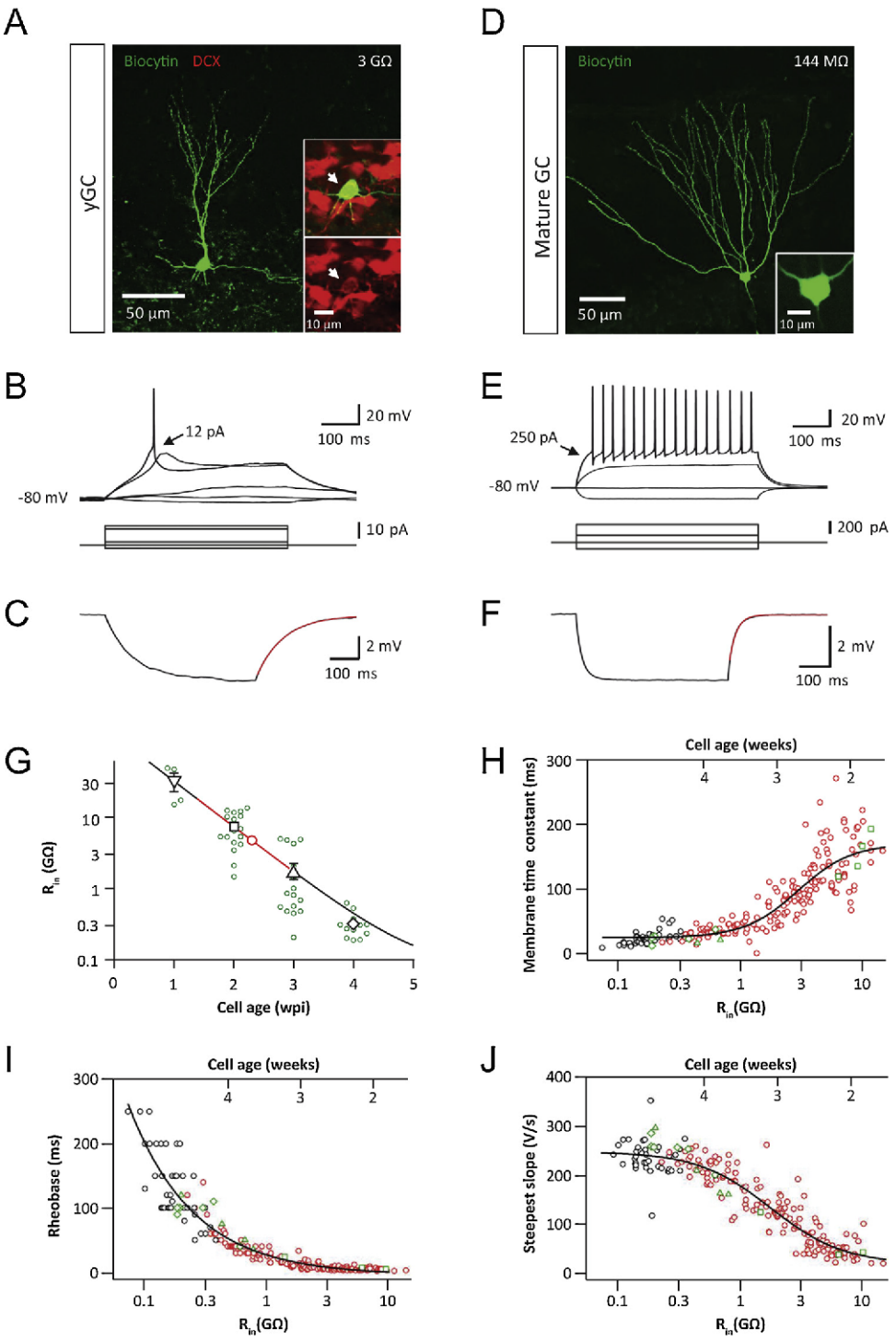

Fig. 1. Intrinsic properties differ between young and mature granule cells. (A) Confocal image of a biocytin-filled (green) newborn granule cell with an input resistance of 3 GΩ corresponding to 2.5 weeks post mitosis. Inset images show immunohistochemical staining of DCX expression (red). (B) Low-threshold Ca^{2+}-spike and AP induced by somatic current injection (same cell as A). Minimal current for AP induction is indicated. (C) Decay after a small hyperpolarization revealed a slow membrane time constant (τ_m = 94 ms, monoexponentially fit in red). (D) Morphology of a mature granule cell with an input resistance of 144 MΩ. (E) Mature firing pattern for the cell in (D). (F) Voltage decay after the current pulse revealed a fast τ_m of 23 ms. (G) Semi-logarithmic plot showing that input resistance (R_{in}) decreases with maturation. Green circles represent individual GFP-positive birth-dated GCs. Black circles represent the mean ± s.e.m. of GFP-positive neurons. Red line indicates the range of the R_{in} of recorded DCX + neurons (1.5–18 GΩ) corresponding to 1.5–3 weeks post mitosis. (H–K) Semi-logarithmic plots of membrane time constant (H), threshold current to evoke an AP (rheobase) (I) and steepest slope of APs (K) of mature GCs (black), $DsRed^+$ young (red) and GFP-positive birth-dated GCs (green). Lines represent sigmoidal (H, K) or double exponential (I) fits. Adapted from Heigele et al., [24].

mice. After cell division the young neurons rapidly start to grow, showing a total dendritic length (TDL) of about 500 µm at 2 weeks post mitosis (wpm) and further increase to about 1000 µm at 3 wpm [18–20]. In Fig. 1A, B a 2.5-week-old biocytin filled neuron is shown with an immature dendritic tree, which fired action potentials (AP) with excitatory currents in the range of a few picoampere (pA) - two orders of magnitude lower than typical mature GCs (Fig. 1D, E). This early growth period is followed by synaptic refinement and dendritic pruning, until the neurons resemble fully mature granule cells with a TDL of about 2 mm at around 6–8 weeks post-mitosis [20,21]. The cell capacitance is initially very small, around 20 pF in the first week, and increases up to about 60 pF during the next 4–6 weeks [22–24]. In addition, young GCs have initially a high membrane resistivity, resulting in a remarkably high electrical input resistance (R_{in}) of about 32 GΩ compared to about 200 MΩ in mature GCs. This means that small currents generate relatively large membrane depolarizations in the young neurons. The high membrane resistance also leads to a slow membrane time constant of about 150 ms at 1–2 wpm, promoting temporal integration of synaptic potentials (Fig. 1C) [2,24,25]. Subsequently, the R_{in} decays exponentially with a 4-fold decrease per week falling below 1 GΩ between 3-4 weeks of cell age (Fig. 1G) [24,26]. The change in R_{in} with maturation is most likely generated by an activity-dependent upregulation in the density of inward-rectifier potassium channels (Kir2, Kir3.2) and ion channels from the two-pore-domain

(K2P) family [23,27,28], which also directly generates a pronounced developmental speed up of the membrane time constant at about 3–4 wpm (Fig. 1H).

The high R_{in} is not only functionally interesting, but also constitutes a challenge for any patch-clamp analysis, potentially generating erroneous results. The small leak conductance introduced at the pipette tip might artificially reduce the recorded R_{in} due to the parallel circuit and depolarize the measured membrane potential (detailed in [24]). Therefore, reported values might actually represent lower estimates of the real values. Nevertheless, using thick-walled glass capillaries and fire polishing of pipette tips allows to obtain seal resistances above 100 GΩ (approximately 10-times higher than R_{in}) and therefore errors are minimized below 10%. If such quality criteria are also used for measuring resting membrane potentials in young GCs, the reported values are relatively similar to mature GCs (−80 mV) [2,24,26].

The high input resistance together with the slow membrane time constant renders young GCs very sensitive to small excitatory currents. As shown in Fig. 1I, the rheobase, i.e. the minimal current to evoke spiking, varies from about 5 pA in young up to 200 pA in fully mature cells, spanning several orders of magnitude. In addition there are low-threshold calcium spikes generated by somato-dendritic T-type calcium channels, which further boost small EPSPs towards the action potential (AP) threshold [2,22,29].

However, already at this stage there are a number of important 'checks and balances'. Firstly, before 3 weeks, young GCs show a higher AP threshold of about −35 mV in contrast to −45 mV in mature GCs [24]. Secondly, voltage-gated sodium and potassium currents were found to be smaller in young as compared to mature GCs, which reduces the AP amplitude, the maximal rate of rise (Fig. 1J) and most importantly the maximal firing frequency [23,24]. As a result, young GCs fire only one or a few spikes during persistent current injection before 3 wpm (Fig. 1B). Finally, the density of excitatory synapses and the amplitude of excitatory synaptic currents are much smaller in young GCs up to 4 weeks of age (see below). Thus, the high R_{in} compensates for the smaller glutamatergic synaptic currents, to finally obtain a synapse-evoked spiking probability in young 2–4 wpm GCs, which is relatively similar to mature cells – at least in the absence of GABAergic inhibition [23,26,30].

Taken together, electrical excitability fundamentally changes during post-mitotic development of newborn GCs in the adult hippocampus. However, increased excitability and increased sensitivity for small excitatory currents do not necessary translate into hyper-excitability and excessive AP firing. In contrast, excitability is balanced by lower density of voltage-gated ion channels, pronounced spike frequency adaptation and lower synaptic connectivity.

3. GABAergic synaptic inputs drive both excitation and shunting inhibition

Post-mitotic granule cells begin to develop GABAergic synaptic contacts as early as 4 days post-mitosis [31] and these synapses gradually increase in strength during the next 6 weeks [5,32,33]. The first interneurons which were found to contact young GCs at about 1 wpm were NO-synthase (NOS) positive neurogliaform/ivy cells and parvalbumin-positive (PV) basket cells [34,35]. In a very elegant study by Linda Overstreet-Wadiche and colleagues it was shown that these early GABAergic synaptic currents have slow time course and small amplitudes, but are nevertheless generated by bona fide synapses and do not represent spillover from neighboring synapses [36]. The functional properties are actually very similar to mature synapses formed by neurogliaform cells onto mature GCs [34].

Similar to embryonic brain development the GABA reversal potential (E_{GABA}) in young neurons is relatively depolarized to about -35 mV until 3 weeks post-mitosis in contrast to about −80 mV measured in mature GCs (Fig. 2) [4,5,24,37]. This is due to a relatively high internal chloride concentration (~25 mM) generated by high expression of NKCC1 and the low expression of KCC2 chloride transporters and has important consequences for the development and survival of young neurons [5,38,39]. More specifically it has been shown that feedback 'inhibition' *via* PV interneurons is critically important for mediating the survival-promoting effect of environmental enrichment during the first 2 weeks after mitosis [35]. In this context it should be noted that the first glutamatergic synapses also form very early at about 7 days post-mitosis. However, these early synapses express predominantly NMDA receptors and very little to no AMPA receptors. Therefore, they might be considered to be functionally silent [33,40]. Nevertheless, it was shown that the depolarizing GABAergic synapses can powerfully unblock NMDA receptors and might thereby induce enough calcium influx to stimulate phosphorylation of CREB and other growth promoting proteins, as well as the unsilencing of glutamatergic synapses [39,41].

Does a depolarized reversal potential of -35 mV mean that GABA is always excitatory? An important factor in this context is the AP threshold. If E_{GABA} is above the AP threshold, excitation is expected to be the predominant outcome. In the case that E_{GABA} is below the threshold, but more depolarized than the resting potential, GABA is expected to generate depolarizing shunting inhibition. In contrast to hyperpolarizing inhibition, shunting inhibition is silent without glutamatergic excitatory synaptic inputs. But when combined with glutamatergic EPSPs, AP initiation is blocked by short circuiting depolarization beyond E_{GABA}. In young GCs before 3 wpm it turned out that E_{GABA} is sitting pretty much exactly at the AP threshold, located at −35 mV [24]. That has important consequences. When only about 10% of connected presynaptic GABAergic interneurons (3–4 cells) fire a brief burst of APs, an average synaptic conductance of about 1.5 nS is generated in a typical 2–3-week-old cell. This conductance was indeed shown to facilitate the generation of APs in young GCs (Fig. 3A). However, a larger number of active GABAergic synapses (> 30% of available connections) was shown to inhibit firing *via* shunting inhibition of AP initiation (Fig. 3B, C) [24]. This large GABAergic conductance promotes rapid depolarization towards E_{GABA}, but at the same time prevents further depolarization beyond this point (Fig. 3A, upper right). Thereby, AP initiation in young GCs can be powerfully controlled by the number of active GABA interneurons.

Currently it is unknown what percentage of interneurons is active under different behavioral conditions. However, the dentate gyrus represents a highly competitive 'winner-takes all' network with strong lateral feedback inhibition [42–44]. PV-positive basket cells can be easily recruited by a small number of active mature GCs, exerting strong inhibition to neighboring GCs locally restricted within about 200 µm [44–46]. Furthermore, *in vivo* recordings in awake animals showed that mature GCs are under strong inhibitory control by local fast-spiking GABAergic interneurons during theta-nested gamma oscillations [47]. On average, the locally generated inhibitory charge outnumbers the excitatory charge generated by perforant-path synapses by a factor of 2.3. Only a small proportion of winner GCs escape from this inhibition from time to time, generating the well-known sparse population code reported for dentate gyrus GCs [48–51]. Thus, it is expected that young GCs will receive substantial GABAergic synaptic inputs, generating both excitation (when about 10% of synapses are active) as well as shunting inhibition (when > 30% of synapses are active), to counterbalance enhanced excitability during increased hippocampal network activity.

At 4 weeks post-mitosis, E_{GABA} becomes very similar to mature GCs sitting close to the resting potential of about −80 mV (Fig. 2B) [6,24]. Nevertheless, GABAergic synapses are still not fully mature at this stage. As pointed out by Alejandro Schinder and colleagues, a prominent feature at this developmental stage still is the slower time course of perisomatic inhibition mediated by PV interneurons relative to mature GCs [6]. Although local stimulation of perforant path (PP) fibers in the molecular layer can generate a ratio of GABAergic and glutamatergic peak conductance amplitudes (I/E ratio) in young GCs similar to mature cells, the slower rise time of inhibitory currents provides a window

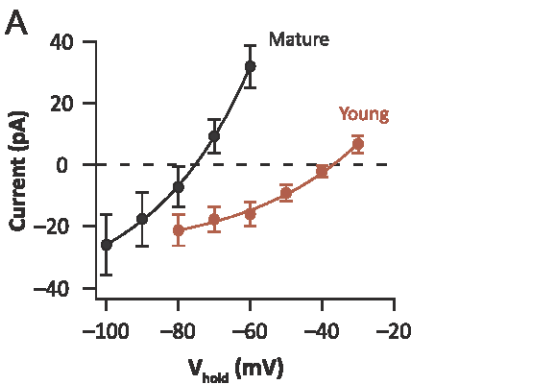

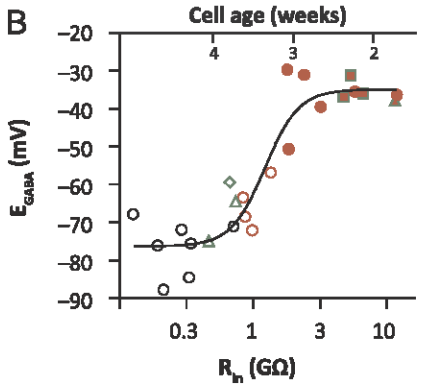

Fig. 2. GABA-reversal of young granule cells is more depolarized than in mature cells. Gramicidin perforated-patch recordings of GABAergic synaptic currents in young and mature granule cells. (A) The average amplitudes of GABAergic synaptic currents from young (red) and mature (black) GCs show a reversal potential of −35 mV and −80 mV, respectively (data presented as mean ± s.e.m). (B) E_{GABA} in individual granule cells was plotted against input resistance (R_{in}) for DCX-DsRed + young (red), GFP virus–labeled (green symbols) and mature GCs (black circles). Adapted from Heigele et al., [24].

of spiking opportunity. Indeed, population analysis in hippocampal slices using calcium imaging revealed that young GCs can be more easily recruited under certain conditions. For example, a single shock stimulation of PP fibers, which recruits about 20% of mature GCs, will recruit 40% of young GCs at 4 wpm [6]. Therefore, during single shock stimuli young neurons are about 2-times more excitable than mature GCs.

More recently, additional studies have shown that at 4wpm the I/E ratio is actually dependent of feedforward *versus* feedback inhibition. While the I/E ratio is smaller in feedforward inhibition of young GCs, feedback inhibition is already rather similar to mature GCs [30,52]. These studies also clearly show that although I/E ratio is overall smaller in young GCs at 4 wpm, GABAergic inhibition can effectively restrict spiking at this stage [30].

Although the smaller I/E ratio may facilitate spiking in young GCs during single shock conditions, the substantially slower decay of the GABAergic conductance also acts to counterbalance excitability during ongoing network activity. Due to stronger temporal summation during continuous activity of local interneurons generated by theta-nested gamma oscillations [47], the slow GABAergic inhibition will generate larger inhibition in young GCs during repetitive activity relative to single stimuli. As a result I/E ratio during trains of stimuli at frequencies between 20–40 Hz is identical in young 4 wpm and mature GCs, effectively blocking spiking [52].

Taken together, young GCs form GABAergic synapses as soon as 4 days post-mitosis and show less pronounced GABAergic inhibition than mature GCs under certain conditions. However, this does not necessarily generate hyper-excitability. There are efficient ways for powerful GABAergic inhibition at all stages of development including effective temporal summation of the slower GABAergic conductance and strong shunting inhibition. This allows for reliable control of young GC spiking by local GABAergic interneurons.

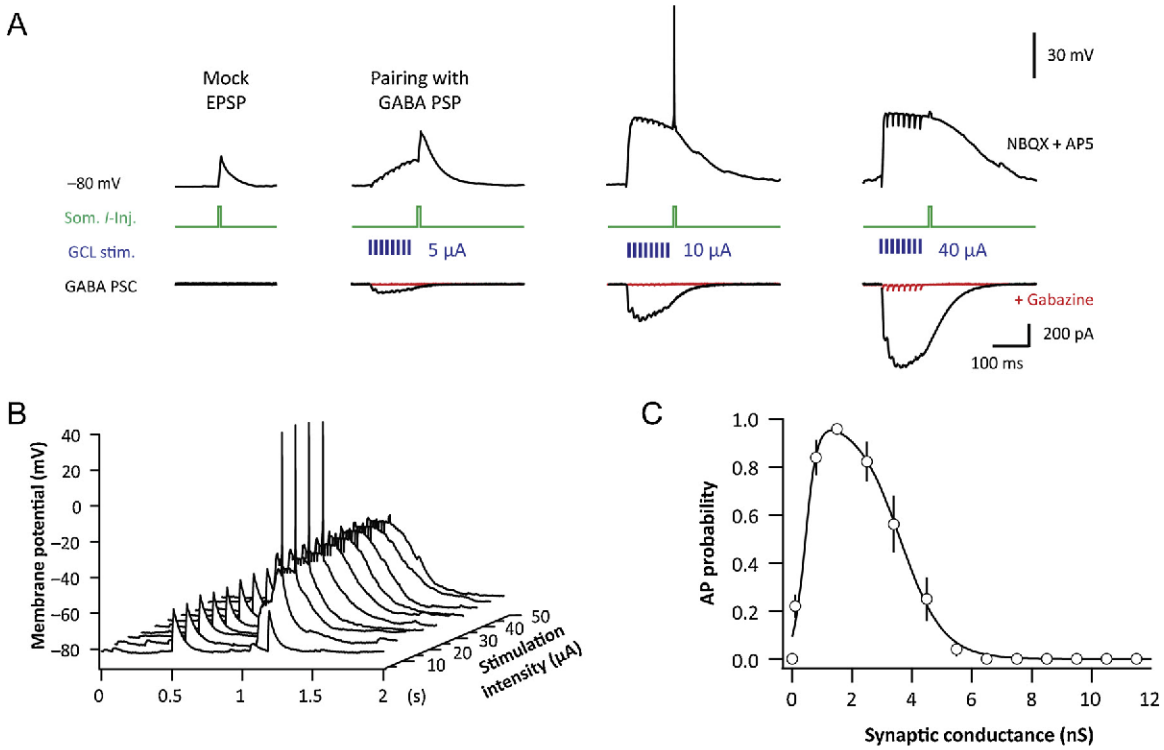

Fig. 3. GABA-induced excitation and inhibition of AP firing in young granule cells. (A) Mock EPSPs were generated by a somatic current injection (10 ms, green) and paired with GABAergic postsynaptic potentials (PSPs) evoked by stimulation pulses of increasing intensity (200 µs, eight times at 50 Hz) in the presence of NBQX and AP5 (upper traces). Lower traces show GABA PSCs using the same stimulation intensity before **(black)** and after application of gabazine (red). (B) A sequence of traces showing pairing with increasing synaptic stimulation intensity, as indicated on the right axis. Spiking is restricted to low stimulation intensities. (C) Firing probability is plotted against the GABA PSC conductance, showing that firing could only be evoked in a certain conductance range (0.4–4 nS). Continuous line represents a fitted curve consisting of the product of a sigmoidal rise and decay. Data are presented as mean ± s.e.m. Adapted from Heigele et al., [24].

4. Selective activation of young neurons *via* NMDA-dependent spiking

At around 7 days post-mitosis the first glutamatergic synapses were reported, which might originate from hilar mossy cells [33,40,53]. During the second post-mitotic week further glutamatergic synapses are formed by axons from lateral and medial entorhinal cortex (LEC, MEC) [40,54]. This shows that the young neurons form synapses with the major afferent glutamatergic input pathways early on. Until 3 wpm glutamatergic synapses show immature functional properties including preferential expression of NMDA receptors [26,41,53]. Similarly, the extrasynaptic membrane of newborn granule cells harbors a large number of NMDA receptors, even in the youngest cells without any synapses [55]. The extrasynaptic NMDA/AMPA receptor conductance ratio is 3-times higher in young GCs before 3 wpm and declines towards a mature ratio of about 1:1 after the loss of DCX expression. These findings suggest that extrasynaptic NMDA receptors are key players in the process of new synapse formation in newly generated granule cells. They might be activated by extrasynaptic glutamate spillover from neighboring preexisting axon terminals and thereby initiate growth of new filopodia and spines in a competitive manner [56–58]. Furthermore, NMDAR activation between 1–2 wpm was shown to be important for survival of the newborn cells, which are otherwise eliminated *via* apoptosis [59].

What is the functional role of NMDA receptors in newborn young neurons? Activation of extrasynaptic NMDA receptors by a small number of glutamate pulses was shown to initiate calcium-induced growth of filopodia and new spines in developing pyramidal cells [60]. Therefore, the high density of extrasynaptic NMDA receptors in young GCs is consistent with the well-documented role of these receptors for glutamatergic synapse formation in early cortical development [61,62] as well as in adult neurogenesis [57,63]. The synaptic NMDAR/AMPAR conductance ratio is initially 10:1 at 2 wpm, substantially higher than the extrasynaptic ratio of 3:1 [26,55], indicating that NMDA receptors are selectively enriched and targeted into developing postsynaptic filopodia. This not only supports synapse formation but also lays the foundation for the adjustment of synaptic strength during activity-dependent synaptic plasticity (see below [2,3],).

NMDAR activation is dependent on several factors besides glutamate binding. In addition to the requirement for postsynaptic depolarization due to the voltage-dependent magnesium block, NMDA receptors need to bind D-serine or glycine as a co-agonist, which is provided by astrocytes [64]. Using a transgenic approach to block vesicular release from astrocytes, it was shown that NMDAR activation and synapse formation in young GCs is critically dependent on astroglial D-serine [63]. The precise conditions for astrocytic D-serine release is not fully understood. However, it was suggested that cooperative neuronal activity within an astrocytic domain activates glial CB1 receptors, leading to calcium-induced release of D-serine, which feeds back to neuronal NMDAR activation [64,65]. Interestingly, this feedback seems to be locally restricted to the neuropil ('synaptic island') controlled by the fine processes of the activated astrocyte [64]. Thus, cooperative neuronal activity will induce locally restricted D-serine release. Thereby synapse formation in young GC dendrites is locally controlled by correlated afferent activity within spatially distinct active synaptic islands [63].

What are the electrophysiological consequences of synaptic NMDA receptor activation in young yGCs? As shown in Fig. 4, electrical stimulation of glutamatergic synapses in the molecular layer with a low intensity readily evokes subthreshold EPSPs in mature as well as in 2-week-old GCs. In contrast to mature neurons, the EPSPs in young neurons are highly sensitive to the NMDAR antagonist AP5 (Fig. 4A, B). Furthermore, brief burst stimulation (5@50 Hz) generates non-linear NMDAR-dependent summation of EPSPs in young GCs with a 10-times larger peak amplitude relative to single EPSPs. By contrast, EPSP summation is sublinear in mature GCs (Fig. 4C, D). As a consequence, the peak amplitude of burst EPSPs in mature and 2-week-old neurons is not significantly different using the same stimulation intensity [26]. Increasing stimulation intensity generates spiking in young cells as well as in mature cells (Fig. 4E, F). In contrast to mature cells, however, spiking in young neurons is critically dependent on NMDA receptors. Thus, the high expression of NMDARs in newly formed synapses of young GCs generates pronounced NMDA-dependent electrogenesis, resulting in highly non-linear summation of glutamatergic EPSPs [26]. This is supported by the small membrane capacitance (20 pF) and high electrical input resistance before 3 wpm (2–30 GΩ), which renders young GCs electrotonically compact and creates a single electrotonic compartment [24].

Interestingly, this resembles NMDA-dependent boosting of EPSPs in single dendritic branches of mature pyramidal and granule cells, which also have a small capacitance and high electrical input impedance [66–71]. Additionally, young GCs can generate simultaneous somatodendritic calcium spikes [29], similar to calcium spikes seen in distal dendritic branches of pyramidal cells [72]. Thus, until around 3 wpm a young GC can be considered to function as a single computational unit similar to individual dendritic branches in mature neurons. Afterwards, the individual dendrites become electrotonically more isolated, and the GC starts to function as a neuron with multiple computational units [66,72].

Does the enhanced excitability and efficient NMDA electrogenesis in young GCs generate hyper-excitability? Again, there are a number of important factors counterbalancing excitability. Most importantly, the number of synaptic connections is dramatically smaller at young developmental stages. It was estimated that the density of immature glutamatergic synapses at 2 and 3 wpm corresponds to only about 2% and 20% of mature values, respectively [18,26]. At 4 wpm the synapse density is still only 35% of mature and further increases during the following weeks [73]. Remarkably, synapse-evoked spiking probability at 2–4 wpm was reported to be very similar in young and mature neurons, using local afferent fiber stimulation in the molecular layer [23,26,73]. This suggests that the high sensitivity for small excitatory currents and NMDA-dependent electrogenesis in young cells does not generate hyperexcitability, but rather balances low connectivity and compensates for the low number of input synapses.

A second factor is related to the narrow cone-shaped dendritic tree structure (Fig. 5A) and the smaller TDL in young neurons of 0.5–1 mm at 2–3 wpm relative to 2 mm in mature GCs [18–21]. It was shown, that synapse-evoked firing in young GCs is efficient in case the connected afferent fiber bundle fires a brief burst (Fig. 5B), but quickly disappears when the location of the stimulation electrode is tangentially shifted to the side [26]. As a consequence, a dendritic 'firing field' is obtained with a substantially smaller width in young *versus* mature GCs (Fig. 5D, E). Furthermore, it was shown that neighboring young neurons with a soma-soma distance of about 50 µm have largely non-overlapping firing fields (15% overlap), while the large fields of mature cells are substantially overlapping (80%, Fig. 5D, E) [26]. Similarly, at 4 wpm connectivity is still sparser than in mature cells as shown by paired voltage-clamp recordings from neighboring GCs [73]. In order to simultaneously evoke EPSCs in two neighboring cells with 50% chance (soma-soma distance < 80 µm), the stimulation intensity needs to be about 2-times higher at 4 wpm than in fully mature GCs [73]. This shows that different young neurons receive inputs from distinct non-overlapping presynaptic fiber populations. This sparse connectivity patterns might support orthogonal coding of neuronal information, because different GCs participate in different cell assemblies with minimal overlap. Or in other words, different entorhinal input patterns, will activate highly distinct cell assemblies in the dentate gyrus.

Firing in mature GCs is strongly reduced by GABAergic synaptic inhibition to finally show similar activity levels than young neurons [26]. In the end, both young and mature GCs show sparse firing in response to afferent fiber stimulation. However, the underlying mechanisms are highly different. While in mature GCs inhibition is most

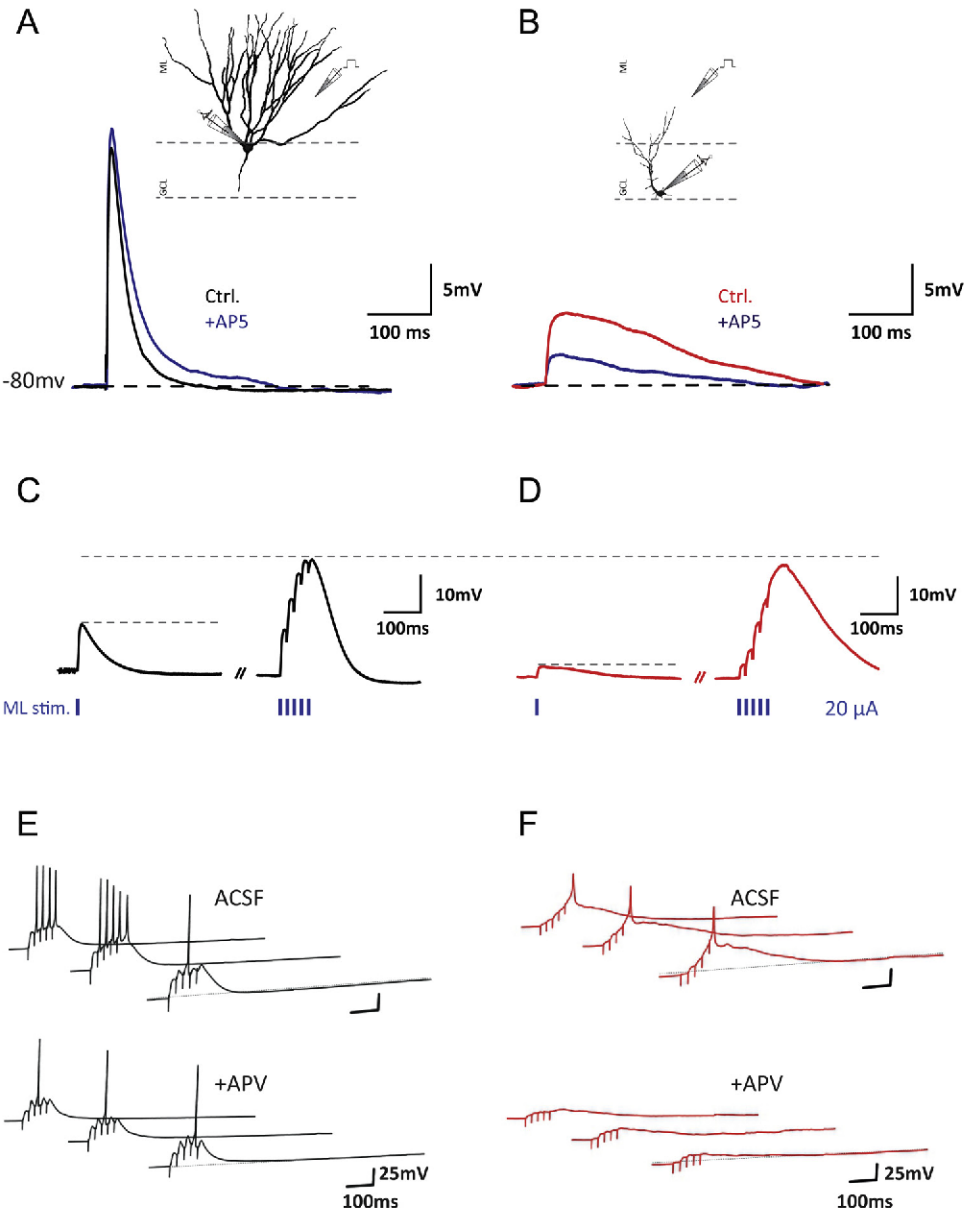

Fig. 4. NMDA-dependent electrogenesis in young GCs. (A, B) Application of AP5 (50 µM) does not significantly affect EPSP amplitude in mature granule cells (A) but decreases EPSP amplitude in a young neuron (B) at 2.5 weeks post mitosis (wpm). There is a significantly larger contribution of AP5-sensitive NMDA receptors to the EPSP in 2–3-week-old DsRed + neurons than in mature GCs. (C, D) Subthreshold summation of five EPSPs evoked by brief burst stimuli (5@50 Hz, 20 µA) in a mature (C) and a young 2.5-week-old GC (D). The ratio of burst EPSP amplitude to single EPSPs is significantly higher in young GCs relative to mature GCs.
(E, F) Increasing burst stimulation intensity (5 @ 50 Hz, 30 µA) evoked AP firing in both mature (E) and young (F) cells. With the application of AP5 (50 µM) firing was still possible in mature neurons, however, it was largely blocked in young GCs showing strong NMDA-receptor dependent spiking. Adapted from Li et al., [26].

important, the response in young GCs is predominantly shaped by the sparse afferent connectivity [30]. The total number of glutamatergic synapses in mature GCs was counted to be about 5000 in adult mice [21]. On the basis of the lower synapse density (2–20%) and shorter dendritic length (young / mature TDL = 0.25-0.5), the total number of connected synapses was estimated in young GCs, revealing a value of only about 25 (0.25*2% = 0.5%) and 500 synapses (0.5*20% = 10%), at 2 and 3 wpm, respectively [18,26]. As neighboring 2–3-week-old cells are connected to different fibers, a small subpopulation of active afferent EC fibers will discharge highly different subsets of young GCs. Similarly, in 4-week-old GCs it was reported that synaptic excitation is difficult when stimulation electrodes were positioned in the LEC or MEC, while efficient synapse-evoked spiking could be reliably achieved if stimulation is locally positioned in the molecular layer of the dentate gyrus (Dieni et al., 2013, 2016). This indicates that young GCs fire APs similarly to mature cells when a distinct small subpopulation of connected afferent fibers is active. However, the recruitment of young GCs is restricted by the sparse connectivity, which generates sparse and orthogonal responses in neighboring young neurons.

Taken together, these studies suggest that between 2–4 wpm young GCs efficiently generate APs given that a specific subset of afferent fibers is activated. The high impact of the low number of connected synapses is based on the high electrical input resistance and non-linear NMDA-dependent electrogenesis in young cells. However, spiking rapidly disappears in young cells with more unspecific stimulation paradigms, under which mature GCs still discharge, indicating that glutamatergic connectivity in young GCs is sparse and firing output is highly orthogonal.

5. Activity of young GCs during hippocampus-dependent learning

What is the functional impact of sparse AP firing in young dentate gyrus GCs for hippocampal information processing? The seminal studies of Marr suggested that the mammalian hippocampus constitutes an auto-associative memory storage based on CA3 connectivity [74]. However, it was pointed out that selectively retrieving a specific firing pattern among several learned neuronal activity patterns stored in the same set of recurrent synapses is highly non-trivial [12]. While auto-associative memory storage systems show the potentially useful property of memory retrieval by partial cues, they also tend to generalize, strongly limiting storage capacity. Computational modeling suggested that this problem could be potentially reduced in the hippocampus by

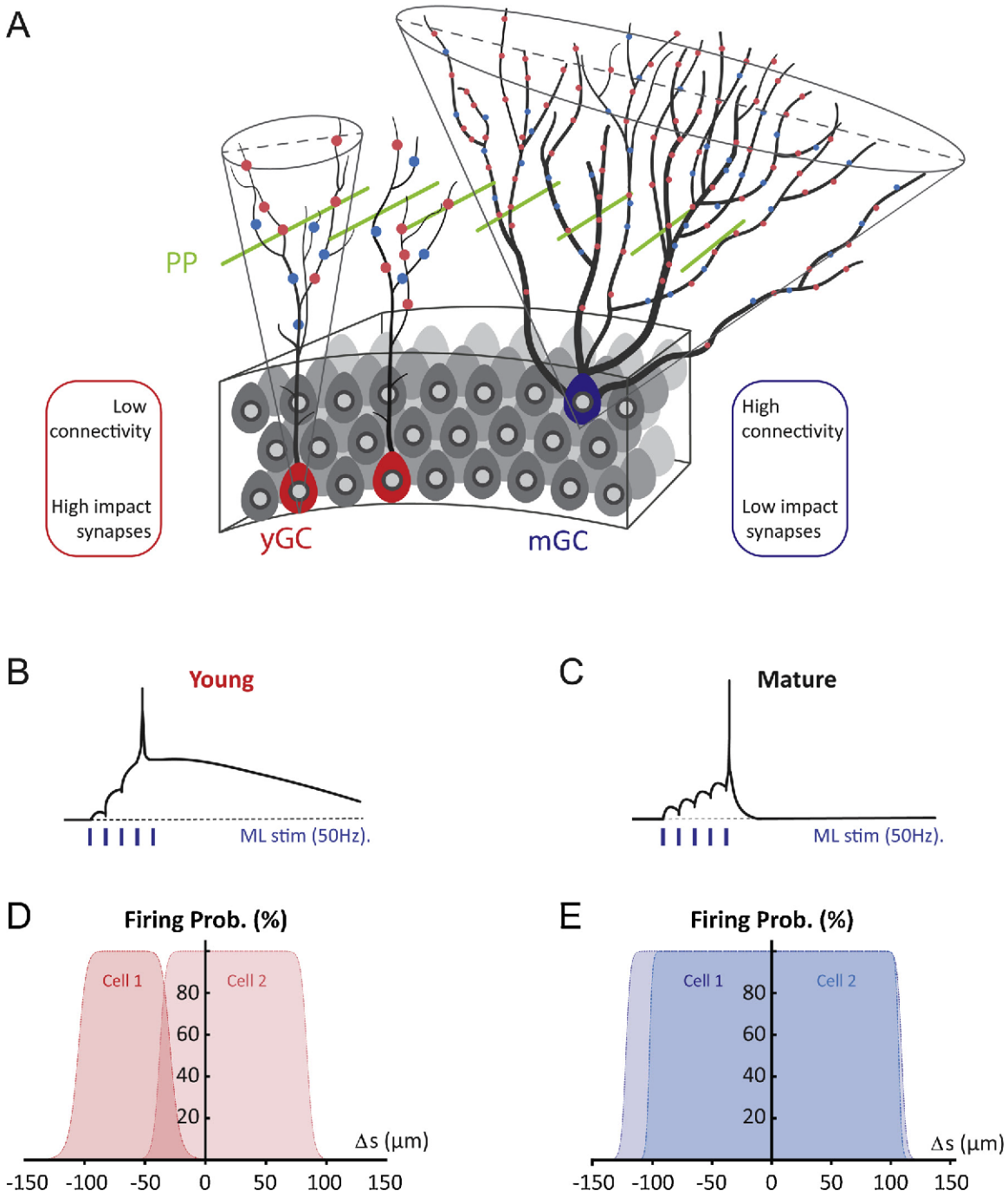

Fig. 5. Low connectivity and high excitability in young granule cells supports orthogonal firing. (A) Schematic representation of the dentate. Young granule cells (shown in red) have smaller dendritic cones (outlined in grey) than mature GCs (blue). Glutamatergic (red circles) and GABAergic (blue circles) synapses are fewer and have a high impact in depolarizing young cells. Perforant path (PP) fibers (green) traverse the molecular layer perpendicular to the dendritic trees of granule cells. The precise orientation of these fibers might vary along the dorso-ventral axis of the hippocampus. Due to the small dendritic cones of young cells, different PP fibers connect with young GCs in a non-overlapping manner. In contrast, in mature GCs glutamatergic and GABAergic synapses are present in large numbers and widely distributed. (B) Despite low numbers, the synaptic connections in young GCs efficiently generate AP firing *via* efficient temporal summation and non-linear NMDAR-dependent electrogenesis. (C) Mature cells have low intrinsic excitability, but when combined with a large number of inputs from many synapses, are able to reliably fire action potentials. (D, E) The firing probability of two neighboring young (D) or mature (E) cells plotted against the location (Δs) of stimulated afferent fibers. While young GCs are activated by distinct sets of afferent fibers, mature GCs are activated by spatially overlapping perforant path fibers.

sparse and orthogonal activity in the dentate-gyrus mossy-fiber system, acting as a 'teacher' for the CA3 network [13].

Indeed sparse activity patterns in dentate were later confirmed by many experimental studies, showing that only about 2% of dentate granule cells are active during a certain behavioral task [48–51]. However, within the CA3 region the relative proportion of active cells is typically an order of magnitude larger (30–40%). This is partially due to the dense recurrent network formed by CA3 pyramidal cells, with each neuron receiving about 4000 EC inputs and more than 10000 recurrent collateral synapses. In contrast, a single CA3 pyramidal cell receives inputs from only a few mossy fibers (~50) with exceptionally strong synaptic weight. Therefore, although the mossy-fiber input is

sparse, a brief burst in a single GCs is able to discharge a CA3 pyramidal neuron [75,76]. As dentate GCs are active in parallel to the direct perforant-path input onto CA3, a sparse and orthogonal mossy fiber input might therefore help to form distinct cell assemblies during learning for different memory items [13]. This may finally help to increase storage capacity of the hippocampus. Although it is still largely unclear how young and mature GCs contribute to this process, a few concepts have begun to emerge.

Behavioral studies suggest that newly generated young GCs improve distinction of similar memory items by promoting hippocampal pattern separation [15,77–81]. Evidently, the contribution of newly generated GCs to learning is largest when they are young, at around 3–4 wpm [10,11]. While reversible optogenetic silencing of a small cohort of 4 wpm GCs during context-fear conditioning disrupts context-dependent memory, silencing a similar cohort of 8 wpm GCs has no significant effect [10].

The number of activated newly generated young GCs has also been compared with the activity of mature GCs using immediate early gene expression, showing that the proportion of active 4-week-old GCs is slightly larger (about 4%) than the proportion of active GCs within the general NeuN-positive GC population under identical conditions (1–2%) [82–85]. Similarly, *in vivo* calcium imaging has shown that cells younger than 6 wpm are on average 1.5-fold more active than mature GCs [15]. Although slightly more active than mature GCs, the activity levels in young GCs are still one order of magnitude lower than reported activities in CA3. Finally, using direct labeling of GCs born at E17 or P7 with Thymidine analogues, no differences has been found in the proportion of c-Fos expressing cells after Watermaze learning relative to adult-born 7.5 week-old cells (1%, [86]. All of these *in vivo* results are fully consistent with the sparse and orthogonal connectivity of young GCs described above.

The sparse activity of young GCs indicates that the mossy fiber input from young neurons onto CA3 pyramidal cells would be well suited to sparsify and orthogonalize CA3 cell assemblies during learning, as suggested by computational modelling studies [13,87]. This is also consistent with the notion that young neurons need to be activated during learning to be beneficial for memory recall [15,88]. Increasing the spine density of young GCs *via* Neuroligin-2 overexpression artificially increases the active proportion of young cells during learning from 4% to about 9% Arc^+ neurons. Remarkably, this boost in activity impaired hippocampus-dependent learning, rather than improving it [85]. This shows that the sparse and orthogonal AP firing in young GCs is required for beneficial effects of adult neurogenesis on storage capacity.

Taken together, young GCs are sparsely active during hippocampus-dependent learning, consistent with their network connectivity and intrinsic properties promoting sparse firing. Reversible silencing of young neurons has shown that they are most beneficial for learning at young developmental stages of 3–4 wpm. Finally, sparse coding in young cells is critically important, because they only improve memory recall, if they are recruited during learning at sparse activity levels.

6. Functional implications of sparse and orthogonal AP firing in young GCs for hippocampal information processing

Although it is well established that newly generated young GCs contribute to learning and memory formation in a unique fashion, it is still largely unclear how this is achieved. Nevertheless, there are a few properties of young cells that nicely fit the predictions for dentate GCs as proposed by computational modeling studies.

It was predicted that the dentate gyrus should form a competitive learning matrix to remove redundancy and generate an orthogonal and sparse set of outputs towards CA3 [13]. The competitive formation of new synapses by young cells starting from the first week after mitosis perfectly fits this requirement [56–58]. The highly non-linear NMDAR-dependent electrogenesis in young GCs further supports this process, which efficiently detects correlative activity in input synapses. The high extrasynaptic NMDAR expression, the enhanced excitability and the enhanced NMDAR-dependent associative synaptic plasticity in young neurons constitute a competitive advantage over the mature GCs [2,3,80]. As a consequence of the NMDAR-dependent electrogenesis, a low number of synapses can powerfully depolarize and discharge young GCs [26]. Therefore, young cells detect and respond to coactive synapses within their small dendritic field. Due to their competitive advantage, they will easily remove such synapses from neighboring mature GC dendrites to form connections with these fibers on their own, mapping these connections to new distinct DG units [56]. Thereby the output patterns of neighboring mature GCs are also sparsified [58]. As suggested by network modeling, this should generate the formation of codes for regularly occurring combinations of active inputs that participate in different episodic memories [13]. Most importantly, the smaller the units which reliably respond to correlations in the input space, the finer the distinction of individual features from partial cues, thus preventing different items falsely activating the same cell assemblies in CA3.

As outlined above, at all stages of development there are different mechanisms to counterbalance enhanced excitability and NMDAR-dependent spiking, providing sparse firing even with increasing synapse load. During the first three weeks, membrane resistivity is high and GABAergic synapses generate less synaptic inhibition under certain conditions. However, firing is restricted by the lower density of voltage-gated ion channels and sparse glutamatergic connectivity. Furthermore, the slow time course of GABAergic synapses generates efficient temporal summation leading to shunting inhibition during enhanced hippocampal activity early on. At around 3–4 weeks, when the number of connected synapses exceeds 500, several important changes occur. Firstly, the membrane time constant drops towards that of mature values, dividing dendrites electrotonically apart from each other. Secondly, E_{GABA} declines to mature values, making GABA more inhibitory. As the time course of GABAergic currents is still slow, there will be more efficient temporal summation of GABAergic synaptic currents during ongoing network activity. Finally, it was reported that at around 4 wpm there is also enhanced long-term depression in young GCs, as well as a phase of dendritic pruning [20,89]. After the full complement of approximately 5000 synapses is reached, sparse firing is maintained by large feedforward and feedback inhibition, increased leak channel density and a high threshold for synaptic plasticity. While these mechanisms still allow for sparse coding and detection of previously learned correlations, learning of new ones will be more difficult at this stage.

In addition to the input synapses, the output synapses of young GCs also show special properties. The mossy fiber boutons from synapses with CA3 pyramidal cells at around 2 wpm reaching mature EPSC amplitudes at about 4 wpm [19,90]. At this stage they show a lower threshold for the induction of the non-associative mossy-fiber LTP than fully mature cells [10]. At the mossy-fiber CA3-pyramidal cell synapse potentiation depends only on presynaptic GC activity, while the activity of the postsynaptic CA3 pyramidal cell is largely irrelevant [76]. Computational studies have suggested that the associative LTP in input synapses together with non-associative LTP at output synapses of GCs is necessary as an instructive teaching signal for the formation of new distinctive cell assemblies in CA3 [12]. Starting at 2 wpm young GCs also from synapses with CA3 interneurons to generate feedforward inhibition, another mechanism to support decorrelation in CA3 cell assemblies [43,91].

Taken together, not only the input synapses, but also the output synapses of young GCs show properties, which nicely match requirements for efficient hippocampal information processing as suggested by computational modeling studies.

7. Conclusions

Although newly generated young GCs have intrinsic properties to increase excitability, they remain sparsely active similar to mature GCs within the dentate network. This is mainly due to sparse connectivity of the young cells, generated by a small number of high-impact synapses. As these synapses are formed in a competitive manner by associative mechanisms, new connections are preferentially formed with afferent fibers showing highly correlated activity patterns. Unique cellular properties of young GCs - for example high expression of NMDA receptors and enhanced synaptic plasticity - provide a competitive advantage over mature GCs for synapse formation and potentiation, but do not generate hyperactivity. At all developmental stages there are mechanisms to counterbalance enhanced excitability including efficient temporal summation of slow GABAergic conductance and powerful shunting inhibition. Altogether this results in sparse and orthogonal firing of the young GCs *in vitro* as well as *in vivo*.

According to modeling studies the dentate gyrus may improve storage capacity of hippocampus–dependent auto-associative memory, by sparse and distinct synaptic inputs to the CA3 network. As young GCs preferentially form synaptic input connections with small bundles of co-active afferent EC fibers, the young GC population will output distinctive feature sets to CA3. As a consequence, they are expected to improve learning and recall of similar memory items as experimentally confirmed by improved behavioral pattern separation. Taken together, present studies support the notion that synaptic properties of newly generated GCs efficiently support sparse and orthogonal coding in the mammalian hippocampus to improve learning and memory.

Acknowledgement

We thank Jan M. Schulz and Nicolas Toni for helpful comments on the manuscript. Supported by the Swiss National Science Foundation (SNSF, Project 31003A_176321/1).

References

[1] H. van Praag, A.F. Schinder, B.R. Christie, N. Toni, T.D. Palmer, F.H. Gage, Functional neurogenesis in the adult hippocampus, Nature 415 (2002) 1030–1034.
[2] C. Schmidt-Hieber, P. Jonas, J. Bischofberger, Enhanced synaptic plasticity in newly generated granule cells of the adult hippocampus, Nature 429 (2004) 184–187.
[3] S. Ge, C. Yang, K. Hsu, G. Ming, H. Song, A critical period for enhanced synaptic plasticity in newly generated neurons of the adult brain, Neuron 54 (2007) 559–566.
[4] L. Overstreet-Wadiche, D. Bromberg, A. Bensen, G. Westbrook, GABAergic signaling to newborn neurons in entate gyrus, J. Neurophysiol. 94 (2005) 4528–4532.
[5] S. Ge, E.L.K. Goh, K.A. Sailor, Y. Kitabatake, G. Ming, H. Song, GABA regulates synaptic integration of newly generated neurons in the adult brain, Nature 439 (2006) 589–593.
[6] A. Marín-Burgin, L.A. Mongiat, M.B. Pardi, A.F. Schinder, Unique processing during a period of high excitation/inhibition balance in adult-born neurons, Science 335 (2012) 1238–1242.
[7] D.A. Laplagne, M.S. Espósito, V.C. Piatti, N.A. Morgenstern, C. Zhao, H. van Praag, F.H. Gage, A.F. Schinder, Functional convergence of neurons generated in the developing and adult Hippocampus macklis J, ed, PLoS Biol. 4 (2006) e409.
[8] J.B. Aimone, W. Deng, F.H. Gage, Adult neurogenesis: integrating theories and separating functions, Trends Cogn. Sci. (Regul. Ed.) 14 (2010) 325–337.
[9] J.B. Aimone, W. Deng, F.H. Gage, Resolving new memories: a critical look at the Dentate Gyrus, adult neurogenesis, and pattern separation, Neuron 70 (2011) 589–596.
[10] Y. Gu, M. Arruda-Carvalho, J. Wang, S.R. Janoschka, S.A. Josselyn, P.W. Frankland, S. Ge, Optical controlling reveals time-dependent roles for adult-born dentate granule cells, Nat. Neurosci. 15 (2012) 1700–1706.
[11] T. Nakashiba, J.D. Cushman, K.A. Pelkey, S. Renaudineau, D.L. Buhl, T.J. McHugh, V.R. Barrera, R. Chittajallu, K.S. Iwamoto, C.J. McBain, M.S. Fanselow, S. Tonegawa, Young dentate granule cells mediate pattern separation, whereas old granule cells facilitate pattern completion, Cell 149 (2012) 188–201.
[12] A. Treves, E.T. Rolls, Computational constraints suggest the need for two distinct input systems to the hippocampal CA3 network, Hippocampus 2 (1992) 189–199.
[13] A. Treves, E.T. Rolls, Computational analysis of the role of the hippocampus in memory, Hippocampus 4 (1994) 374–391.
[14] V.C. Piatti, L.A. Ewell, J.K. Leutgeb, Neurogenesis in the dentate gyrus: carrying the message or dictating the tone, Front. Neurosci. 7 (2013) 50.
[15] N.B. Danielson, P. Kaifosh, J.D. Zaremba, M. Lovett-Barron, J. Tsai, C.A. Denny, E.M. Balough, A.R. Goldberg, L.J. Drew, R. Hen, A. Losonczy, M.A. Kheirbek, Distinct contribution of adult-born hippocampal granule cells to context encoding, Neuron 90 (2016) 101–112.
[16] S.T. Johnston, M. Shtrahman, S. Parylak, J.T. Gonçalves, F.H. Gage, Paradox of pattern separation and adult neurogenesis: a dual role for new neurons balancing memory resolution and robustness, Neurobiol. Learn. Mem. 129 (2016) 60–68.
[17] A.I. Ramsaran, P.W. Frankland, The young and the promiscuous, Neuron 90 (2016) 6–8.
[18] C. Zhao, E.M. Teng, R.G. Summers, G.-L. Ming, F.H. Gage, Distinct morphological stages of dentate granule neuron maturation in the adult mouse hippocampus, J. Neurosci. 26 (2006) 3–11.
[19] G.J. Sun, K.A. Sailor, Q.A. Mahmood, N. Chavali, K.M. Christian, H. Song, G. Ming, Seamless reconstruction of intact adult-born neurons by serial end-block imaging reveals complex axonal guidance and development in the adult hippocampus, J. Neurosci. 33 (2013) 11400–11411.
[20] J.T. Gonçalves, C.W. Bloyd, M. Shtrahman, S.T. Johnston, S.T. Schafer, S.L. Parylak, T. Tran, T. Chang, F.H. Gage, In vivo imaging of dendritic pruning in dentate granule cells, Nat. Neurosci. 19 (2016) 788–791.
[21] C. Schmidt-Hieber, P. Jonas, J. Bischofberger, Subthreshold dendritic signal processing and coincidence detection in dentate gyrus granule cells, J. Neurosci. 27 (2007) 8430–8441.
[22] P. Ambrogini, D. Lattanzi, S. Ciuffoli, D. Agostini, L. Bertini, V. Stocchi, S. Santi, R. Cuppini, Morpho-functional characterization of neuronal cells at different stages of maturation in granule cell layer of adult rat dentate gyrus, Brain Res. 1017 (2004) 21–31.
[23] L.A. Mongiat, M.S. Espósito, G. Lombardi, A.F. Schinder, Reliable activation of immature neurons in the adult Hippocampus reh TA, ed, PLoS One 4 (2009) e5320.
[24] S. Heigele, S. Sultan, N. Toni, J. Bischofberger, Bidirectional GABAergic control of action potential firing in newborn hippocampal granule cells, Nat. Neurosci. 19 (2016) 263–270.
[25] L.S. Overstreet, S.T. Hentges, V.F. Bumaschny, F.S.J. de Souza, J.L. Smart, A.M. Santangelo, M.J. Low, G.L. Westbrook, M. Rubinstein, A transgenic marker for newly born granule cells in dentate gyrus, J. Neurosci. 24 (2004) 3251–3259.
[26] L. Li, S. Sultan, S. Heigele, C. Schmidt-Salzmann, N. Toni, J. Bischofberger, Silent synapses generate sparse and orthogonal action potential firing in adult-born hippocampal granule cells, Elife 6 (2017) e23612.
[27] C.C. Young, M. Stegen, R. Bernard, M. Müller, J. Bischofberger, R.W. Veh, C.A. Haas, J. Wolfart, Upregulation of inward rectifier K^+ (Kir2) channels in dentate gyrus granule cells in temporal lobe epilepsy, J. Physiol. (Paris) 587 (2009) 4213–4233.
[28] J.C. Gonzalez, S.A. Epps, S.J. Markwardt, J.I. Wadiche, L. Overstreet-Wadiche, Constitutive and synaptic activation of GIRK channels differentiates mature and newborn dentate granule cells, J. Neurosci. 38 (2018) 6513–6526.
[29] G. Stocca, C. Schmidt-Hieber, J. Bischofberger, Differential dendritic Ca^{2+} signalling in young and mature hippocampal granule cells, J. Physiol. (Paris) 586 (2008) 3795–3811.
[30] C.V. Dieni, A.K. Nietz, R. Panichi, J.I. Wadiche, L. Overstreet-Wadiche, Distinct determinants of sparse activation during granule cell maturation, J. Neurosci. 33 (2013) 19131–19142.
[31] J. Song, J. Sun, J. Moss, Z. Wen, G.J. Sun, D. Hsu, C. Zhong, H. Davoudi, K.M. Christian, N. Toni, G. Ming, H. Song, Parvalbumin interneurons mediate neuronal circuitry–neurogenesis coupling in the adult hippocampus, Nat. Neurosci. 16 (2013) 1728–1730.
[32] M.S. Espósito, V.C. Piatti, D.A. Laplagne, N.A. Morgenstern, C.C. Ferrari, F.J. Pitossi, A.F. Schinder, Neuronal differentiation in the adult hippocampus recapitulates embryonic development, J. Neurosci. 25 (2005) 10074–10086.
[33] N. Sah, B.D. Peterson, S.T. Lubejko, C. Vivar, H. van Praag, Running reorganizes the circuitry of one-week-old adult-born hippocampal neurons, Sci. Rep. 7 (2017) 10903.
[34] S.J. Markwardt, C.V. Dieni, J.I. Wadiche, L. Overstreet-Wadiche, Ivy/neurogliaform interneurons coordinate activity in the neurogenic niche, Nat. Neurosci. 14 (2011) 1407–1409.
[35] D.D. Alvarez, D. Giacomini, S.M. Yang, M.F. Trinchero, S.G. Temprana, K.A. Büttner, N. Beltramone, A.F. Schinder, A disynaptic feedback network activated by experience promotes the integration of new granule cells, Science 354 (80) (2016) 459–465.
[36] S.J. Markwardt, J.I. Wadiche, L.S. Overstreet-Wadiche, Input-specific GABAergic signaling to newborn neurons in adult dentate gyrus, J. Neurosci. 29 (2009) 15063–15072.
[37] Y.J.G. Karten, M.A. Jones, S.I. Jeurling, H.A. Cameron, GABAergic signaling in young granule cells in the adult rat and mouse dentate gyrus, Hippocampus 16 (2006) 312–320.
[38] Y. Ben-Ari, Excitatory actions of gaba during development: the nature of the nurture, Nat. Rev. Neurosci. 3 (2002) 728–739.
[39] R. Jagasia, K. Steib, E. Englberger, S. Herold, T. Faus-Kessler, M. Saxe, F.H. Gage, H. Song, D.C. Lie, GABA-cAMP response element-binding protein signaling regulates maturation and survival of newly generated neurons in the adult hippocampus, J. Neurosci. 29 (2009) 7966–7977.
[40] A. Deshpande, M. Bergami, A. Ghanem, K.-K. Conzelmann, A. Lepier, M. Götz, B. Berninger, Retrograde monosynaptic tracing reveals the temporal evolution of inputs onto new neurons in the adult dentate gyrus and olfactory bulb, Proc Natl Acad Sci U S A 110 (2013) E1152–61.
[41] J.H. Chancey, E.W. Adlaf, M.C. Sapp, P.C. Pugh, J.I. Wadiche, L.S. Overstreet-Wadiche, GABA depolarization is required for experience-dependent synapse unsilencing in adult-born neurons, J. Neurosci. 33 (2013) 6614–6622.
[42] J.R. Geiger, J. Lübke, A. Roth, M. Frotscher, P. Jonas, Submillisecond AMPA

receptor-mediated signaling at a principal neuron–Interneuron synapse, Neuron 18 (1997) 1009–1023.
[43] S.G. Temprana, L.A. Mongiat, S.M. Yang, M.F. Trinchero, D.D. Alvarez, E. Kropff, D. Giacomini, N. Beltramone, G.M. Lanuza, A.F. Schinder, Delayed coupling to feedback inhibition during a critical period for the integration of adult-born granule cells, Neuron 85 (2015) 116–130.
[44] C. Espinoza, S.J. Guzman, X. Zhang, P. Jonas, Parvalbumin+ interneurons obey unique connectivity rules and establish a powerful lateral-inhibition microcircuit in dentate gyrus, Nat. Commun. 9 (2018) 4605.
[45] L.A. Ewell, M.V. Jones, Frequency-tuned distribution of inhibition in the dentate gyrus, J. Neurosci. 30 (2010) 12597–12607.
[46] S. Sambandan, J.-F. Sauer, I. Vida, M. Bartos, Associative plasticity at excitatory synapses facilitates recruitment of fast-spiking interneurons in the dentate gyrus, J. Neurosci. 30 (2010) 11826–11837.
[47] A.J. Pernía-Andrade, P. Jonas, Theta-gamma-Modulated synaptic currents in hippocampal granule cells in vivo define a mechanism for network oscillations, Neuron 81 (2014) 140–152.
[48] M.W. Jung, B.L. McNaughton, Spatial selectivity of unit activity in the hippocampal granular layer, Hippocampus 3 (1993) 165–182.
[49] M.K. Chawla, J.F. Guzowski, V. Ramirez-Amaya, P. Lipa, K.L. Hoffman, L.K. Marriott, P.F. Worley, B.L. McNaughton, C.A. Barnes, Sparse, environmentally selective expression ofArc RNA in the upper blade of the rodent fascia dentata by brief spatial experience, Hippocampus 15 (2005) 579–586.
[50] J.K. Leutgeb, S. Leutgeb, M.-B. Moser, E.I. Moser, Pattern separation in the Dentate Gyrus and CA3 of the Hippocampus, Science 315 (80) (2007) 961–966.
[51] T. Hainmueller, M. Bartos, Parallel emergence of stable and dynamic memory engrams in the hippocampus, Nature 558 (2018) 292–296.
[52] M.B. Pardi, M.B. Ogando, A.F. Schinder, A. Marin-Burgin, Differential inhibition onto developing and mature granule cells generates high-frequency filters with variable gain, Elife 4 (2015).
[53] J.H. Chancey, D.J. Poulsen, J.I. Wadiche, L. Overstreet-Wadiche, Hilar mossy cells provide the first glutamatergic synapses to adult-born dentate granule cells, J. Neurosci. 34 (2014) 2349–2354.
[54] N.I. Woods, C.E. Vaaga, C. Chatzi, J.D. Adelson, M.F. Collie, J.V. Perederiy, K.R. Tovar, G.L. Westbrook, Preferential targeting of lateral entorhinal inputs onto newly integrated granule cells, J. Neurosci. 38 (2018) 5843–5853.
[55] C. Schmidt-Salzmann, L. Li, J. Bischofberger, Functional properties of extrasynaptic AMPA and NMDA receptors during postnatal hippocampal neurogenesis, J. Physiol. (Paris) 592 (2014) 125–140.
[56] N. Toni, E.M. Teng, E.A. Bushong, J.B. Aimone, C. Zhao, A. Consiglio, H. van Praag, M.E. Martone, M.H. Ellisman, F.H. Gage, Synapse formation on neurons born in the adult hippocampus, Nat. Neurosci. 10 (2007) 727–734.
[57] Y. Mu, C. Zhao, N. Toni, J. Yao, F.H. Gage, Distinct roles of NMDA receptors at different stages of granule cell development in the adult brain, Elife 4 (2015) e07871.
[58] E.W. Adlaf, R.J. Vaden, A.J. Niver, A.F. Manuel, V.C. Onyilo, M.T. Araujo, C.V. Dieni, H.T. Vo, G.D. King, J.I. Wadiche, L. Overstreet-Wadiche, Adult-born neurons modify excitatory synaptic transmission to existing neurons, Elife 6 (2017) e19886.
[59] A. Tashiro, V.M. Sandler, N. Toni, C. Zhao, F.H. Gage, NMDA-receptor-mediated, cell-specific integration of new neurons in adult dentate gyrus, Nature 442 (2006) 929–933.
[60] H.-B. Kwon, B.L. Sabatini, Glutamate induces de novo growth of functional spines in developing cortex, Nature 474 (2011) 100–104.
[61] G.M. Durand, Y. Kovalchuk, A. Konnerth, Long-term potentiation and functional synapse induction in developing hippocampus, Nature 381 (1996) 71–75.
[62] M. Maletic-Savatic, R. Malinow, K. Svoboda, Rapid dendritic morphogenesis in CA1 hippocampal dendrites induced by synaptic activity, Science 283 (1999) 1923–1927.
[63] S. Sultan, L. Li, J. Moss, F. Petrelli, F. Cassé, E. Gebara, J. Lopatar, F.W. Pfrieger, P. Bezzi, J. Bischofberger, N. Toni, Synaptic integration of adult-born hippocampal neurons is locally controlled by astrocytes, Neuron 88 (2015) 957–972.
[64] T. Papouin, J. Dunphy, M. Tolman, J.C. Foley, P.G. Haydon, Astrocytic control of synaptic function, Philos Trans R Soc B Biol Sci 372 (2017) 20160154.
[65] L.M. Robin, et al., Astroglial CB1 receptors determine synaptic D-serine availability to enable recognition memory, Neuron 98 (2018) 935–944 e5.
[66] P. Poirazi, T. Brannon, B.W. Mel, Pyramidal neuron as two-layer neural network, Neuron 37 (2003) 989–999.
[67] A. Polsky, B.W. Mel, J. Schiller, Computational subunits in thin dendrites of pyramidal cells, Nat. Neurosci. 7 (2004) 621–627.
[68] T. Branco, M. Häusser, The single dendritic branch as a fundamental functional unit in the nervous system, Curr. Opin. Neurobiol. 20 (2010) 494–502.
[69] T. Branco, M. Häusser, Synaptic integration gradients in single cortical pyramidal cell dendrites, Neuron 69 (2011) 885–892.
[70] R. Krueppel, S. Remy, H. Beck, Dendritic integration in hippocampal dentate granule cells, Neuron 71 (2011) 512–528.
[71] J.M. Schulz, F. Knoflach, M.-C. Hernandez, J. Bischofberger, Dendrite-targeting interneurons control synaptic NMDA-receptor activation via nonlinear α5-GABAA receptors, Nat. Commun. 9 (2018) 3576.
[72] M.E. Larkum, T. Nevian, M. Sandler, A. Polsky, J. Schiller, Synaptic integration in tuft dendrites of layer 5 pyramidal neurons: a new unifying principle, Science 325 (2009) 756–760.
[73] C.V. Dieni, R. Panichi, J.B. Aimone, C.T. Kuo, J.I. Wadiche, L. Overstreet-Wadiche, Low excitatory innervation balances high intrinsic excitability of immature dentate neurons, Nat. Commun. 7 (2016) 11313.
[74] D. Marr, Simple memory: a theory for archicortex, Philos Trans R Soc B Biol Sci 262 (1971) 23–81.
[75] D.A. Henze, L. Wittner, G. Buzsáki, Single granule cells reliably discharge targets in the hippocampal CA3 network in vivo, Nat. Neurosci. 5 (2002) 790–795.
[76] J. Bischofberger, D. Engel, M. Frotscher, P. Jonas, Timing and efficacy of transmitter release at mossy fiber synapses in the hippocampal network, Pflügers Arch - Eur J Physiol 453 (2006) 361–372.
[77] C.D. Clelland, M. Choi, C. Romberg, G.D. Clemenson, A. Fragniere, P. Tyers, S. Jessberger, L.M. Saksida, R.A. Barker, F.H. Gage, T.J. Bussey, A functional role for adult hippocampal neurogenesis in spatial pattern separation, Science 325 (2009) 210–213.
[78] D.J. Creer, C. Romberg, L.M. Saksida, H. van Praag, T.J. Bussey, Running enhances spatial pattern separation in mice, Proc. Natl. Acad. Sci. U. S. A. 107 (2010) 2367–2372.
[79] A. Sahay, D.A. Wilson, R. Hen, Pattern separation: a common function for new neurons in Hippocampus and olfactory bulb, Neuron 70 (2011) 582–588.
[80] M.A. Kheirbek, L. Tannenholz, R. Hen, NR2B-dependent plasticity of adult-born granule cells is necessary for context discrimination, J. Neurosci. 32 (2012) 8696–8702.
[81] L. Bolz, S. Heigele, J. Bischofberger, Running improves pattern separation during novel object recognition, Brain Plast (Amsterdam, Netherlands) 1 (2015) 129–141.
[82] V. Ramirez-Amaya, D.F. Marrone, F.H. Gage, P.F. Worley, C.A. Barnes, Integration of new neurons into functional neural networks, J. Neurosci. 26 (2006) 12237–12241.
[83] N. Kee, C.M. Teixeira, A.H. Wang, P.W. Frankland, Preferential incorporation of adult-generated granule cells into spatial memory networks in the dentate gyrus, Nat. Neurosci. 10 (2007) 355–362.
[84] A. Tashiro, H. Makino, F.H. Gage, Experience-specific functional modification of the Dentate Gyrus through adult neurogenesis: a critical period during an immature stage, J. Neurosci. 27 (2007) 3252–3259.
[85] M. Krzisch, C. Fülling, L. Jabinet, J. Armida, E. Gebara, F. Cassé, S. Habbas, A. Volterra, J.-P. Hornung, N. Toni, Synaptic adhesion molecules regulate the integration of new granule neurons in the postnatal mouse Hippocampus and their impact on spatial memory, Cereb. Cortex 27 (2016) 4048–4059.
[86] S.S.D. Stone, C.M. Teixeira, K. Zaslavsky, A.L. Wheeler, A. Martinez-Canabal, A.H. Wang, M. Sakaguchi, A.M. Lozano, P.W. Frankland, Functional convergence of developmentally and adult-generated granule cells in dentate gyrus circuits supporting hippocampus-dependent memory, Hippocampus 21 (2011) 1348–1362.
[87] P. Mishra, R. Narayanan, Disparate forms of heterogeneities and interactions among them drive channel decorrelation in the dentate gyrus: degeneracy and dominance, Hippocampus 29 (2019) 378–403.
[88] J.-M. Zhuo, H. Tseng, M. Desai, M.E. Bucklin, A.I. Mohammed, N.T. Robinson, E.S. Boyden, L.M. Rangel, A.P. Jasanoff, H.J. Gritton, X. Han, Young adult born neurons enhance hippocampal dependent performance via influences on bilateral networks, Elife 5 (2016) e22429.
[89] F. Massa, M. Koehl, M. Koelh, T. Wiesner, N. Grosjean, J.-M. Revest, P.-V. Piazza, D.N. Abrous, S.H.R. Oliet, Conditional reduction of adult neurogenesis impairs bidirectional hippocampal synaptic plasticity, Proc. Natl. Acad. Sci. U. S. A. 108 (2011) 6644–6649.
[90] N. Toni, D.A. Laplagne, C. Zhao, G. Lombardi, C.E. Ribak, F.H. Gage, A.F. Schinder, Neurons born in the adult dentate gyrus form functional synapses with target cells, Nat. Neurosci. 11 (2008) 901–907.
[91] L. Restivo, Y. Niibori, V. Mercaldo, S.A. Josselyn, P.W. Frankland, Development of adult-generated cell connectivity with excitatory and inhibitory cell populations in the Hippocampus, J. Neurosci. 35 (2015) 10600–10612.

7.2 Rizzi G, Lodge ME, Tan KR (2016). Design and construction of a low-cost nose poke system for rodents. *MethodsX*, *3*: 326-332.

MethodsX 3 (2016) 326–332

Contents lists available at ScienceDirect

MethodsX

journal homepage: www.elsevier.com/locate/mex

Design and construction of a low-cost nose poke system for rodents

Giorgio Rizzi*, Meredith E. Lodge, Kelly R. Tan*

Biozentrum, University of Basel, Klingelbergstrasse 50/70, 4056 Basel, Switzerland

A B S T R A C T

Operant behavioral tasks for animals have long been used to probe the function of multiple brain regions (i.e., understanding the role of dopamine in electrical brain stimulation reward [1], or determining the rewarding properties of feeding oriented brain pathways [2]). The recent development of tools and techniques has opened the door to refine the answer to these same questions with a much higher degree of specificity and accuracy, both in biological and spatial-temporal terms [3,4]. A variety of systems designed to test operant behavior are now commercially available, but have prohibitive costs. Here, we provide a low-cost alternative to a nose poke system for mice. Adapting a freely available sketch for ARDUINO boards, in combination with an in-house built PVC box and inexpensive electronic material we constructed a four-port nose poke system that detects and counts port entries. To verify the applicability and validity of our system we tested the behavior of DAT-CRE transgenic mice injected with an adeno-associated virus to express ChannelRhodopsin 2 in the Ventral tegmental area (VTA) and used the BNC output to drive a blue laser coupled to a fiber implanted above the VTA. Over 6 days, mice perform as it has been reported previously [5] exhibiting a remarkable preference for the port that triggers optogenetic stimulation of VTA dopamine neurons.

- We provide a low cost alternative to commercially available nose poke system.
- Our custom made apparatus is open source and TTL compatible.
- We validate our system with optogenetic self-stimulation of dopamine neurons.

A R T I C L E I N F O

Method name: Arduino based nose poke system for rodents

Keywords: Operant behavior, Rodent, Reward, Nose poke, Optogenetics, Lowcost

Article history: Received 4 February 2016; Accepted 6 April 2016; Available online 19 April 2016

* Corresponding authors.
E-mail addresses: Giorgio.rizzi@unibas.ch (G. Rizzi), Kelly.tan@unibas.ch (K.R. Tan).

http://dx.doi.org/10.1016/j.mex.2016.04.002

Method

Operant behavioral tasks designed for rodents are often used to probe the involvement and function of different brain regions linked to a variety of physiological and pathological brain states. The systems used to perform these experiments are often very expensive and beyond the reach of small labs or low budget projects.

Here we recapitulate the steps taken to construct a custom-made nose poke system designed for mice, taking advantage of open source technology and inexpensive materials.

Arduino boards are becoming increasingly popular due to their versatility and low cost. They have dedicated software and hardware that allow them to be programmed and therefore be applied to suit any need.

Starting from a freely available sketch (Supl. Ref. 1) containing source code designed to make a laser tripwire, we applied the same principle to detect the nose entries to a port and built a nose poke system around it.

The circuit is composed of a light dependent resistor (LDR) that gets exposed to a light source, in our case a red LED, a second LED (here green) that turns on every time the light beam onto the LDR is interrupted and an output BNC connector that drives the laser (GMP S.A. MBL-F-473-500 mW) for optogenetic stimulation.

For a list of all the necessary electronic components to build the Arduino based four-port nose poke system see Table 1.

Our system includes four different ports that have separate circuits connected in parallel. The ARDUINO UNO board processes all of the inputs and outputs.

As schematized in Fig. 1, the red LEDs (LED1) used as light sources for the LDRs are each connected in series with a 100 Ω resistor (R1) and all connected to the 5 V port of the Arduino board and the ground port, creating a very simple circuit to provide power to the LED1. The light sensing circuits are composed of an LDR connected between the 3.3 V port of the Arduino board and the ANALOG-IN ports A1 to A4. A voltage divider is created connecting a 10 kΩ resistor (R3) between the LDRs and ground (Fig. 1).

The green LED (LED2) circuits are formed connecting a 120 Ω resistor (R2) between DIGITAL ports D8 to D11 and the LED2s, which then are connected to ground (Fig. 1).

Finally the DIGITAL port D13 is connected to the live contact of the BNC connector and the shielding to ground (Fig. 1).

We designed the frame that would hold all the electronic components to fit a rectangular PVC box normally used for open field experiments with mice (Fig. 2E and F). We developed our design using SketchUp, a freely available and intuitive 3D modeling software (see Supl. Fig. 1). The frame is composed of two semi-closed compartments one designed to hold the mice while they perform the tasks and the other designed to hold all electronic components and connections (Fig. 2A and B). The front compartment has only a platform and a wall with four 15 mm diameter holes (nose poke ports)

Table 1
Inventory. List of all the electronic materials needed to build a four-port nose poke system designed for mice.

Item	Quantity	Item Number	Company	Schematic Name
Arduino Uno	1	642818	Distrelec	Arduino Uno
100 Ω Resistor	4	722324	Distrelec	R1
120 Ω Resistor	4	728023	Distrelec	R2
10 kΩ Resistor	4	728104	Distrelec	R3
Red LED	4	632048	Distrelec	LED1
Green LED	4	632043	Distrelec	LED2
LDR	4	631603	Distrelec	LDR
BNC Connector	1	103032	Distrelec	BNC
Breadboard	1	920250	Distrelec	N/A
Jumper Cables	50–100	1705	Pololu	N/A

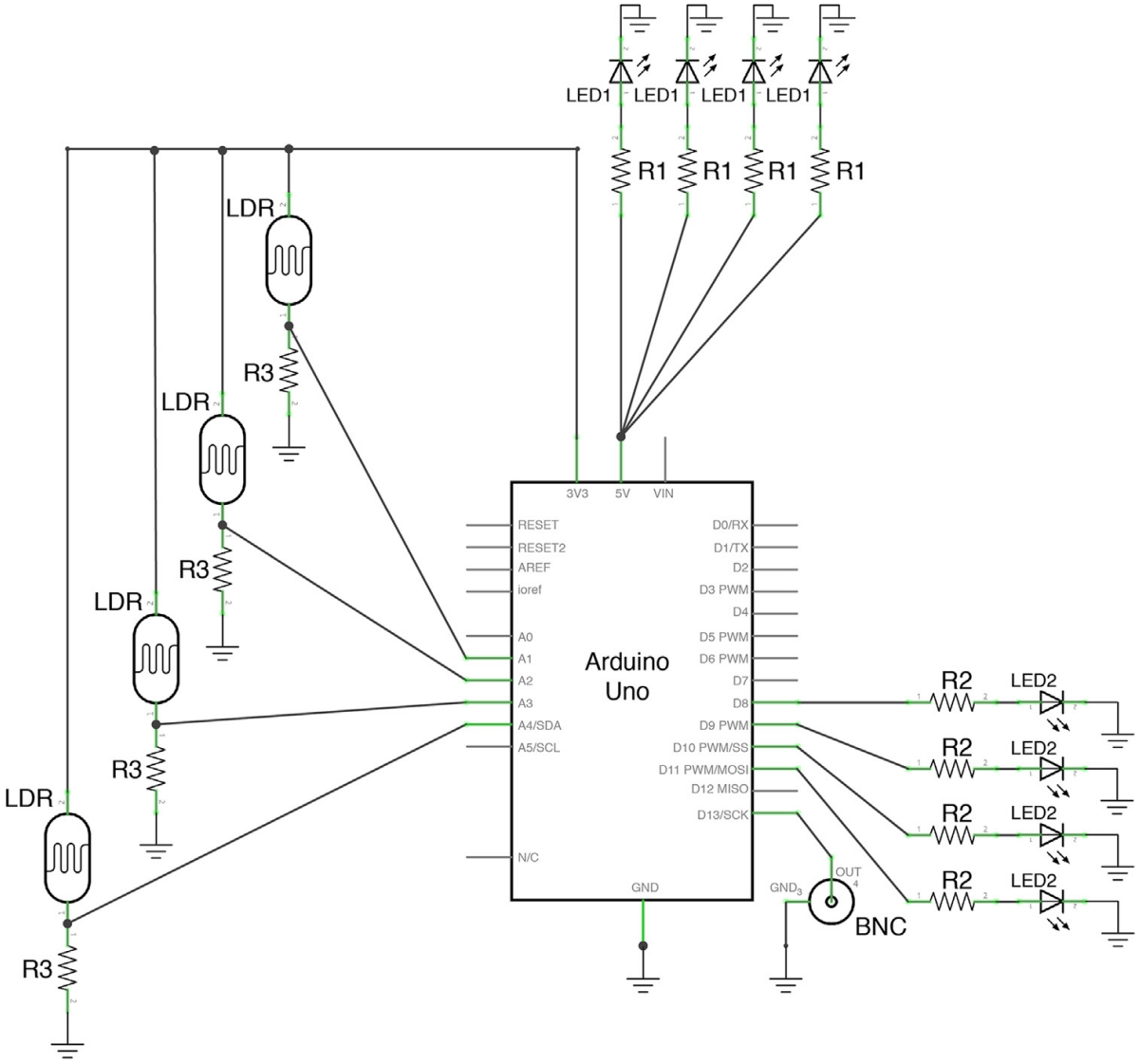

Fig. 1. Electronic circuit schematic of the nose poke system.
Schematic diagram of the circuitry needed for the custom-made nose poke system depicting positioning and connection of each component. The names used in this schematic are reported in Table 1 for the correct selection of each component.

equally spaced and with the lower edge 1 cm from the floor platform, each having a 5 mm diameter hole above that holds the green LED2s.

On the back compartment, surrounding each nose port, there is a structure with 5 mm holes directly above and below the port designed to be aligned vertically and hold the red LED1 above and the LDR below. Thus, when the mouse snout gets into the port it creates a shadow over the LDR changing the value of the resistance (Supl. Fig. 1).

To facilitate the assembly of the electronic components onto the frame we used a breadboard to hold all resistors and used a 3D-printed case that holds the Arduino board (Fig. 2C, G and H). The SketchUp design was then implemented and constructed by the in-house workshop using PVC material. All the detailed measurements of our design can be found in the (Supl. File 1).

Once all the components were placed in the frame, the code (Supl. File 2) could be loaded on the Arduino board allowing the system to be used. For a detailed guide on how to upload sketches on Arduino boards see Supl. Ref. 2.

The Arduino board must be connected to a computer in order to communicate the nose pokes. Power can be supplied to the Arduino Uno either via USB cable or an external power adapter. To initialize an experiment once the board is connected to the PC, the Arduino IDE needs to be launched. Once the serial port monitor window is opened, the board is reset and starts executing the code. The

Fig. 2. Illustrating images of the nose poke system.
Images of the frame and electronic components assembled and ready to use. (A) Front view. (B) Rear view. (C) Back view. (D) Top view. (E) Rear view of the frame placed inside an open field box to prevent the mice from falling off the platform. (F) Top view of the frame placed inside open field. (G) Close view of the breadboard used to interface the connections between electric components and the Arduino board. (H) 3D printed case housing the Arduino board.

first header line will be transmitted through the serial port, listing the port number, poke number and a time stamp. From that point on, every time there is a nose poke, its information will be transmitted as a new row of text with comma separated values. At the end of the session the list must be manually copied to a text file, which will then be saved in a comma separated values format. Closing and opening the serial monitor window of the Arduino IDE will reset the board and prepare it for a new session.

The serial port can be also monitored through third party software and/or a secondary code can be implemented to automatically copy and store the data transmitted by the Arduino board as an alternative to the manual process.

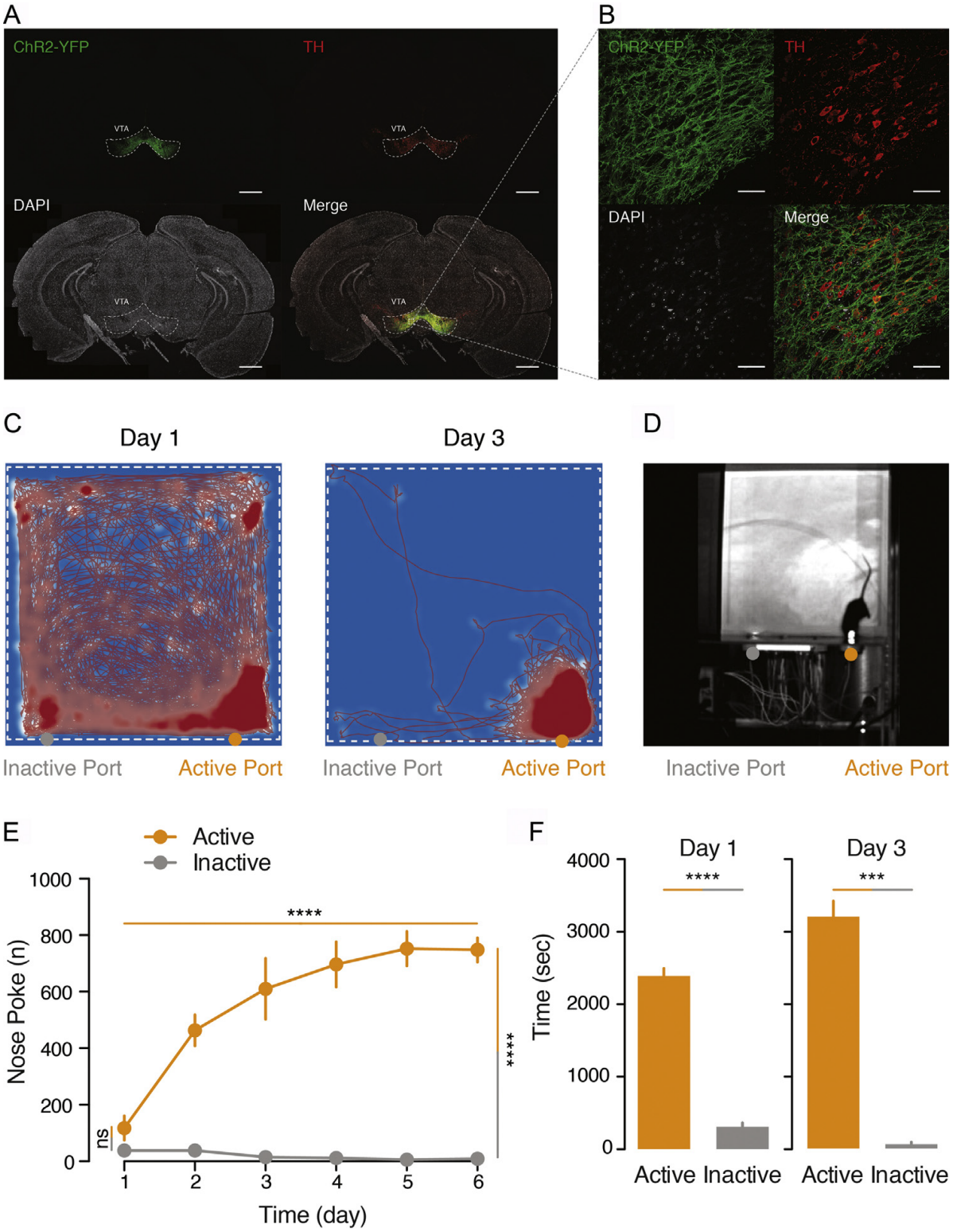

Fig. 3. Quantification of dopamine neuron optogenetic self-stimulation.
Validation of the system through dopamine self-stimulation in DAT-CRE transgenic mice. A) Infection site and TH counter stain verifying infection and dopamine selectivity of ChR2-YFP. Scale bar 1 mm. B) Magnified view of the VTA area showing overlap of TH staining and ChR2-YFP expression. Scale bar 100 μm. C) Example track plot of the first and third sessions of a single mouse overlaid with a normalized heatmap illustrating the distribution of time spent on the platform. D) Example image of a mouse nose poking in the active port. E) Quantification of the nose pokes in the active and inactive ports over time (two-way Anova repeated measures, effect across days $F(5,20) = 19.76$; $p < 0.0001$, effect between ports $F(1,4) = 115.98$; $p = 0.0004$). F) Quantification of the time spent near the active and inactive ports on the first day (2392 ± 102.3SEM and 308 ± 55.87SEM; $p < 0.0001$ *t*-test) and the third day (3205 ± 216.5SEM and 59 ± 29.74SEM; $p = 0.0001$ *t*-test).

To test the functionality of our system we decided to use DAT-CRE transgenic mice (Jackson Laboratory stock number: 006660) injected with DIO-ChR2-EYFP in the VTA and implanted with an optic fiber [6] above this region to deliver light and activate dopamine neurons. For this specific experiment the two central ports of the frame were blocked so that mice could only nose poke in either port most lateral to the frame (Fig. 3). The Arduino code was modified to make one of the ports inactive, the nose pokes were quantified but no light delivery was triggered following an entry to the inactive port. In response to an entry to the active port the BNC output connector triggered a 3 s light delivery at 50 Hz with pulse duration of 5 ms. During the 3 s light simulation no nose pokes were quantified.

Six to eight weeks old DAT-CRE transgenic mice (n = 3) underwent stereotactical surgery during which 300nl of AAV5-EF1α-DIO-ChR2-H134R-EYFP bilaterally with the following coordinates from bregma (−3.4 mm AP; 0.45 mm ML; 4.35 mm DV). During the same surgery a single optic fiber implant was placed with a 10° angle above the VTA to deliver light stimulation.

Three weeks after the surgery all animals were placed in the nose poke system for a daily 60 min session for a total of six days. The behavior of the animals during each session was recorded and tracked (Fig. 3D, Supl. Video 1), using AnyMaze software. The time spent nearby the active and inactive port was quantified automatically and the number of nose pokes in each port was counted and monitored by the Arduino board through the serial port monitor of its dedicated software.

As expected the animals displayed a very strong preference for the active port having an average number of nose pokes of 37.33 ± 11.33SEM in the inactive port and 116.7 ±43.10SEM in the active port on day 1 and 8 ± 4SEM in the inactive port and 746 ± 42.53SEM in the active port on day 6 (Fig. 3E, effect between ports $F(1,4) = 115.98$; $p = 0.0004$ two-way Anova repeated measures,).

As displayed in Fig. 3C and F already on the third day of testing there was a significant preference for the active port (day 1 $p < 0.0001$ and day 3 $p = 0.0001$ *t*-tests) in all the animals confirming the validity of the preparation and the nose poke system. After the sixth day of testing all animals were intracardially perfused and fixed, the brains were slices and the infection and optic fiber placement were verified (Fig. 3A and B). Confocal images of the brains confirmed the restriction of the ChR2 infection to the VTA area and immunohistochemistry counterstaining with tyrosine hydroxylase (TH) confirmed the selectivity of ChR2 expression in dopamine neurons.

Here we provide a recapitulation of the making and testing of a custom-made Arduino-based nose poke system that allows for operant behavioral testing in mice at a fraction of the cost of commercially available systems. Due to the versatility of its microcontroller, this system can easily be modified to modulate any external device that is TTL compatible, and adapted to other types of operant switches such as lever presses or pressure plates.

Acknowledgments

We thank the in-house workshop for their efficient collaboration. We thank the Biozentrum Imaging Core Facility (IMCF, Basel) for providing support, access and maintenance of confocal microscopy. This work was supported by the Swiss National Science Foundation (PP00P3_1150683).

MethodsX thanks the reviewers (Anonymous) of this article for taking the time to provide valuable feedback.

Appendix A. Supplementary data

Supplementary data associated with this article can be found, in the online version, at http://dx.doi.org/10.1016/j.mex.2016.04.002.

References

[1] A.G. Phillips, D.A. Carter, H.C. Fibiger, Dopaminergic substrates of intracranial self-stimulation in the caudate-putamen, Brain Res. 104 (1976) 221–232.

[2] J.H. Jennings, G. Rizzi, A.M. Stamatakis, R.L. Ung, G.D. Stuber, The inhibitory circuit architecture of the lateral hypothalamus orchestrates feeding, Science 341 (2013) 1517–1521, doi:http://dx.doi.org/10.1126/science.1241812.

[3] H.-C. Tsai, F. Zhang, A. Adamantidis, G.D. Stuber, A. Bonci, L. de Lecea, et al., Phasic firing in dopaminergic neurons is sufficient for behavioral conditioning, Science 324 (2009) 1080–1084, doi:http://dx.doi.org/10.1126/science.1168878.
[4] S.M. Sternson, B.L. Roth, Chemogenetic tools to interrogate brain functions, Annu. Rev. Neurosci. 37 (2014) 387–407, doi:http://dx.doi.org/10.1146/annurev-neuro-071013-014048.
[5] V. Pascoli, J. Terrier, A. Hiver, C. Lüscher, Sufficiency of mesolimbic dopamine neuron stimulation for the progression to addiction, Neuron 88 (2015) 1054–1066, doi:http://dx.doi.org/10.1016/j.neuron.2015.10.017.
[6] D.R. Sparta, A.M. Stamatakis, J.L. Phillips, N. Hovelsø, R. van Zessen, G.D. Stuber, Construction of implantable optical fibers for long-term optogenetic manipulation of neural circuits, Nat. Protoc. 7 (2012) 12–23, doi:http://dx.doi.org/10.1038/nprot.2011.413.

Supplementary References

[1] http://robotix.com.au/#/user/videos/8.
[2] https://www.arduino.cc/en/Guide/HomePage.

8. Glossary

ACSF	artificial cerebrospinal fluid
AMPA	α-Amino-3-hydroxy-5-methyl-4-isoxazolepropionic acid
AP	action potential
ChETA	channelrhodopsin-2 with E123T mutation
ChR2	channelrhodopsin-2
DCX	doublecortin
Dpi	days post injection
DSRed	Discosoma sp. reef coral red fluorescent protein
E_{GABA}	reversal potential for GABAA receptor-mediated postsynaptic currents
EPSC	excitatory postsynaptic current
GABA	γ-aminobutyric acid
GC	granule cell
GCL	granule cell layer
GFP/eGFP	green fluorescent protein/enhanced green fluorescent protein
GPSC	GABAergic postsynaptic current
IN	interneuron
KCC2	K^+-Cl^- extruder, a Cl^- extruder
LTP	long-term potentiation
ML	molecular layer
NBQX	2,3-dioxo-6-nitro-1,2,3,4-tetrahydrobenzo[f]quinoxaline-7-sulfonamide; an AMPA-receptor blocker
NKCC1	Na^+-K^+-$2Cl^-$ cotransporter; a Cl^- importer expressed in young neurons
NMDA	N-Methyl-D-aspartic acid

PV	parvalbumin; a calcium binding protein
R_{in}	input resistance
R_S	series resistance
R_{Seal}	seal resistance
SOM	somatostatin, a peptide hormone
V_{Hold}	holding membrane potential
V_{Rest}	resting membrane potential
wpi	weeks post injection
yGC	young granule cell

9. Acknowledgments

Foremost, I would like to acknowledge my advisor Prof. Josef Bischofberger for the opportunity he gave me to complete my PhD in his lab, and for the continual support and guidance he has given me over the past three years. Additionally, I would like to recognize Dr Jan Schulz for his co-supervision of this project, and his helpful feedback on this thesis.

I would also like to thank the rest of my committee- Prof. Tania Rinaldi Barkat and Prof. Christoph Handschin- for their invaluable support, encouragement and insightful comments.

I thank my fellow lab members-Katharina Behr, Ekaterina Verdiyan and Seraphima Verbitsky - and those within the Pecho-Vrieseling group for helpful feedback in lab meetings. A huge thank you to Selma Becherer for constant technical support, and Heidi Ramstein for administrative help.

Finally, I would like to acknowledge the staff working within the Biozentrum Animal Facility, who ensure the health and wellbeing of the experimental animals.

This research was supported by by the Swiss National Science Foundation (SNSF, Project 31003A_13301).